

**University of Alberta**

**Protein Detection Using Dynamic DNA Assembly**

by

Feng Li

A thesis submitted to the Faculty of Graduate Studies and Research  
in partial fulfillment of the requirements for the degree of

**Doctor of Philosophy**

**Department of Chemistry**

©Feng Li  
Spring 2013  
Edmonton, Alberta

Permission is hereby granted to the University of Alberta Libraries to reproduce single copies of this thesis and to lend or sell such copies for private, scholarly or scientific research purposes only. Where the thesis is converted to, or otherwise made available in digital form, the University of Alberta will advise potential users of the thesis of these terms.

The author reserves all other publication and other rights in association with the copyright in the thesis and, except as herein before provided, neither the thesis nor any substantial portion thereof may be printed or otherwise reproduced in any material form whatsoever without the author's prior written permission.

## Abstract

Dynamic DNA assemblies are useful to generate or amplify signals for detection of nucleic acids. However, application of DNA assemblies to proteins is more challenging. The major research goal of my thesis is to expand the scope of dynamic DNA assemblies to proteins.

I developed a fluorescence turn-on assay and studied thermal stability of DNA functionalized gold nanoparticles (DNA-AuNPs) as a function of organosulfur anchor groups and DNA surface densities. An attempt to use DNA-AuNPs as detection probes in western blot protein analyses revealed nonspecific protein adsorptions. By applying dynamic DNA assembly to Aptamer-functionalized gold nanoparticles (Apt-AuNPs), I designed a competitive protection strategy that was able to effectively eliminate nonspecific protein adsorptions on Apt-AuNPs, enabling specific and sensitive detection of target proteins from human serum samples.

To broaden the use of dynamic DNA assembly as tools for protein detection, I developed a binding-induced DNA strand-displacement strategy that could convert protein bindings to the release of pre-designed output DNA molecules. The output DNA molecules were used to trigger various DNA assemblies. Using this strategy, I developed a binding-induced strand-displacement beacon and a binding-induced catalytic DNA circuit, both of which could be used as isothermal and enzyme-free signal amplification strategies for protein detection. I have further developed a molecular translator that acted by binding-induced dynamic

DNA assemblies on AuNPs, enabling highly sensitive and specific detection of different protein targets in homogeneous solutions.

The techniques and strategies described in this thesis can be potentially used to construct a variety of protein-mediated DNA assemblies and nanostructures. A promising application is in the area of point-of-care diagnostics, taking advantage of binding-induced DNA assembly, molecular and/or signal amplification, and nanoparticle-based visualization.

## **Acknowledgements**

First, I would like to express my sincere gratitude to my supervisor Dr. Chris Le for his great support in both science and life. I always suspect that Chris has some kind of superpower like “mind-reading” or “super-brain”, because he knows everything in my mind no matter how bad I expressed, and he can magically make everything so easy and comfortable no matter how hard they are. Thus, working with Chris is always an enjoyable journey for me. Chris never forced me to learn anything or to do anything, but he has taught me so much little by little, from conducting a simple lab operation to forming a complete research idea, from presenting my work in a group meeting to showcasing my project to a huge conference, and from writing a research proposal to publishing a research manuscript. Furthermore, Chris always believes in me and gives me a lot of freedom and opportunities to work on diverse research projects. Without him, I won't be able to learn so much and grow up so much in academia.

I would also like to thank the members of my supervisory committee, Dr. Jonathan Sweedler, Dr. Robert Campbell, Dr. Julianne Gibbs-Davis, and Dr. Mark McDermott for giving me so many insightful suggestions and comments.

I would also like to thank Dr. Hongquan Zhang for teaching me so much on basic lab techniques and reading skills, and thank Dr. Xing-Fang Li for giving me so many good suggestions about my projects and my life. I also need to thank my good friends Katerina, Xiufen, Qiang, Baowei, Yichao, Hanyong, Chenming, Zonglin, Lydia and all members of Chris's group and AET division for making my life in Edmonton such enjoyable, and I will always treasure your friendships. I

also need to thank all my friends in Department of Chemistry and throughout my campus life in University of Alberta. You make my life so colorful here!

最后，我想把我最诚挚的感激之情献给我的父亲，母亲，妻子，和一起成长与奋斗的好朋友们。无论身在何方，你们的鼓舞与支持永远是我不断前进的动力。

# Table of Contents

|  |           |
|--|-----------|
| <b>Chapter One: Introduction .....</b>   | <b>1</b>  |
| 1.1 DNA nanotechnology .....   | 1         |
| 1.2 DNA functionalized gold nanoparticles for bio-analysis.....                          | 2         |
| 1.2.1 Colorimetric biosensors using DNA-AuNPs .....                                      | 3         |
| 1.2.2 Fluorescent biosensors using DNA-AuNPs.....  | 5         |
| 1.3 Dynamic DNA assembly for bioanalysis.....  | 9         |
| 1.3.1 Assays based on toehold-mediated DNA strand-displacement<br>reactions .....        | 9         |
| 1.3.2 Assays based on hybridization chain reactions.....                                 | 13        |
| 1.3.3 Assays based on catalytic DNA circuits and DNA machines.....                       | 16        |
| 1.4 Binding-induced DNA assemblies for protein assays .....                              | 20        |
| 1.4.1 Binding-induced DNA annealing assays .....   | 20        |
| 1.4.2 Proximity ligation assays .....  | 24        |
| 1.4.3 Assays based on binding-induced DNA assembly .....                                 | 26        |
| 1.5 Rationale and objective.....   | 29        |
| 1.6 References .....   | 32        |
| <b>Chapter Two: Thermal Stability of DNA Functionalized Gold Nanoparticles<br/>.....</b> | <b>39</b> |
| 2.1 Introduction.....  | 39        |

|   |           |
|---|-----------|
| 2.2 Experimental .....  | 42        |
| 2.2.1 Materials and reagents .....  | 42        |
| 2.2.2 Preparation of DNA-AuNPs .....  | 43        |
| 2.2.3 Characterization of DNA-AuNPs .....   | 44        |
| 2.2.4 Monitoring the thermal dissociation of DNA-AuNPs .....  | 45        |
| 2.2.5 Monitoring the chemical-induced dissociation of DNA-AuNPs .....   | 46        |
| 2.3 Results and discussion .....  | 46        |
| 2.3.1 Experimental design.....  | 46        |
| 2.3.2 Effect of anchor groups on the thermal stability of DNA-AuNPs .....                                       | 49        |
| 2.3.3 Effect of packing densities on the thermal stability of DNA-AuNPs .....                                   | 54        |
| 2.3.4 Enhancing the thermal stability of DNA-AuNPs containing sicDNA<br>using double-stranded DNA probes .....  | 57        |
| 2.4 Conclusions .....   | 60        |
| 2.5 References .....  | 61        |
| <b>Chapter Three: Dynamic DNA Assembly on Aptamer Functionalized Gold<br/>Nanoparticles for Bioassays .....</b> | <b>64</b> |
| 3.1 Introduction .....  | 64        |
| 3.2 Experimental .....  | 67        |
| 3.2.1 Materials and reagents .....  | 67        |
| 3.2.2 Preparation of Apt-AuNPs .....  | 69        |

|  |    |
|--|----|
| 3.2.3 Characterization of Apt-AuNPs .....                                | 70 |
| 3.2.4 Gel electrophoresis, protein transfer, and membrane blotting ..... | 73 |
| 3.2.5 Protein detection using competitive protected Apt-AuNPs .....      | 73 |
| 3.2.6 Signal amplification using layer-by-layer assembly of Apt-AuNPs.   | 74 |
| 3.2.7 Signal amplification using targeted growth of Apt-AuNPs .....      | 74 |
| 3.3 Results and discussion .....   | 75 |
| 3.3.1 Competitive protection strategy for Aptamer-AuNPs .....            | 75 |
| 3.3.2 Design and characterization of the protection oligonucleotide..... | 78 |
| 3.3.3 Layer-by-layer assembly of Apt-AuNPs for signal amplification .... | 84 |
| 3.3.4 Targeted growth of Apt-AuNPs for signal amplification .....        | 86 |
| 3.4 Conclusions .....  | 90 |
| 3.5 References .....   | 91 |

**Chapter Four: Dynamic DNA Assemblies Mediated by Binding-Induced DNA Strand-Displacement Reactions .....** **93**

|  |    |
|--|----|
| 4.1 Introduction .....   | 93 |
| 4.2 Experimental .....   | 96 |
| 4.2.1 Materials and reagents .....   | 96 |
| 4.2.2 Probe preparation for binding-induced DNA strand displacement...                       | 98 |
| 4.2.3 Monitoring the binding-induced DNA strand displacement using gel electrophoresis ..... | 98 |

|  |     |
|--|-----|
| 4.2.4 Binding-induced DNA strand-displacement beacon.....  | 99  |
| 4.2.5 Binding-induced catalytic DNA circuit .....  | 100 |
| 4.3 Results and discussion .....   | 101 |
| 4.3.1 Binding-induced DNA strand displacement for streptavidin.....                                    | 101 |
| 4.3.2 Binding-induced strand-displacement beacon .....   | 104 |
| 4.3.3 Estimating the conversion efficiency of the binding-induced strand-<br>displacement beacon ..... | 108 |
| 4.3.4 Minimizing the target-independent displacement by tuning the length<br>of DNA probes .....       | 112 |
| 4.3.5 Binding-induced catalytic DNA circuit .....  | 116 |
| 4.4 Conclusions.....   | 119 |
| 4.5 References.....  | 120 |

**Chapter Five: Binding-Induced Molecular Translator for Homogeneous Protein Assays ..... 122**

|  |     |
|--|-----|
| 5.1 Introduction.....  | 122 |
| 5.2 Experimental .....   | 123 |
| 5.2.1 Materials and reagents .....   | 123 |
| 5.2.2 Construction of binding-induced molecular translator .....                               | 126 |
| 5.2.3 Monitoring binding-induced molecular translator by a fluorescence<br>turn-on assay ..... | 127 |

|  |            |
|--|------------|
| 5.2.4 Detection of PDGF-BB using binding-induced molecular translator .....  | 128        |
| 5.2.5 Estimation of melting temperatures for designing binding-induced molecular translator .....  | 128        |
| 5.3 Results and discussion .....   | 129        |
| 5.3.1 Experimental Design.....   | 129        |
| 5.3.2 Binding-induced molecular translator for streptavidin .....  | 132        |
| 5.3.3 Effect of competing oligo length on binding-induced molecular translator .....   | 135        |
| 5.3.4 Effect of blocking oligo on binding-induced molecular translator .   | 137        |
| 5.3.5 Temperature effect on binding-induced molecular translator.....  | 140        |
| 5.3.6 Binding-induced molecular translator for PDGF-BB .....   | 141        |
| 5.4 Conclusions.....   | 146        |
| 5.5 References.....  | 147        |
| <b>Chapter Six: Conclusions and Future Work.....</b>   | <b>149</b> |
| <b>Appendix A: List of Publications from the PhD Program .....</b>   | <b>154</b> |
| <b>Appendix B: Detection of <i>Escherichia coli</i> O157:H7 Using Gold Nanoparticle Labeling and Inductively Coupled Plasma Mass Spectrometry.....</b> | <b>157</b> |

## List of Tables

|            |   |     |
|------------|---|-----|
| Table 2-1. | DNA sequences and modifications.....  | 42  |
| Table 2-2. | Summary of three DNA-AuNP probes.....   | 50  |
| Table 2-3. | Effects of packing density on thermal dissociation kinetics of DNA-AuNPs.....             | 55  |
| Table 3-1. | DNA sequences and calculated melting temperature.....                                     | 70  |
| Table 4-1. | DNA sequences and modifications.....  | 99  |
| Table 5-1. | DNA sequences for constructing binding-induced molecular translator for streptavidin..... | 126 |
| Table 5-2. | DNA sequences for constructing binding-induced molecular translator for PDGF-BB.....      | 127 |

## List of Figures

|              |   |    |
|--------------|---|----|
| Figure 1-1.  | Aggregation of DNA functionalized gold nanoparticles in the presence of complementary target oligonucleotide..... | 4  |
| Figure 1-2.  | Schematic representation of scanometric DNA assay on a glass chip.....  | 5  |
| Figure 1-3.  | Fluorescent biosensors making use of DNA-AuNPs.....   | 7  |
| Figure 1-4.  | Schematic representation of nano-flares for multiple mRNA detection.....  | 8  |
| Figure 1-5.  | Assays using toehold-mediated strand-displacement reactions.  | 12 |
| Figure 1-6.  | Assays using hybridization chain reactions.....   | 15 |
| Figure 1-7.  | Assays using catalytic DNA circuit.....   | 19 |
| Figure 1-8.  | Binding-induced DNA annealing assays.....   | 23 |
| Figure 1-9.  | Proximity ligation assays.....  | 26 |
| Figure 1-10. | Binding-induced DNA Assembly.....   | 29 |
| Figure 2-1.  | DNA-AuNP probes constructed by conjugating oligonucleotides having different organosulfur anchor groups .....     | 41 |
| Figure 2-2.  | UV/Vis extinction spectra of bare AuNPs and DNA-AuNPs....   | 45 |
| Figure 2-3.  | Thermal dissociation of FAM-labelled DNA from <b>SP-1</b> .....   | 48 |
| Figure 2-4.  | Fraction of FAM-labeled DNA released from the three DNA-AuNP probes .....   | 50 |
| Figure 2-5.  | Dissociation of FAM-labeled DNA from the DNA-AuNPs when the DNA-AuNPs were treated with 50 $\mu$ M MCH.....       | 53 |
| Figure 2-6.  | Effect of packing density on thermal dissociation of DNA-AuNPs.....   | 55 |
| Figure 2-7.  | Designs of double-stranded DNA-AuNP probes to enhance the stability of the sicDNA.....                            | 59 |

|              |   |     |
|--------------|---|-----|
| Figure 3-1.  | Schematic illustrating the principle of competitive protection...   | 66  |
| Figure 3-2.  | Transmission electron microscopy (TEM) images of the modified and unmodified gold nanoparticles.....  | 71  |
| Figure 3-3.  | UV/Vis absorption spectra of AuNPs and Apt-AuNPs before and after incubating with protection oligos.....  | 72  |
| Figure 3-4.  | Schematic showing the application of competitive protected Apt-AuNPs to protein analysis on western blot membrane.....                            | 76  |
| Figure 3-5.  | Western blot analysis of human $\alpha$ -thrombin in 10-time diluted human serum.....   | 77  |
| Figure 3-6.  | Membrane images from the western blot analysis of human $\alpha$ -thrombin and human prothrombin.....   | 80  |
| Figure 3-7.  | Membrane images from the western blot analysis of human $\alpha$ -thrombin in 10-time diluted human serum.....                                    | 81  |
| Figure 3-8.  | Membrane images from the western blot analysis of human $\alpha$ -thrombin in 10-time diluted human serum.....                                    | 83  |
| Figure 3-9.  | Schematic showing the layer-by-layer assembly of Apt-AuNPs for signal amplification.....  | 85  |
| Figure 3-10. | Signal enhancement strategies for detecting human $\alpha$ -thrombin on the western blot membrane with Apt-AuNPs.....                             | 87  |
| Figure 3-11. | Targeted growth strategy for detecting human $\alpha$ -thrombin in 10-time diluted human serum.....   | 89  |
| Figure 4-1.  | Schematic illustrating the principle of the binding-induced DNA strand displacement.....  | 95  |
| Figure 4-2.  | Schemactic illustrating that the binding of streptavidin to biotinylated DNA results in binding-induced DNA assembly and strand displacement..... | 102 |
| Figure 4-3.  | Native PAGE analysis of the binding-induced DNA strand displacement that release the output DNA <b>O</b> .....                                    | 103 |
| Figure 4-4.  | Native PAGE analysis of the binding-induced DNA strand displacement that release the output DNA <b>L</b> .....                                    | 103 |

|              |   |     |
|--------------|---|-----|
| Figure 4-5.  | (A) Schematic illustrating the principle of the binding-induced strand-displacement beacon; (B) Evaluation of the binding-induced strand-displacement beacon..... | 106 |
| Figure 4-6.  | Characterization of the toehold-mediated strand-displacement beacon.....  | 107 |
| Figure 4-7.  | Schematic showing the model for calculating theoretical concentrations of the released output DNA <b>O</b> .....  | 109 |
| Figure 4-8.  | Optimization of the ratio between <b>T</b> and <b>O</b> .....   | 110 |
| Figure 4-9.  | Estimation of the conversion efficiency from the target streptavidin to the output DNA at different streptavidin concentrations.....                              | 111 |
| Figure 4-10. | Optimization of the binding-induced DNA strand-displacement strategy to minimize the target-independent strand displacement.....                                  | 114 |
| Figure 4-11. | Native PAGE characterization of the binding-induced strand-displacement strategy that is able to eliminate the target-independent displacement.....               | 117 |
| Figure 4-12. | (A) Schematic illustrating the principle of the binding-induced catalytic DNA circuit; (B) Evaluation of the binding-induced catalytic DNA circuit.....           | 120 |
| Figure 5-1.  | Schematic illustrating the principle of the binding-induced molecular translator.....   | 131 |
| Figure 5-2.  | Schematic showing that the binding of streptavidin to biotinylated DNA results in a stable binding-induced DNA assembly.....                                      | 133 |
| Figure 5-3.  | Evaluation of the binding-induced molecular translator for streptavidin using a fluorescent turn-on assay.....  | 134 |
| Figure 5-4.  | (A) Three designs of competing DNA-2, showing competing sequences of 7, 8, and 9 n.t.....   | 136 |

|              |   |     |
|--------------|---|-----|
| Figure 5-5.  | Schematic illustrating the effect of blocking oligo on the binding-induced molecular translator for streptavidin.....                   | 138 |
| Figure 5-6.  | (A) Three designs of blocking oligo, showing blocking sequences of 10, 11, and 12 n.t.....  | 139 |
| Figure 5-7.  | Effect of temperature on the performance of binding-induced molecular translator.....   | 140 |
| Figure 5-8.  | (A-C) Schematic illustrations of three design strategies to construct molecular translators for PDGF-BB.....                            | 143 |
| Figure 5-9.  | Effect of DNA-1/DNA-3 duplex density on the performance of the binding-induced molecular translator Design-1 for PDGF-BB detection..... | 144 |
| Figure 5-10. | Results of specificity test.....  | 145 |

## List of Abbreviations

|           |   |
|-----------|---|
| Apt-AuNPs | aptamer-functionalized gold nanoparticles |
| AuNPs     | gold nanoparticles                        |
| BINDA     | binding-induced DNA Assembly              |
| BSA       | bovine serum albumin                      |
| DNA       | deoxyribonucleic acid                     |
| DNA-AuNPs | DNA functionalized gold nanoparticles     |
| DTPA      | dithiol phosphoramidite                   |
| DTT       | dithiothreitol                            |
| EDTA      | ethylene diamine tetraacetic acid         |
| FAM       | fluorescein amidite                       |
| FRET      | fluorescence resonance energy transfer    |
| HSA       | human serum albumin                       |
| IgG       | immunoglobulin G                          |
| MCH       | 6-mercapto-1-hexanol                      |
| ME        | $\beta$ -mercaptoethanol                  |
| miRNA     | microRNA                                  |
| mRNA      | messenger RNA                             |
| MW        | molecular weight                          |
| n.t.      | nucleotide                                |
| PAGE      | Polyacrylamide gel electrophoresis        |

|        |   |
|--------|---|
| PBS    | phosphate buffered saline                                     |
| PCR    | polymerase chain reaction                                     |
| PLA    | proximity ligation assay                                      |
| PDGF   | platelet derived growth factor                                |
| RCA    | rolling circle amplification                                  |
| RNA    | Ribonucleic acid  |
| SELEX  | systematic evolution of ligands by<br>exponential enrichment  |
| TCEP   | Tris(2-carboxyethyl)phosphine                                 |
| TE     | Tris-EDTA buffer  |
| TE-Mg  | Tris-EDTA buffer supplemented with 10 mM<br>MgCl <sub>2</sub> |
| TEM    | transmission electron microscopy                              |
| UV-Vis | ultraviolet-visible   |

# Chapter One: Introduction<sup>1</sup>

## 1.1 DNA nanotechnology

DNA nanotechnology deals with the design and manufacture of artificial nucleic acid structures as non-biological engineering materials for technological uses,<sup>1</sup> and can be broadly divided into structural DNA nanotechnology and dynamic DNA nanotechnology.<sup>2</sup> Structural DNA nanotechnology (also well known as DNA origami) has achieved static DNA structures,<sup>1,3-6</sup> e.g. 2-dimensional and 3-dimensional crystal lattices, nanotubes, arbitrary shapes, as well as assembled networks of other nanomaterials through DNA hybridization,<sup>7-9</sup> e.g. gold nanoparticles, quantum dots, and carbon nanotubes. In contrast, dynamic DNA nanotechnology is exemplified by switchable DNA nanostructures or nanodevices such as autonomous DNA machines and DNA computers.<sup>2,10-14</sup> In recent years, both structural and dynamic DNA nanotechnologies have been realized as unique tools for generation or amplification of detection signals for bio-analysis and thus have greatly promoted the field of molecular diagnostics and imaging.<sup>15-18</sup>

In this chapter, I will review recent advances of dynamic DNA nanotechnology for sensitive detection of biomolecules, including nucleic acids, proteins, and small biomolecules, with an emphasis on DNA-functionalized gold nanoparticles, dynamic DNA assemblies, and binding-induced DNA assemblies. These DNA assembly-based techniques form a basis of discussion for the main

---

<sup>1</sup>A portion of this chapter has been published in Zhang, H.; Li, F.; Dever, B.; Li, X.-F.; Le, X. C. *Chem. Rev.* Published online December 11, 2012. DOI: 10.1021/cr300340p.

subject of this thesis: harnessing the dynamic DNA nanotechnology to construct facile protein diagnostic tools for potential point-of-care applications.

## **1.2 DNA functionalized gold nanoparticles for bio-analysis**

Gold nanoparticles (AuNPs) possess many distinct physical properties, including localized surface plasmon resonance (LSPR), high fluorescent quenching efficiency, and electronic properties, making them attractive tools as biosensors for nucleic acids, proteins, and small molecules.<sup>19,20</sup> The combination of dynamic DNA nanotechnology with AuNPs yields DNA-functionalized gold nanoparticles (DNA-AuNPs) possessing further advantages for biosensing due to the programmability through exquisite Watson-Crick base pairing.<sup>19-21</sup>

Biosensors that make use of DNA-AuNPs can easily be made to recognize and respond to target nucleic acids using complementary DNA probes. Proteins and small molecules can also be recognized by DNA-AuNPs when functional nucleic acids, e.g. aptamers are conjugated onto AuNPs. Aptamers are short, synthetic single-stranded oligonucleotides (DNA or RNA) selected from random sequence libraries, using the systematic evolution of ligands by exponential enrichment (SELEX) techniques.<sup>22-27</sup> They can bind to a wide range of target molecules, including proteins, peptides, small molecules, and whole cells with high affinity and specificity.<sup>28</sup> Aptamers that have sufficient binding affinity and specificity are usually present in their favored secondary structures when bound to the target. The conformational change in aptamers' secondary structure upon their binding to the target is very useful to construct homogeneous biosensors when aptamers are conjugated on AuNPs.<sup>28-30</sup>

### 1.2.1 Colorimetric biosensors using DNA-AuNPs

The aggregation of AuNPs induces interparticle surface plasmon coupling, resulting in a visible color change from red to blue.<sup>20</sup> This unique optical property of AuNP provides a practical platform for developing colorimetric biosensors.<sup>19-21</sup> The first DNA-AuNP based colorimetric biosensor was designed by Mirkin and co-workers for facile detection of oligonucleotide.<sup>31</sup> In their seminal work, two DNA-AuNP probes were used for recognizing the target oligonucleotide (Figure 1-1). The DNA sequences on AuNP probes were designed in a way that they were complementary to both ends of the target oligonucleotides. Thus, DNA-AuNP probes were cross-linked to form aggregation and a concomitant red-to-blue color change happened in the presence of the target oligonucleotide (Figure 1-1). In addition to the color change, sharp DNA melting transitions were also observed when using DNA-AuNP as detection probes, enabling high degree discrimination of single nucleotide polymorphisms (SNPs). Upon the discovery of these unique properties of DNA-AuNPs, great efforts have been made to further improve the colorimetric sensors based on AuNPs for homogeneous detection of nucleic acids.<sup>21</sup>

The colorimetric detection strategy through assembly or disassembly of DNA-AuNP probes can also be applied to detection of proteins and small molecules by using aptamer functionalized AuNPs (Apt-AuNPs). For example, Tan and co-workers demonstrated a colorimetric detection method for platelet derived growth factor (PDGF) using PDGF aptamer derived AuNPs by assembling Apt-AuNPs through PDGF bindings.<sup>32</sup> Liu and Lu developed fast

colorimetric sensors for adenosine and cocaine by disassembling Apt-AuNPs upon target bindings.<sup>33</sup>

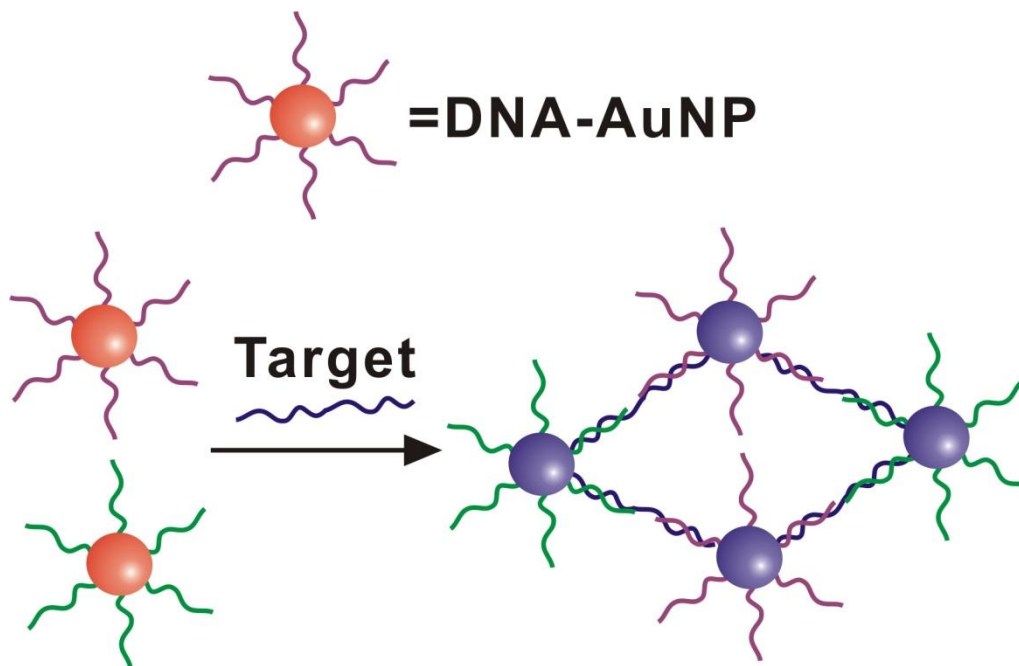


**Figure 1-1.** Aggregation of DNA functionalized gold nanoparticles (DNA-AuNPs) in the presence of complementary target oligonucleotide.

DNA-AuNPs have also been used to construct facile colorimetric biosensors on different solid supports.<sup>34-37</sup> For example, scanometric DNA array was developed for ultrasensitive colorimetric detection of nuclei acids on glass chips (Figure 1-2).<sup>34</sup> The scanometric DNA array consisted of a capture DNA immobilized on a glass chip that was able to recognize the target oligonucleotide. A second DNA probe, which could also recognize the same target oligonucleotide but at a separate sequence, was conjugated to AuNP. In the presence of the target, the DNA-AuNP probe was captured onto glass chip through the binding complex

among two DNA probes and the target. After removing the nonspecifically bound target strands by a thermal stringency wash, catalytic reduction of silver onto the AuNP surfaces was applied to amplify the target signal. As a result, target oligonucleotides could be visualized with a flatbed scanner with a detection limit of 50 fM. Besides detection of nucleic acids, this strategy has also been used to detect membrane blotted human  $\alpha$ -thrombin by adopting thrombin aptamer functionalized AuNPs.<sup>35,36</sup> Lu and co-workers applied Apt-AuNPs to the lateral flow dipstick, enabling the colorimetric detection of adenosine and cocaine.<sup>37</sup>

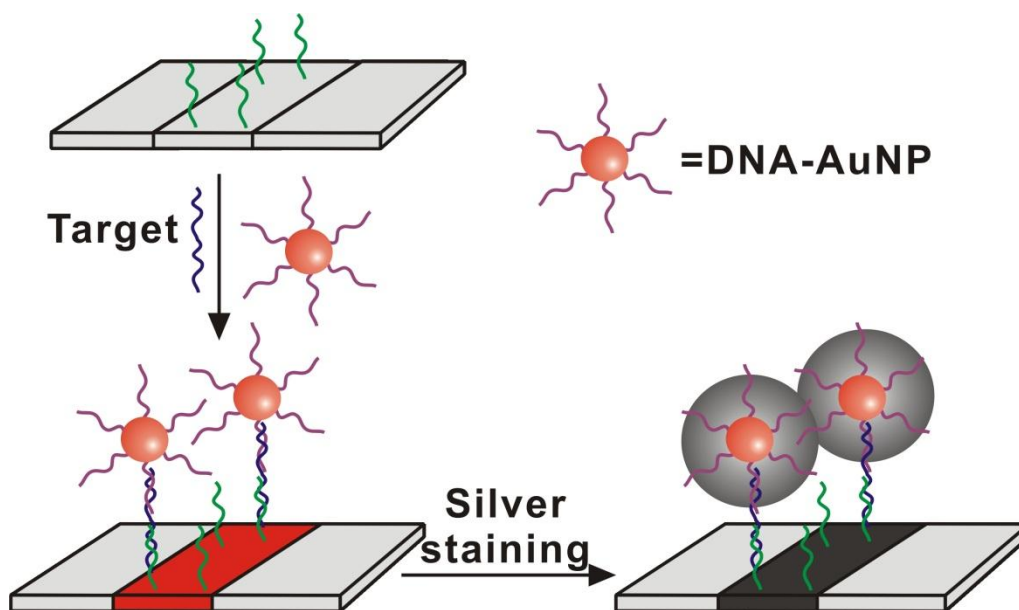


**Figure 1-2.** Schematic representation of scanometric DNA assay on a glass chip.

### 1.2.2 Fluorescent biosensors using DNA-AuNPs

DNA-AuNPs are superior tools for constructing fluorescent biosensors for nucleic acids and small molecules. Different interaction mechanisms form a variety of fluorescent biosensors that could potentially be used for point-of-care

diagnostics. Depending on the conjugation methods and interaction mechanisms, we categorize recent fluorescent biosensors making use of DNA-AuNPs into three types and summarize them in the following part (Figure 1-3). In the first type of sensors, AuNPs are mainly served as quenchers and scaffolds to support the functional DNA probes (Figure 1-3A). Detection signals are generated through the conformational changes of functional DNA probes, including molecular beacons and aptamers. Molecular beacon, developed by Tyagi and Kramer in 1996, is a simple but effective way to detect nucleic acids in homogeneous solutions.<sup>38</sup> Replacing organic quenchers with gold nanoparticles was demonstrated to be more efficient and thus enhanced the sensitivity up to 100-fold.<sup>39</sup> Furthermore, using gold nanoparticle as scaffold was able to create more stringent environment for nucleic acid detection which increased the ability to differentiate single mismatch to 8-fold.<sup>39</sup> Another advantage of using AuNP as detection scaffold is that multiple targets detection can be achieved on a single particle when multiple fluorescent dyes are used. Song, *et al* used 15 nm AuNP to conjugate with three different DNA hairpin probes, each of which linked with a different fluorescent dye.<sup>40</sup> Three different target nucleic acids were able to be detected at the same time with high sensitivity and specificity. They further designed a multicolour detection method for three different small molecules with the same principle but using aptamers instead of DNA hairpins.<sup>41</sup> Designing of the second type of detection probes relied on both conjugation and DNA interaction with AuNPs (Figure 1-3B). For example, Nie's group has developed a hybrid probe composed of a 2.5 nm gold nanoparticle and an ssDNA with one end

conjugated to AuNPs through thiol group and the other end adsorbed on AuNPs with a fluorescent dye molecule.<sup>42</sup> Upon the presence of the target nucleic acid, ssDNA hybridized with target which released fluorescent dye molecule from AuNPs and turned on the fluorescent signal. This type of probe is able to detect nucleic acids similar to molecular beacons but with no requirement on the hairpin structure which simplifies the designing process. In the third type of sensors, DNA-AuNPs are used to construct fluorescent sensors through assembling or disassembling with other DNA functionalized materials, e.g. quantum dots (Figure 1-3C).<sup>43</sup>

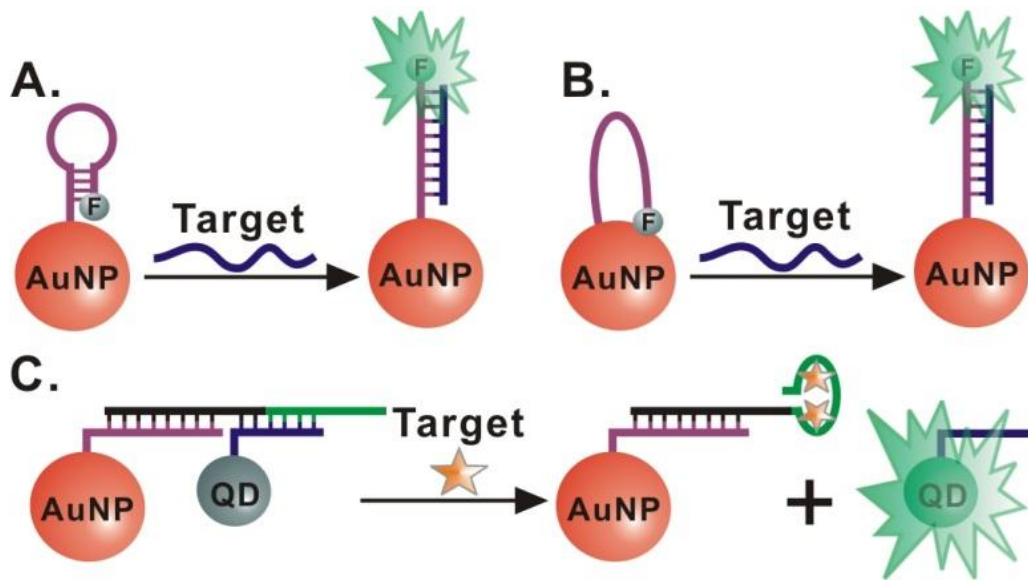


**Figure 1-3.** Fluorescent biosensors making use of DNA-AuNPs.

Fluorescent biosensors making use of DNA-AuNPs can also be designed to monitor concentration levels of mRNA and small molecules in living cells. For example, Mirkin and co-workers have developed DNA-AuNPs (nano-flares) to

visualize and quantify RNA in living cells.<sup>44,45</sup> Fluorescently labeled DNA reporter probes were initially hybridized to DNA-AuNPs, and the fluorescence of these reporter probes was quenched by AuNPs. The presence of target RNA then displaced and released the reporter probes from AuNPs, and fluorescence signal was turned on (Figure 1-4).<sup>44</sup> By attaching two different types of fluorescent reporter probes on a single AuNP, the authors designed a multiplexed nanoflare capable of detecting two distinct mRNA targets simultaneously inside a living cell (Figure 1-4).<sup>45</sup> When adenosine aptamer was used as functional DNA on AuNPs, nano-flares were able to be turned on upon the presence of adenosine in living cells.<sup>46</sup> Besides sensing ability, nano-flares have also displayed many distinct features, including direct cellular uptake without the need of transfection agents,<sup>47</sup> ability to regulate cell function,<sup>47,48</sup> enhanced enzymatic stability of DNA probes,<sup>49</sup> and favored strand-displacement kinetics on AuNP,<sup>50</sup> making them extremely powerful tools to control and monitor biological functions in living cells.

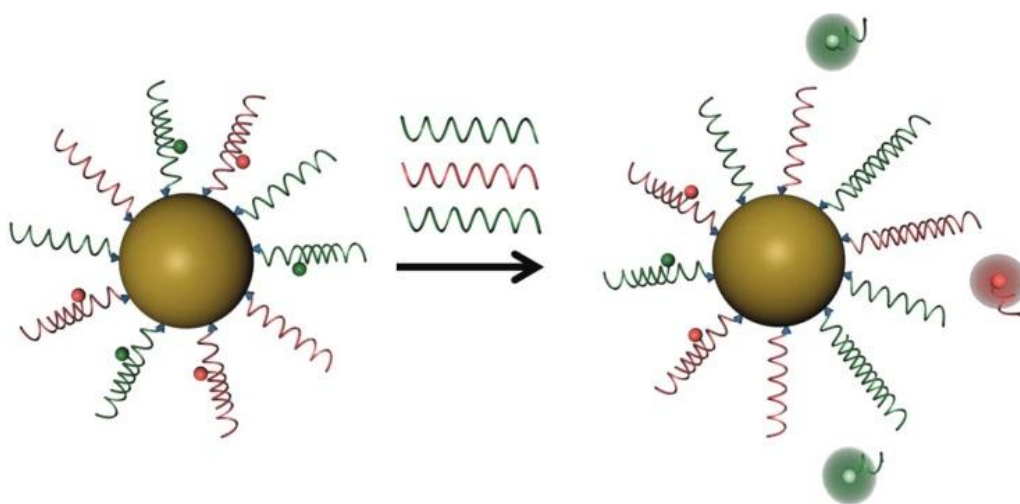


**Figure 1-4.** Schematic representation of nano-flares for multiple mRNA detection.

### **1.3 Dynamic DNA assembly for bioanalysis**

In this part, I will summarize the applications of dynamic DNA assembly as promising signal generation and amplification tools in bioanalysis. Important features include high sensitivity, high specificity, isothermal amplification, no requirement for protein enzymes, and no requirement for any separation steps.

#### **1.3.1 Assays based on toehold-mediated DNA strand-displacement reactions**

As one of the most powerful strategies to construct and control dynamic DNA nanostructures and nanodevices, DNA strand displacement reaction is the process through which two strands with partial or full complementarity hybridize to each other, displacing one or more pre-hybridized strands in the process.<sup>2</sup> The strand displacement reaction is initiated at complementary single-stranded domains termed as DNA “toeholds” and progresses through a branch migration process. A toehold in a double-stranded DNA refers to a sticky end consisting of typically 5-8 nucleotides. By varying the length and sequence of toeholds,<sup>51</sup> the rate of the toehold-mediated strand displacement reactions can be enhanced by a factor of  $10^6$ . Toehold-mediated strand displacement reactions have been successfully applied to homogeneous assays for nucleic acids.

Li and co-workers demonstrated the use of the toehold-mediated strand displacement beacons for nucleic acid detections.<sup>52</sup> As shown in Figure 1-5A, two complementary DNA strands were labeled with a quencher and a fluorophore respectively. One of the strands had a few nucleotides longer than the other, leaving a toehold part for target binding. In the absence of target nucleic acid, a stable DNA duplex was formed and the fluorescence signal was quenched. Upon

target binding, the toehold-mediated strand displacement reaction resulted in the release of the shorter DNA strand and turned on fluorescence. This strand displacement beacon showed two distinct advantages over the commonly used molecular beacons. One was the sharper transition observed in the melting curve of the strand displacement beacon than observed in a variety of molecular beacons. The other advantage was a wider detection window between the perfectly matched and single mismatch targets. These observations suggest the potential use of strand displacement beacons to detect SNPs with higher sensitivity and specificity.

Indeed, by establishing a theoretical framework for the analysis of nucleic acid hybridization specificity, Yin and co-workers have designed toehold exchange probes that were able to achieve high hybridization specificity across a wide range of temperatures, salinities, and oligonucleotide concentrations (Figure 1-5B).<sup>53</sup> Two toeholds were designed on the same strand displacement beacon probe at 3' and 5' (Figure 1-5B). The hybridization of the probe to the correct target was initiated at the 3' toehold region and completed via the spontaneous dissociation of the 5' toehold region to release the ssDNA that was labeled with the quencher. The two toeholds allowed both forward and reverse reactions to proceed with fast kinetics, and the standard free energy of the forward reaction was close to zero. This process mimicked hybridization behaviour of the probe at close to its melting temperature, which was commonly used as optimal condition to discriminate fully matched target DNA from the single-base mismatched DNA. Using the toehold exchange probes to test five different DNA targets against 55

single-base mismatched spurious analogues, the authors achieved discrimination factors between three and over 100 (median, 26) under a wide range of conditions.<sup>53</sup>

Multiple toehold-mediated strand-displacement reactions can be programmed to generate signals for detection of nucleic acids.<sup>54,55</sup> For example, Ghadiri and co-workers have developed universal translators that were able to convert any target nucleic acid input into a unique output molecule by combining multiple strand-displacement reactions (Figure 1-5C).<sup>54</sup> In the presence of target nucleic acid, an intermediate DNA was released through a toehold-mediated strand-displacement reaction. The intermediate DNA triggered a secondary strand displacement reaction to release a universal output DNA, which was then detected by a strand displacement beacon. Through this translator, several biologically relevant input DNA sequences were successfully translated into a unique output DNA in 5 min at room temperature without any separation steps.

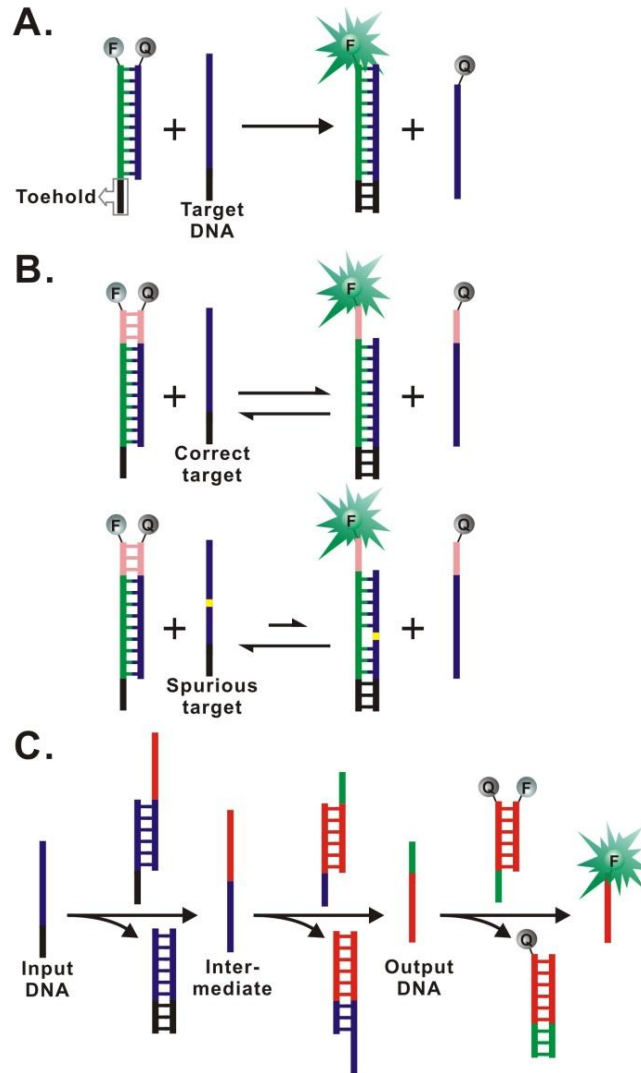


**Figure 1-5.** Assays using toehold-mediated strand-displacement reactions. (A) Strand-displacement beacon for nucleic acid detection; (B) Toehold exchange reactions for detection of specific single nucleotide polymorphism (SNP); (C) Universal molecular translators for nucleic acid analyses using multiple strand-displacement reactions.

### 1.3.2 Assays based on hybridization chain reactions

Dynamic DNA assembly can be programmed through cascade of strand-displacement reactions to amplify the detection signal for target molecules. One of the most widely used strategies is known as hybridization chain reaction (HCR).<sup>56-60</sup> In HCR, DNA molecules can be assembled into nicked dsDNA structures similar to alternating copolymers from a cascade of hybridization events triggered by a single target nucleic acid molecule. The detection signal can be amplified by monitoring the long double stranded DNA with hundreds of repeated units.<sup>56-60</sup> Pierce and Dirks introduced the concept of HCR in 2004, and then explored its potentials as label-free biosensors and as amplification probes for multiplexed imaging of mRNA expression.<sup>56,57</sup> Soon after the discovery of HCR, many efforts have been made to apply it as signal amplification strategies for homogeneous binding assays.<sup>58-60</sup>

For a typical HCR (Figure 1-6A), two DNA hairpins H1 and H2 are used. H1 and H2 are stable in the absence of the target DNA. But in the presence of the target DNA, a toehold-mediated strand displacement is initiated at the sticky end of H1, opening its hairpin. The newly exposed end of H1 nucleates at the sticky end of H2 and opens the hairpin to expose the end of H2 which is identical in sequence to the target. Hence, each copy of the target DNA can propagate a chain reaction of hybridization events between alternating H1 and H2 hairpins to form a nicked double-helix, amplifying the signal of the target DNA. To monitor the HCR product, Pierce and Dirks developed a fluorescence quenching assay using the adenine analog, 2-aminopurine (2AP). 2AP fluoresced when incorporated in

the single-stranded form, but was significantly quenched when in a stacked double-helical conformation.<sup>56</sup>

To develop a fluorescence turn-on assay for nucleic acids using HCR, Tan and co-workers designed pyrene-excimer based HCR probes.<sup>58</sup> As shown in Figure 1-6B, the DNA hairpins for HCR were dual-labeled at both ends with pyrene moieties. In the absence of target DNA, the two pyrene moieties on each hairpin were spatially separated by the extra length of the sticky end, and only emitted at a low wavelength range (375 and 398 nm). In the presence of target DNA, the HCR process was triggered. A pyrene moiety on one probe was brought into close proximity to a pyrene moiety on the neighboring probe, forming pyrene excimers which turned on the fluorescent signal at 485 nm. Numerous pyrene excimers were formed by HCR and the target DNA was detected at the sub pM range.

Willner and co-workers further improved the HCR signal amplification for homogeneous binding assays by incorporating DNazymes into the HCR product.<sup>59,60</sup> For example, an  $Mg^{2+}$ -dependant DNzyme was split into two subunits, each of which was imbedded in a DNA hairpin for HCR (Figure 1-6C).<sup>59</sup> In the presence of target DNA, HCR was triggered and two DNzyme subunits were brought into close proximity to form a complete DNzyme. The DNzyme catalyzed the cleavage of the fluorophore/quencher-modified substrates, turning on fluorescence. A detection limit of 10 fM was achieved for DNA detection. A colorimetric detection method was also developed by the same

group for DNA analyses when a HRP-mimicking DNAzyme was incorporated in HCR.<sup>60</sup>

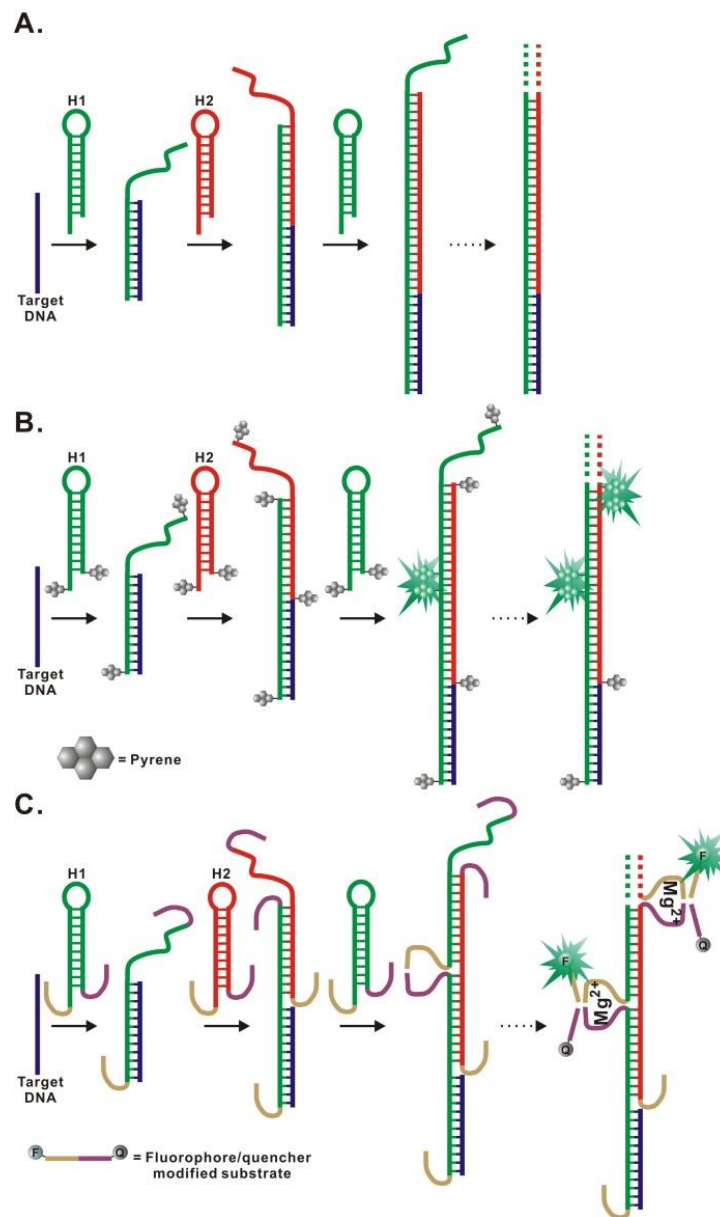


**Figure 1-6.** Assays using hybridization chain reactions (HCR). (A) A typical process of HCR using two hairpin probes (H1 and H2). (B) HCR using pyrene excimer as a fluorescence turn-on probes. (C) HCR using DNAzyme as signal amplification probes.

### 1.3.3 Assays based on catalytic DNA circuits and DNA machines

The recent advances in the field of dynamic DNA nanotechnology have also yielded enzyme-free DNA catalytic circuits that can be adapted to amplify signals for detecting biomolecules.<sup>13-16,61-64</sup> Winfree and co-workers designed entropy-driven DNA circuit that has potential to be used as signal amplification tool for homogeneous nucleic acid detection.<sup>61-63</sup> As shown in Figure 1-7A, the target DNA was used to catalyze the reaction between the fuel strand (F) and the substrate (S). The target DNA was first used to displace a side product DNA (SP) through a toehold-mediated strand displacement reaction. Through the second toehold on the substrate, the fuel (F) displaced both the output DNA (O) and the target DNA by forming the F-S duplex. The target DNA was used again to trigger another round of reaction, and the output DNA was detected through a displacement beacon. This target catalyzed DNA circuit was thermodynamically driven forward by the entropic gain of the liberated molecules. As low as 1 pM of target DNA could be detected after amplification.

Pierce, Yin, and co-workers described another DNA circuit based on catalyzed hairpin assembly in their seminal work on programming DNA self-assembly pathways.<sup>13</sup> Chen, Ellington, and co-workers further adapted this signal amplification strategy with a strand-displacement beacon and explored its modularity to multiple detection methods commonly used in bioanalysis.<sup>15</sup> As shown in Figure 1-7B, a pair of DNA hairpins (H1 and H2) were designed to potentially hybridize partially to each other. However, the spontaneous hybridization between H1 and H2 was kinetically hindered by caging complementary regions in the stem parts of the hairpins. In the presence of the

target DNA, the stem part of H1 was opened by the toehold-mediated strand-displacement reactions initiated from the sticky end of H1. The newly exposed sticky end of H1 nucleates at the sticky end of H2 and triggered another strand-displacement reaction, forming a H1-H2-target complex. This complex was inherently unstable, and target DNA dissociated from the H1-H2 complex, completing the reaction and allowing the target to act as a catalyst to trigger the formation of other H1-H2 complexes. By coupling to a strand-displacement beacon, detection signal was amplified linearly by 20 to 50 folds with negligible background. Using the same DNA circuit but a different read-out format, Yang and co-workers developed a colorimetric assay for homogeneous detection of nucleic acids by releasing HRP-mimicking catalytic beacon as end products.<sup>64</sup>

It is possible to engineer DNA circuit capable of amplifying the detection signal exponentially by combining multiple catalytic DNA reactions.<sup>13</sup> For example, Pierce, Yin and co-workers designed a cross-catalytic DNA circuit that have shown an exponential kinetics by using four metastable DNA hairpins (Figure 1-7C).<sup>13</sup> Using this strategy, they amplified and detected fluorescently 5 fM of target DNA.

Toehold-mediated strand displacement reactions can also be applied to construction of DNA machines for amplified detection of nucleic acids.<sup>65</sup> For example, Willner and co-workers have fabricated an autonomous ligation DNAzyme machine that combines the function of a  $Zn^{2+}$ -dependent ligation DNAzyme with DNA strand displacement reaction for enzyme-free DNA detection.<sup>65</sup> A  $Zn^{2+}$ -dependent ligation DNAzyme was modified to respond to a

target DNA by including a target recognition domain in a hairpin structure. In the absence of the target DNA, the stem part of the hairpin structure blocked the formation of the complete ligation DNAzyme. However, in the presence of the target DNA, the hybridization of the target DNA with the recognition domain opened the hairpin structure, enabling the assembly of the two substrate components to form a complete DNAzyme. As a result, two substrate components were ligated into a new DNA sequence as the product. This DNA product was designed to contain a DNA toehold capable of displacing the target DNA from the target recognition part on the hairpin structure. This toehold-mediated strand displacement reaction regenerated both the target DNA and the catalytic region on the DNAzyme. Therefore, one target DNA was able to trigger multiple rounds of ligation reactions, amplifying the detection signals. To monitor this signal amplification process, the hairpin structure was functionalized with a quencher at 3'-end, and a fluorophore at the complementary part of the internal position. Thus fluorescent signals were turned on upon the binding of target DNA or the newly generated ligated DNA to the hairpin portion of the DNAzyme. This ligation DNAzyme machine was applied to detection of Tay-Sachs genetic disorder mutant, and a detection limit of 10 pM was achieved.

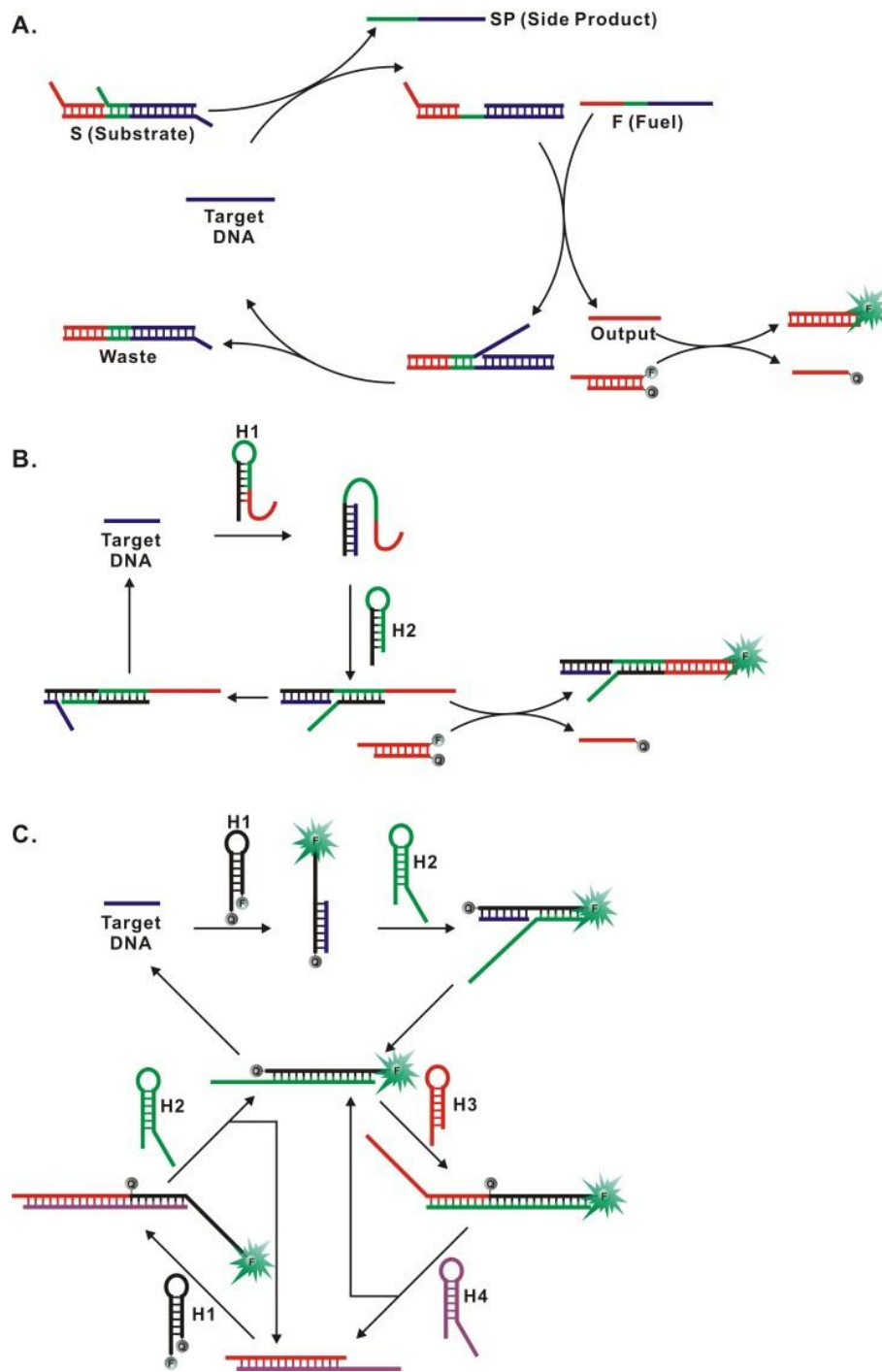


**Figure 1-7.** Assays using catalytic DNA circuit. (A) Linear amplification using entropy-driven DNA circuit; (B) Linear amplification using double hairpin DNA circuit; (C) Exponential amplification using multiple catalytic DNA circuits.

## **1.4 Binding-induced DNA assemblies for protein assays**

Recent advances in DNA assembly and affinity binding have led to exciting developments of nanosensors and ultrasensitive assays for specific proteins.<sup>66-70</sup> These sensors and assays share three main attractive features: (i) the detection of proteins can be accomplished by the detection of amplifiable DNA, thereby dramatically enhancing the sensitivity; (ii) assembly of DNA is triggered by affinity binding of two or more probes to a single target molecule, resulting in increased specificity; and (iii) the assay is conducted in solution with no need for separation, making it attractive for potential point-of-care applications. We illustrate here the principle of assembling DNA through affinity binding and highlight novel applications to the detection of proteins.

### **1.4.1 Binding-induced DNA annealing assays**

A set of simple but effective binding-induced DNA annealing assays have been developed for detecting proteins,<sup>67,68,71-76</sup> taking the advantage of the drastic increase in the local effective concentration of DNA probes upon target binding to the affinity ligands that are conjugated to the DNA probes. A pair of DNA probes is generally designed to have short complementary regions (Figure 1-8A), the  $T_m$  of which is much lower than the experimental temperature. Such a design minimizes the inter-molecular hybridization between the two DNA probes, ensuring low target-independent response. After incubation of DNA probes with target molecules, binding of two DNA probes to a same target molecule through affinity ligands greatly increases the  $T_m$  of the two DNA probes due to the increase of the local effective concentration, resulting in a stable intra-molecular

DNA duplex. Thus, the target molecule can be detected indirectly quantifying the intra-molecular DNA duplex.

Using the principle of target-induced DNA annealing, Heyduk and coworkers developed a class of optical sensors based on fluorescence resonance energy transfer (FRET) (Figure 1-8B).<sup>67,71-75</sup> They first designed a pair of DNA probes and conjugated them to a pair of affinity ligands that were able to recognize non-overlapping epitopes of the same target protein. One of the DNA probes was then labeled with a fluorescence donor (e.g. fluorescein) and the other with a fluorescence acceptor (e.g. Cy5). For efficient FRET, the fluorescence donor and acceptor had to be brought into a close proximity (~ 5 nm), which could not be achieved unless the two DNA probes anneal. Binding of the target molecules to the two probes induced DNA annealing and produced stable DNA duplexes, resulting in FRET. By adopting different types of affinity ligands, including antibodies, peptides, and aptamers, they have successfully achieved sensitive detection of various proteins, e.g. thrombin,<sup>67</sup> cardiac troponin I,<sup>72</sup> insulin,<sup>74</sup> and C-reactive protein,<sup>75</sup> with pM detection limit.

Christopher and coworkers incorporated the concept of the binding-induced DNA annealing to an electrochemical detection platform and constructed the electrochemical proximity assay (ECPA).<sup>76</sup> As shown in Figure 1-8C, one DNA probe was attached to a gold electrode through thiolated gold bond, and the other DNA probe was conjugated to methylene blue (MB). The binding of two DNA probes to the same target molecule through affinity ligands brought MB close to the gold electrode, resulting in electron transfer from MB to the gold electrode

and the consequent increase in electrical current. The increase in electrical current was proportional to the concentration of the specific target molecule. Aptamer-modified DNA probes were used to construct an ECPA sensor for thrombin detection. Antibody-modified DNA probes were used in the detection of insulin, with a detection limit of 128 fM and a dynamic range of over 4 orders of magnitude in concentration.

The intra-molecular DNA duplex formed in the binding-induced DNA annealing assay can also be amplified directly through a DNA polymerase-mediated primer extension reaction followed by polymerase chain reaction (PCR) (Figure 1-8D).<sup>68</sup> One of the two DNA probes was designed to have a long overhang sequence (shown in red in Figure 1-8D), serving as a template for the primer extension reaction. In the absence of target molecules, the complementary region of the two DNA probes was too short to form a stable DNA duplex and thus no primer extension reaction could take place. However, in the presence of the target, the binding-induced DNA annealing generated a stable intra-molecular DNA duplex, serving as a primer for the primer extension reaction. The newly formed DNA strand from the primer extension reaction (red-green-orange color in Figure 1-8D) was then amplified by PCR to enhance the detection signal. Using this strategy, Liu and coworkers were able to detect as low as 200 zmol of streptavidin. They also developed a multiplexed format that was able to identify ligand-target pairs of a wide range of affinities from protein/small molecule libraries.

The intra-molecular DNA duplex can also be amplified by rolling circle amplification (RCA). King and coworkers demonstrated the binding-induced DNA annealing and RCA for thrombin detection.<sup>77</sup> They used two DNA aptamers, one aptamer was linked to a circular DNA template, and the other aptamer was extended to have a 3' overhang that could be annealed with the circular aptamer only when both aptamers were bound to the same thrombin molecule. Upon aptamer binding to thrombin, a RCA reaction was initiated from the overhang strand, producing an elongated DNA consisting of repeat units of the template sequence. The linear amplification by RCA leads to a modest detection limit of 30 pM thrombin.

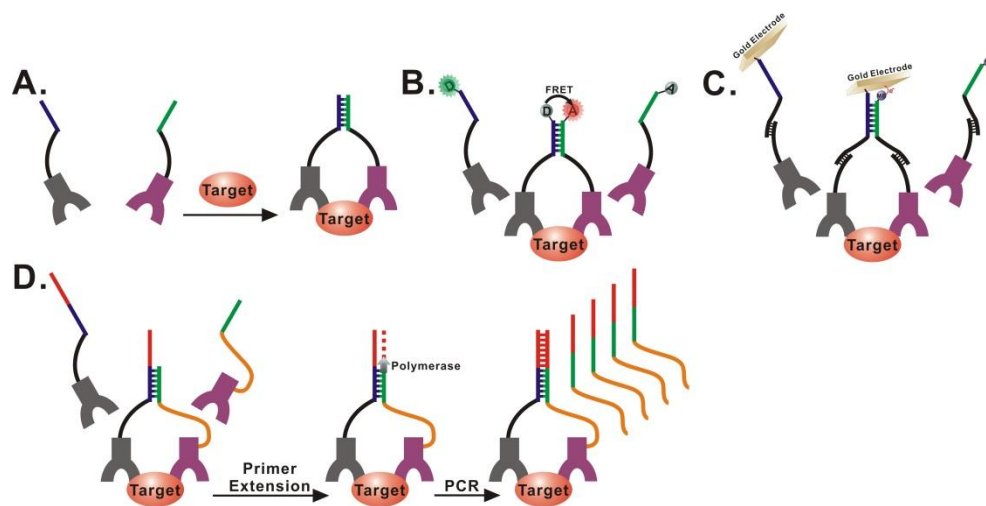


**Figure 1-8.** Binding-induced DNA annealing assays. (A) Principle of binding-induced DNA annealing; (B) Assays based on fluorescence resonance energy transfer (FRET); (C) Assays based on electrochemical detection; (D) Assays based on primer extension and PCR amplification.

### 1.4.2 Proximity ligation assays

Proximity ligation assays (PLA) make use of affinity binding to bring DNA probes to close proximity, enabling DNA ligation. The detection of a target molecule is converted to the detection of new DNA strands that are formed by ligation.<sup>66</sup> A pair of DNA probes, each conjugated to a specific affinity ligand recognizing the target, are brought into close proximity upon two binding events. Two DNA probes then hybridize with a connector oligo, facilitating the enzymatic ligation of the two DNA probes (Figure 1-9A). Various techniques can then be used to amplify and detect the ligated new DNA strand.<sup>78</sup> While the concentration of the connector oligo is usually more than 10,000 folds higher than the concentrations of the DNA in the affinity probes, hybridization of two DNA probes with the connector oligo only takes place when both affinity probes bind to the same target molecule, where the local concentrations of both DNA probes are greatly increased. Background signal is from the target-independent hybridization of two DNA probes with the connector. Therefore, the length of the connector oligo is crucial for the signal-to-background ratio. Landegren and co-workers first used this strategy in combination with real-time PCR to detect the homo dimers of platelet derived growth factor (PDGF-BB).<sup>66</sup> Aptamers for PDGF-BB served as the affinity ligands and were extended to constitute the DNA probes. They successfully achieved a detection limit of 24,000 molecules of PDGF-BB in a 5  $\mu$ l sample.

Landegren et al devised a variant of this assay by adding a third affinity probe bearing the connector oligo.<sup>79</sup> This variant was named 3PLA because it used three affinity probes, as compared to the original assay (named 2PLA thereafter) that

used two affinity probes. In the 3PLA format, three monoclonal antibodies recognizing distinct epitopes of a target molecule were covalently conjugated to three oligos forming three antibody-oligo probes. Binding of the three affinity probes to the same target molecule was followed by two ligation events, producing a new strand of DNA that was amplified and detected (Figure 1-9B). The requirement of a target molecule binding to three affinity probes enhanced the specificity and reduced background, thus improving the detection by ~100 folds. Using 3PLA, they achieved a detection limit of 60 molecules of vascular endothelial growth factor (VEGF) in 5  $\mu$ l buffer. Tavoosidana et al developed a 4PLA assay to detect prostasome,<sup>80</sup> a microvesicle with a mean diameter of 150 nm, which is secreted by prostate cells. This 4PLA required the use of four antibodies to bind to four different proteins on prostasome surface. Each antibody was conjugated to an oligonucleotide. Binding of the four probes to the prostasome vesicle was followed by two ligation events, generating a new amplifiable DNA strand for detection.

PLA has been combined with rolling circle amplification (RCA) (Figure 1-9C).<sup>81</sup> Two affinity probes were incubated with fixed cells or tissue, and two binding events triggered the ligation between the circularizable probe and the connector oligo, forming a circular DNA product after ligation. The circular DNA served as the template for RCA to produce hundreds of repeating units that subsequently hybridized with fluorescence probes, generating in situ signal for direct observation under a microscope. Jarvius et al used this in situ PLA to detect

phosphorylated PDGF receptor  $\beta$  in the cells,<sup>82</sup> and Leuchowius et al reported the screening of inhibitors for PDGF receptor  $\beta$ .<sup>83</sup>

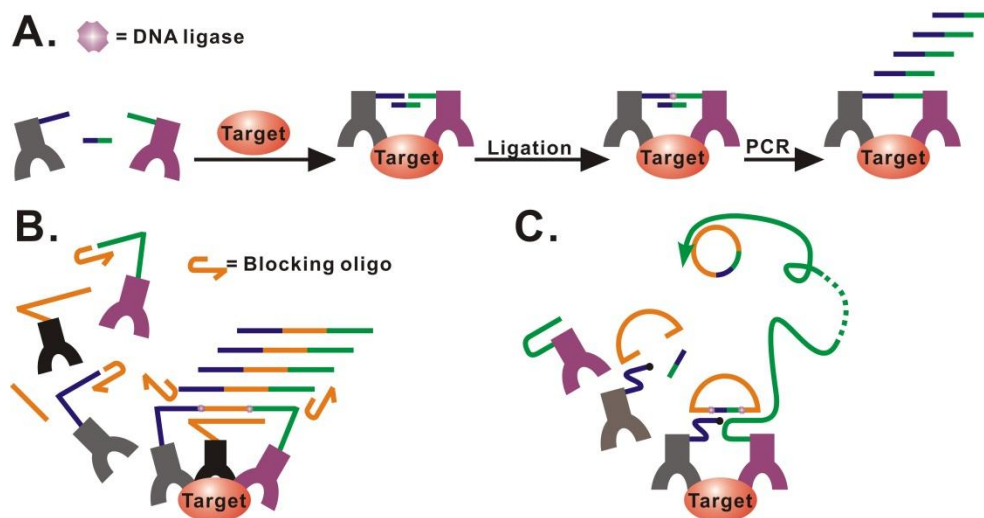


**Figure 1-9.** Proximity ligation assays (PLA). (A) 2-PLA; (B) 3-PLA; (D) In situ PLA.

### 1.4.3 Assays based on binding-induced DNA assembly

Our group has developed binding-induced DNA assembly (BINDA), enabling ultrasensitive assays and functional nanostructures. The directed assembly of DNA motifs and DNA-modified nanomaterials was triggered by binding to the target molecule. Without the target, no assembly took place, leading to very clean background.

We first used a protein molecule to assemble two DNA motifs that were conjugated to aptamers or antibodies, recognizing the target protein.<sup>69</sup> The DNA motifs contained a short region of complementary sequences so that when assembled, these complementary sequences formed the stem of a stable hairpin

motif (Figure 1-10A). The length of the complementary sequence was optimized so that hybridization was unstable in the absence of BINDA. When the two DNA motifs bound to a single target, the local concentration of the DNA was dramatically increased resulting in hybridization to form a hairpin motif. Blocker oligonucleotides partially hybridized with the DNA motifs to further minimize target-independent assembly. DNA ligase was used to join the 3'-end of one motif with the 5'-end of the other motif to form a new DNA sequence that was then detected using real-time PCR. By eliminating the background that could result from target-independent DNA assembly, we achieved detection of yoctomole to zeptomole levels of streptavidin, platelet derived growth factor (PDGF), and prostate specific antigen (PSA).

We then assembled DNA motifs on a gold nanoparticle (AuNP) scaffold to develop a binding-induced molecular translator for the detection of proteins.<sup>70</sup> The binding-induced molecular translator was designed in such a way that the input target protein was able to be converted to a pre-designed output DNA through the process of binding-induced DNA strand displacement. By using this strategy, we have achieved homogeneous protein assays with high sensitivity and specificity. For example, we developed a binding-induced molecular translator to detect PDGF-BB (Figure 1-10B). This molecular translator was composed of target-recognition and signal-readout elements. The target recognition was achieved by two affinity ligands binding to the same target protein. One affinity ligand was conjugated to the AuNP that served as scaffold for the molecular translator. The second affinity ligand was conjugated to a competing DNA probe. A fluorophore-

labeled output DNA was hybridized to a supporting DNA that was conjugated to the same AuNP scaffold, and thus the fluorophore was initially quenched by AuNP. The competing DNA was also designed to be able to hybridize to the supporting DNA, but with 2-4 n.t. shorter than the output DNA. Thus, in the absence of target binding, displacement of the output DNA with the competing DNA was minimum. Binding of PDGF-BB to the two aptamer molecules assembled competing DNA onto the AuNP scaffold, enhanced local effective concentrations of DNA probes, and thus triggered the DNA strand displacement between the competing DNA and the output DNA. As a result, the fluorophore-labeled output DNA was released from the AuNP scaffold and the fluorescent signal was turned on. Using this strategy, sub nM concentrations of streptavidin and PDGF-BB could be detected without any separation steps.

Another assay that uses BINDA resulted in the interaction of silver nanoclusters (AgNC) with guanine rich DNA sequences to enhance fluorescence signal (Figure 1-10C).<sup>84</sup> The simultaneous binding of thrombin to an aptamer probe conjugated to a AgNC nucleation sequence and to another aptamer probe conjugated to a guanine-rich DNA sequence resulted in binding-induced hybridization between the two complementary regions in the sequences. This resulted in the placement of the guanine-rich sequence in close proximity to the AgNC to increase the fluorescence signal to detect 1 nM of thrombin. Besides those aforementioned methods, we are currently expanding the concept and strategy of binding-induced DNA assembly to diverse applications, ranging from the detection of DNA damage, to the biomarker screening, to the design of

binding-induced dynamic DNA assembly, and to the construction of binding-induced DNA assemblies on nanomaterials, e.g. quantum dots.

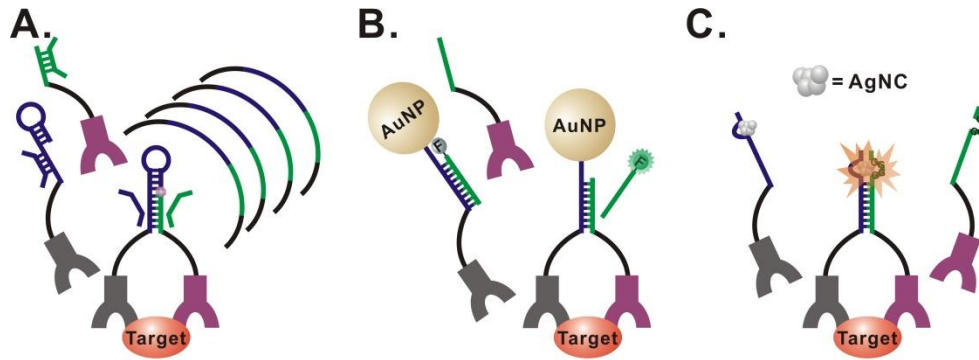


**Figure 1-10.** Binding-induced DNA Assembly (BINDA). (A) BINDA with PCR amplification; (B) Binding-induced molecular translator; (C) BINDA with silver nanocrystals (AgNC) as signal read-out.

## 1.5 Rationale and objective

Molecular diagnostic and imaging applications of dynamic DNA nanotechnologies have recently been a subject of great interest. Many unique features of DNA, including predictable molecular structures, the ability to be tailored or amplified by diverse DNA enzymes, the ability to serve as templates for constructing versatile and dynamic DNA nanostructures, make it desirable to construct ultrasensitive detection tools for point-of-care (POC) diagnostics.

Successful applications of DNA assembly systems have been limited to nucleic acids and a few non-nucleic acid targets possessing structure switching aptamers. However, using dynamic DNA nanotechnology to construct protein detection tools remains a challenge. Unlike nucleic acids, protein molecules

cannot be amplified. Techniques that make use of binding-induced DNA assemblies are very promising. One drawback of these techniques is that they usually require PCR and/or other enzymatic DNA amplification techniques to facilitate the signal amplification. The requirements for thermal cycling and enzyme stability make these techniques less than ideal for point-of-care applications. Making use of AuNPs to facilitate dynamic DNA nanotechnology can produce simple colorimetric signals for detection of nucleic acids and proteins. However, many issues, such as the stability of DNA-AuNPs under chemical or thermal stressed conditions, and the nonspecific adsorption of AuNPs to proteins, may compromise the performance of such biosensors.

The objective of this thesis is to apply the techniques and concepts of dynamic DNA nanotechnology to addressing the aforementioned challenges and to constructing simple but robust tools for detecting specific proteins. The thesis projects are outlined as follows.

**Chapter 2: Stability of DNA functionalized gold nanoparticles.** I systematically investigated how organosulfur anchor groups and DNA surface densities affect the thermal stability of DNA-AuNPs. By understanding the thermal stability of DNA-AuNPs, I designed a dual thiol labelled strategy to stabilize DNA-AuNPs with short internal complementary strands.

**Chapter 3: DNA assembly on aptamer functionalized gold nanoparticles for protein assays.** I investigated nonspecific adsorption of serum proteins to aptamer-functionalized gold nanoparticles (Apt-AuNPs). I then applied Apt-AuNPs as detection probes to western blot for protein analyses. By understanding

the adsorption behavior of proteins to Apt-AuNPs, I designed a competitive protection strategy that effectively eliminated nonspecific protein adsorptions on Apt-AuNPs, enabling specific and sensitive detection of target proteins in human serum samples.

**Chapter 4: Dynamic DNA assemblies mediated by binding-induced DNA strand-displacement reactions.** I designed a binding-induced DNA strand displacement strategy that is able to expand the scope of dynamic DNA assemblies to proteins. Using this strategy, I further developed two dynamic DNA assembly systems, including a binding-induced DNA strand displacement beacon and a binding-induced catalytic DNA circuit. Both systems are able to respond to protein bindings.

**Chapter 5: Binding-induced molecular translator for homogeneous protein assays.** I developed a binding-induced molecular translator that is able to convert protein bindings to the release of fluorescently labelled output DNA molecules from AuNPs. This strategy took advantage of the enhancement of local effective concentrations of DNA probes on AuNPs to accelerate DNA strand-displacement reactions. Using this strategy, I developed homogeneous nanosensors that are able to detect streptavidin and PDGF-BB at the sub nanomolar concentrations.

**Chapter 6: Conclusions.** This chapter summarizes the overall contents of this thesis research and briefly discusses potential future directions.

## 1.6 References

1. Seeman, N.C. *Annu. Rev. Biophys. Biomol. Struct.* **1998**, 27, 225.
2. Zhang, D. Y.; Seelig, G. *Nat. Chem.* **2011**, 3, 103.
3. Aldaye, F. A.; Palmer, A. L.; Sleiman, H. F. *Science* **2008**, 321, 1795.
4. Douglas S. M.; Dietz, H.; Liedl, T.; Hogberg, B.; Graf, F.; Shih, W. M. *Nature* **2009**, 459, 414.
5. Pinheiro, A. V.; Han D.; Shih, W. M.; Yan, H. *Nat. Nanotech.* **2011**, 6, 763.
6. Wei, B.; Dai, M.; Yin, P. *Nature*, **2012**, 485, 623.
7. Park, S. Y.; Lytton-Jean, A. K. R.; Lee, B.; Weigand, S.; Schatz, G. C.; Mirkin, C. A. *Nature*, **2008**, 451, 553.
8. Nykypanchun, D.; Maye, M. M.; van der Lelie, D.; Gang, O. *Nature*, **2008**, 451, 549.
9. Tikhomirov, G.; Hoogland, S.; Lee, P. E.; Fischer, A.; Sargent, E. H.; Kelley, S. O. *Nat. Nanotechnol.* **2011**, 6, 485.
10. Bath, J.; Turberfield, A. J. *Nat. Nanotechnol.* **2007**, 2, 275.
11. Winfree, E.; Liu, F.; Wenzler, L. A.; Seeman, N. C. *Nature* **1998**, 394, 539.
12. Venkataraman, S.; Dirks, R. M.; Ueda, C. T.; Pierce, N. A. *Proc. Natl. Acad. Sci. U. S. A.* **2010**, 107, 16777.
13. Yin, P.; Choi, H. M. T.; Calvert, C. R.; Pierce, N. A. *Nature* **2008**, 451, 318.
14. Qian, L.; Winfree, E. *Science* **2011**, 332, 1196.
15. Li, B.; Ellington, A. D.; Chen, X. *Nucleic Acids Res.* **2011**, 39, e110.
16. Li, B.; Jiang, Y.; Chen, X.; Ellington, A.D. *J. Am. Chem. Soc.* **2012**, 134, 13918.

17. Lin C.; Jungmann, R.; Leifer, A. M.; Li, C.; Levner, D.; Church, G. M.; Shih, W. M.; Yin, P. *Nat. Chem.* **2012**, *4*, 832.
18. Schweller, R. M.; Zimak, J.; Duose, D. Y.; Qutub, A. A.; Hittelman, W. N.; Diehl, M. R. *Angew. Chem. Int. Ed.* **2012**, *51*, 9292.
19. Rosi, N. L.; Mirkin, C. A. *Chem. Rev.* **2005**, *105*, 1547.
20. Saha, K.; Agasti, S. S.; Kim, C.; Li, X.; Rotello, V. M. *Chem. Rev.* **2012**, *112*, 2739.
21. Giljohann, D. A.; Seferos, D. S.; Daniel, W. L.; Massich, M. D.; Patel, P. C.; Mirkin, C. A. *Angew. Chem. Int. Ed.* **2010**, *49*, 3280.
22. Ellington, A. D.; Szostak, J. W. *Nature* **1990**, *345*, 818.
23. Tuerk, C.; Gold, L. *Science* **1990**, *249*, 505.
24. Mendonsa, S. D.; Bowser, M. T. *J. Am. Chem. Soc.* **2004**, *126*, 20.
25. Berezovski, M.; Musheev, M.; Drabovich, A.; Krylov, S. N. *J. Am. Chem. Soc.* **2006**, *128*, 1410.
26. Lou, X.; Qian, J.; Xiao, Y.; Viel, L.; Gerdon, A. E.; Lagally, E. T.; Atzberger, P.; Tarasow, T. M.; Heeger, A. J.; Soh, H. T. *Proc. Natl. Acad. Sci. U.S.A.* **2009**, *106*, 2989.
27. Shangguan, D.; Li, Y.; Tang, Z.; Cao, Z. C.; Chen, H. W.; Mallikaratchy, P.; Sefah, K.; Yang, C. J.; Tan, W. *Proc. Natl. Acad. Sci. U.S.A.* **2006**, *103*, 11838.
28. Hamula, C.; Zhang, H.; Li, F.; Wang, Z.; Le, X. C.; Li, X.-F. *Trends in Analytical Chemistry* **2011**, *30*, 1587.

29. Hamula, C.; Guthrie, J.; Zhang, H.; Li, X. C.; Le, X.-F. *Trends in Analytical Chemistry* **2006**, *25*, 681.
30. Gold, L.; Polisky, B.; Uhlenbeck, O.; Yarus, M. *Annu. Rev. Biochem.* **1995**, *64*, 763.
31. Elghanian, R.; Storhoff, J. J.; Mucic, R. C.; Letsinger, R. L.; Mirkin, C. A. *Science* **1997**, *277*, 1078.
32. Huang C-C.; Huang Y-F.; Cao, Z.; Tan, W.; Chang, H-T. *Anal. Chem.* **2005**, *77*, 5735.
33. Liu, J.; Lu, Y. *Angew. Chem. Int. Ed.* **2006**, *45*, 90.
34. Taton, T. A.; Mirkin C. A.; Letsinger, R. L. *Science* **2000**, *289*, 1757.
35. Wang, Y.; Li, D.; Ren, W.; Liu, Z.; Dong, S.; Wang, E. *Chem. Commun.* **2008**, *44*, 2520.
36. Jana, N. R.; Ying, J. Y. *Adv. Mater.* **2008**, *20*, 430.
37. Liu, J.; Mazumdar, D.; Lu, Y. *Angew. Chem. Int. Edt.* **2006**, *45*, 7955.
38. Tyagi, S.; Kramer, F. R. *Nat. Biotechnol.* **1996**, *14*, 303.
39. Dubertret, B.; Calame, M.; Libchaber, A. J. *Nat. Biotechnol.* **2001**, *19*, 680.
40. Song, S.; Liang, Z.; Zhang, J.; Wang, L.; Li, G.; Fan, C. *Angew. Chem. Int. Ed.* **2009**, *48*, 8670.
41. Zhang, J.; Wang, L.; Zhang, H.; Boey, F.; Song, S.; Fan, C. *Small* **2010**, *6*, 201.
42. Maxwell, D. J.; Taylor, J. R.; Nie, S. *J. Am. Chem. Soc.* **2002**, *124*, 9606.
43. Liu, J.; Lee, J. H.; Lu, Y. *Anal. Chem.* **2007**, *79*, 4120.

44. Seferos, D. S.; Giljohann, D. A.; Hill, H. D.; Prigodich, A. E.; Mirkin, C. A. *J. Am. Chem. Soc.* **2007**, *129*, 15477.
45. Prigodich, A. E.; Randeria, P. S.; Briley, W. E.; Kim, N. J.; Daniel, W. L.; Giljohann, D.; Mirkin, C. A. *Anal. Chem.* **2012**, *84*, 2062.
46. Zheng, D.; Seferos, D. S.; Giljohann, D. A.; Patel, P. C.; Mirkin, C. A. *Nano Lett.* **2009**, *9*, 3258.
47. Rosi, N. L.; Giljohann, D. A.; Thaxton, C. S.; Lytton-Jean, A. K. R.; Han, M. S.; Mirkin, C. A. *Science* **2006**, *312*, 1027.
48. Prigodich, A. E.; Seferos, D. S.; Massich, M. D.; Giljohann, D. A.; Lane, B. C.; Mirkin, C. A. *ACS Nano* **2009**, *3*, 2147.
49. Seferos, D. S.; Prigodich, A. E.; Giljohann, D. A.; Patel, P. C.; Mirkin, C. A. *Nano Lett.* **2009**, *9*, 308.
50. Prigodich, A. E.; Lee, O.-S.; Daniel, W. L.; Seferos, D. S.; Schatz, G. C.; Mirkin, C. A. *J. Am. Chem. Soc.* **2010**, *132*, 10638.
51. Zhang, D. Y.; Winfree, E. *J. Am. Chem. Soc.* **2009**, *131*, 17303.
52. Li, Q.; Luan, G.; Guo, Q.; Liang, J. *Nucleic Acids Res.* **2002**, *30*, E5.
53. Zhang, D. Y.; Chen, S. X.; Yin, P. *Nat. Chem.* **2012**, *4*, 208.
54. Picuri, J. M.; Frezza, B. M.; Ghadiri, M. R. *J. Am. Chem. Soc.* **2009**, *131*, 9368.
55. Duose, D. Y.; Schweller, R. M.; Zimak, J.; Rogers, A. R.; Hittelman, W. N.; Diehl, M. R. *Nucleic Acids Res.* **2012**, *40*, 3289.
56. Dirks, R. M.; Pierce, N. A. *Proc. Natl. Acad. Sci. U.S.A.* **2004**, *101*, 15275.

57. Choi, H. M. T.; Chang, J. Y.; Trinh, L. A.; Padilla, J. E.; Fraser, S. E.; Pierce, N. A. *Nat. Biotechnol.* **2010**, *28*, 1208.
58. Huang, J.; Wu, Y.; Chen, Y.; Zhu, Z.; Yang, X.; Yang, C. J.; Wang, K.; Tan, W. *Angew. Chem. Int. Ed.* **2011**, *50*, 401.
59. Wang, F.; Elbaz, J.; Orbach, R.; Magen, N.; Willner, I. *J. Am. Chem. Soc.* **2011**, *133*, 17149.
60. Shimron, S.; Wang, F.; Orbach, R.; Willner, I. *Anal. Chem.* **2012**, *84*, 1042.
61. Seelig, G.; Soloveichik, D.; Zhang, D. Y.; Winfree, E. *Science* **2006**, *314*, 1585.
62. Zhang, D. Y.; Turberfield, A. J.; Yurke, B.; Winfree, E. *Science* **2007**, *318*, 1121.
63. Zhang, D. Y.; Winfree, E. *Nucleic Acids Res.* **2010**, *38*, 4182.
64. Zheng, A.-X.; Li, J.; Wang, J.-R.; Song, X.-R.; Chen, G.-N.; Yang, H.-H. *Chem. Comm.* **2012**, *48*, 3112.
65. Wang, F.; Elbaz, J.; Willner, I. *J. Am. Chem. Soc.* **2012**, *134*, 5504.
66. Fredriksson, S.; Gullberg, M.; Jarvius, J.; Olsson, C.; Pietras, K.; Gústafsdóttir, S. M.; Ostman, A.; Landegren, U. *Nat. Biotechnol.* **2002**, *20*, 473.
67. Heyduk, E.; Heyduk, T. *Anal. Chem.* **2005**, *77*, 1147.
68. McGregor, L. M.; Gorin, D. J.; Dumelin, C. E.; Liu, D. R. *J. Am. Chem. Soc.* **2010**, *132*, 15522.
69. Zhang, H.; Li, X.-F.; Le, X. C. *Anal. Chem.* **2012**, *84*, 877.
70. Li, F.; Zhang, H.; Lai, C.; Li, X.-F.; Le, X. C. *Angew. Chem. Int. Ed.* **2012**, *51*, 9317.

71. Heyduk, T. *Biophys. Chem.* **2010**, *151*, 91.
72. Heyduk, E.; Dummit, B.; Chang, Y.-H.; Heyduk, T. *Anal. Chem.* **2008**, *80*, 5152.
73. Tian, L.; Heyduk, T. *Anal. Chem.* **2009**, *81*, 5218.
74. Heyduk, E.; Heyduk, T. *Anal. Biochem.* **2010**, *396*, 298.
75. Heyduk, E.; Moxley, M. M.; Salvatori, A.; Corbett, J. A.; Heyduk, T. *Diabetes* **2010**, *59*, 2360.
76. Hu, J.; Wang, T.; Kim, J.; Shannon, C.; Easley, C. J. *J. Am. Chem. Soc.* **2012**, *134*, 7066.
77. Di Giusto, D. A.; Wlassoff, W. A.; Gooding, J. J.; Messerle, B. A.; King, G. *C. Nucleic Acids Res.* **2005**, *33*, e64.
78. Conze, T.; Shetye, A.; Tanaka, Y.; Gu, J.; Larsson, C.; Göransson, J.; Tavoosidana, G.; Söderberg, O.; Nilsson, M.; Landegren, U. *Annu. Rev. Anal. Chem.* **2009**, *2*, 215.
79. Schallmeiner, E.; Oksanen, E.; Ericsson, O.; Spangberg, L.; Eriksson, S.; Stenman, U.-H.; Pettersson, K.; Landegren, U. *Nat. Methods* **2007**, *4*, 135.
80. Tavoosidana, G.; Ronquist, G.; Darmanis, S.; Yan, J.; Carlsson, L.; Wu, D.; Conze, T.; Ek, P.; Semjonow, A.; Eltze, E. et al., *Proc. Natl. Acad. Sci. U.S.A* **2011**, *108*, 8809.
81. Soderbert, O.; Gullberg, M.; Jarvius, M.; Ridderstrale, K.; Leuchowius, K.-J.; Jarvius, J.; Wester, K.; Hydbring, P.; Bahram, F.; Larsson, L.-G. et al., *Nat. Methods* **2006**, *3*, 995.

82. Jarvius, M.; Paulsson, J.; Weibrecht, I.; Leuchowius, K.-J.; Andersson, A.-C.; Wählby, C.; Gullberg, M.; Botling, J.; Sjöblom, T.; Markova, B.; et al., *Mol. Cell. Proteomics* **2007**, *6*, 1500.
83. Leuchowius, K.-J.; Jarvius, M.; Wickström, M.; Rickardson, L.; Landegren, U.; Larsson, R.; Söderberg, O.; Fryknäs, M.; Jarvius, J. *Mol. Cell. Proteomics* **2010**, *9*, 178.
84. Li, J.; Zhong, X.; Zhang, H.; Le, X. C.; Zhu, J.-J. *Anal. Chem.* **2012**, *84*, 5170–5174.

# Chapter Two: Thermal Stability of DNA Functionalized Gold Nanoparticles

## 2.1 Introduction

DNA functionalized gold nanoparticles (DNA-AuNPs) have shown great potential and exciting opportunities for disease diagnostic and therapeutic treatment.<sup>1-13</sup> DNA-AuNPs have been used for gene regulation,<sup>1-3</sup> drug delivery,<sup>4</sup> cancer cell imaging,<sup>5-7</sup> and photothermal therapies.<sup>8-13</sup> Stable conjugation between DNA oligonucleotides and gold nanoparticles is critical to any of the practical applications, because long term incubations at elevated temperatures (*e.g.* 37 °C)<sup>1-7</sup> or photothermal treatments to release DNA from AuNPs are commonly involved.<sup>8-13</sup> The covalent bond between gold and sulfur (Au-S, also known as thiolated-gold bond), usually mediated through the sulfhydryl (SH) functional group in thiols (RSH), is the most widely used interaction to achieve the stable conjugation between DNA oligonucleotides and AuNPs.<sup>14</sup> However, such Au-S bond is known to subject to dissociation that can be induced by other thiols or elevated temperatures.<sup>15-17</sup>

Efforts have been made to improve the stability of DNA-AuNP formed through Au-S bond by comparing conjugates formed with different organosulfur anchors including alkanethiol, acyclic disulfide, cyclic disulfide, and other types of multidentate thiolated anchor groups.<sup>16-19</sup> However, most studies have been focused on salt-dependent colloidal stability of DNA-AuNPs as a function of the extent of the colloidal aggregation rather than directly monitoring the dissociation of Au-S bond. Furthermore, most comparison studies were based merely on

chemical stabilities, where thiols, such as dithiolthreitol (DTT) or mercaptohexanol (MCH) were used to displace the thiolated DNA from AuNP surfaces.<sup>16-18</sup> Only limited studies have explored the thermal stability of DNA-AuNPs at room temperature or elevated temperatures without interference from other thiols.<sup>15,20</sup> For example, with the aim to find the most desired condition for storage of purified DNA-AuNPs, Liu *et al.* studied the long term DNA dissociation kinetics at 4 °C and at room temperature as a function of ionic strength, pH, and organic solvents.<sup>20</sup> Taton *et al.* studied the short term dissociation kinetics of DNA-AuNPs at elevated temperatures (40 °C to 95 °C).<sup>15</sup> Both studies focused only on Au-S bond formed with alkanethiol (RSH) as an anchor. To our knowledge, no systematic thermal stability study for DNA-AuNPs has been established regarding Au-S bonds formed with other types of organosulfur anchor groups. To understand the influence of different anchor groups on the thermal stability of DNA-AuNPs, we have designed DNA-AuNP probes with three different anchor groups (Figure 2-1). We report here a systematic study of their thermal stability by monitoring their thermal dissociation kinetics using a fluorescence turn-on assay. We also report the effect of packing densities on both thermal and chemical stability of DNA-AuNPs. DNA packing densities on AuNPs can influence the stability of DNA-AuNPs, as a result of the strong intermolecular repulsions among the largely negatively charged phosphodiester backbones of DNA molecules.<sup>23</sup> Such density effect on the thermal stability of DNA-AuNPs has not been reported previously.

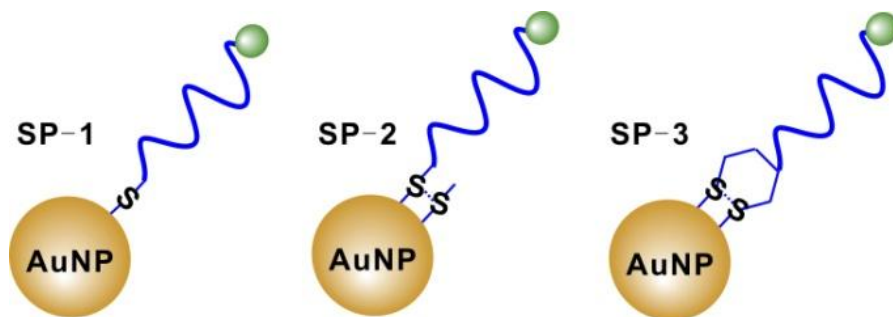


**Figure 2-1.** DNA functionalized gold nanoparticle (DNA-AuNP) probes constructed by conjugating oligonucleotides having different organosulfur anchor groups. **SP-1**, **SP-2**, and **SP-3** represent DNA-AuNPs modified with thiol, acyclic disulfide, and cyclic disulfide (DTPA), respectively.

## 2.2 Experimental

### 2.2.1 Materials and reagents

Gold nanoparticles with 20 nm diameter were purchased from Ted Pella (Redding, CA). All DNA samples were purchased from Integrated DNA Technologies (Coralville, IA) and purified by HPLC. The DNA sequences and modifications are listed in Table 2-1. Phosphate buffered saline (PBS) 10× solution and Tween20 were purchased from Fisher Scientific. Tris (2-carboxyethyl) phosphine hydrochloride (TCEP), 6-Mercapto-1-hexanol (MCH), DL-Dithiothreitol (DTT), and β-Mercaptoethanol (ME) were purchased from Sigma-Aldrich (Oakville, ON, Canada). NANOpure H<sub>2</sub>O (> 18.0 MΩ), purified using an Ultrapure Milli-Q water system, was used for all experiments.

**Table 2-1.** DNA sequences and modifications

| Probes | Sequences & Modifications                     | Antisense sequences & Modifications    |
|--------|---|--|
| SP-1   | 5'-FAM-TTT CTG TCG CGC<br>TTT TT-ThioMC3-D-3' | N.A.                                   |
| SP-2   | 5'-FAM-TTT CTG TCG CGC<br>TTT TT-ThioMC3-D-3' | N.A.                                   |
| SP-3   | 5'-FAM-TTT CTG TCG CGC<br>TTT TT-DTPA-3'      | N.A.                                   |
| DP-1   | 5'-FAM-TTT CTG TCG CGC<br>TTT TT-ThioMC3-D-3' | 5'-ThioMC6-D-AAA AAG<br>CGC GAC AGA-3' |
| DP-2   | 5'-FAM-TTT CTG TCG CGC<br>TTT TT-DTPA-3'      | 5'-ThioMC6-D-AAA AAG<br>CGC GAC AGA-3' |
| DP-3   | 5'-FAM-TTT CTG TCG CGC<br>TTT TT-DTPA-3'      | 5'-DTPA-AAA AAG CGC<br>GAC AGA-3'      |

### 2.2.2 Preparation of DNA-AuNPs

All organosulfur modified DNA oligonucleotides were received in disulfide or cyclic disulfide forms. To prepare DNA conjugated AuNP probe (**SP-1**) with thiol as the anchor, the disulfide modified oligonucleotide with a concentration of 50  $\mu\text{M}$  was treated with 100  $\mu\text{M}$  TCEP for 1 hr at room temperature to reduce the disulfide bond. This solution was then added to 1 mL 20nm AuNP solution (concentration 1 nM), and the mixture was placed at room temperature for 12 hrs. To this mixture was slowly added 20  $\mu\text{L}$  of 3 M NaCl, and followed by sonication for 10 seconds. This process was repeated for 5 times with 1 hr interval. The repeated process was to maximize the oligonucleotide loading amounts.<sup>24</sup> The final solution was stored at room temperature for 24 hrs. Then it was centrifuged at 13,500 rpm for 30 min to separate the AuNPs from the unreacted reagents. The DNA-AuNPs were washed 3 times with  $\frac{1}{2} \times$  PBS buffer (pH 7.4) containing 1% Tween20, and finally re-dispersed in the same PBS buffer. To prepare DNA conjugated AuNP probes with disulfide (**SP-2**) and DTPA (**SP-3**) as anchors, the same experimental procedure was used for disulfide modified DNA oligonucleotide and DTPA modified DNA oligonucleotide, except there was no TCEP reduction step.

To prepare DNA-AuNP probes with different densities, the initial ratio between DNA and AuNP was adjusted to 1000: 1, 500: 1, and 250: 1. To fine tune the density of DNA oligonucleotides on AuNP surfaces, we further adjusted final NaCl concentrations to 0.3 M, 0.5 M, and 0.7 M during the salt aging step. After washing, we measured surface densities of all nine DNA-AuNP probes, and selected five probes with distinct densities for subsequent experiments.

Double-stranded DNA-AuNP probes (**DP-1, DP-2, and DP-3**) were prepared by hybridizing two complementary organosulfur modified DNA strands before conjugating to AuNPs. Briefly, two complementary single stranded DNA oligonucleotides (50  $\mu$ M, 20  $\mu$ L each) were mixed together with 160  $\mu$ L 1  $\times$  PBS buffer. The solution was then heated up to 70  $^{\circ}$ C for 5 minutes and left at room temperature for 1 hr. The rest of the procedure was the same as mentioned above for **SP-1**.

### **2.2.3 Characterization of DNA-AuNPs**

DNA conjugated AuNPs were characterized by UV/Visible absorption spectrometry. A Lambda 35 UV/Vis absorption spectrophotometer (Perkin Elmer) was used to collect extinction spectra of DNA-AuNPs from 400 nm to 700 nm (Figure 2-2). We also determined the number of oligonucleotides loaded on each particle by measuring the concentration of AuNPs and concentration of fluorescent DNA in each sample according to the previous reported methods.<sup>25</sup>

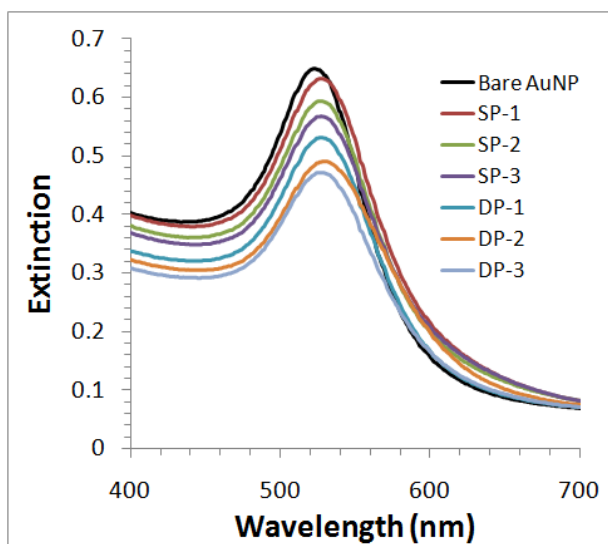


**Figure 2-2.** UV/Vis extinction spectra of bare gold nanoparticles (AuNPs) and DNA functionalized AuNPs (DNA-AuNPs). Unmodified AuNPs was dissolved in deionized water, and the solution showed a maximum absorption at 522 nm. The DNA-AuNPs were dissolved in  $\frac{1}{2} \times$  PBS buffer containing 0.01% Tween20. A small red shift of 5 nm was observed for all 6 DNA-AuNPs formed with different organosulfur anchor groups, indicating the formation of DNA layers on AuNPs.<sup>1</sup> No aggregation was observed for any of the DNA-AuNPs. The scanning rate was 120 nm/min and the resolution was 1 nm.

#### 2.2.4 Monitoring the thermal dissociation of DNA-AuNPs

A solution of 200  $\mu$ L DNA-AuNPs was centrifuged at 13,500 rpm for 30 minutes to remove all possible oligonucleotides released during storage. The pellet was redispersed in 200  $\mu$ L  $\frac{1}{2} \times$  PBS buffer and then incubated at different temperatures. Fluorescence signal increase was monitored with a multimode microplate reader (DTX880, Beckman Coulter) at time points of 0, 1, 2, 4, 8, 20 hrs. After 20 hrs incubation, a solution of 5  $\mu$ L  $\beta$ -mercaptomethonal (ME) was added to each sample at a final concentration of 50 mM. All the oligonucleotides were released into solution during an overnight incubation, and fluorescence

signal was read with microplate reader. The value of [Released] / [Total] was defined as fluorescence signal at each time point over the final fluorescence signal after ME treatment.

### **2.2.5 Monitoring the chemical-induced dissociation of DNA-AuNPs**

To a 95  $\mu\text{L}$  solution of FAM labeled DNA conjugated AuNPs in  $\frac{1}{2} \times$  PBS buffer was added 5  $\mu\text{L}$  MCH with different concentrations at room temperature. The increase of fluorescent signal was monitored every 10 minutes with the microplate reader for 400 minutes. Finally, a solution of 5  $\mu\text{L}$  ME was added to each sample to a concentration of 50 mM. All the oligonucleotides were released into solution during an overnight incubation, and fluorescence signal was collected again with the same microplate reader. The value of [Released] / [Total] was defined as fluorescence signal at every 10 minutes over the final fluorescent signal after ME treatment.

## **2.3 Results and discussion**

### **2.3.1 Experimental design**

To systematically study the thermal stability of DNA-AuNPs, we designed a set of single-stranded DNA-AuNP probes, as shown in Figure 2-1. **SP-1**, **SP-2**, and **SP-3** represent single stranded DNA-AuNP probes modified with three most widely used organosulfur anchor groups, including thiol,<sup>1-13</sup> acyclic disulfide,<sup>16-18</sup> and DTPA (cyclic disulfide).<sup>1,26-28</sup> We then studied thermal stabilities of these DNA-AuNP probes by monitoring the kinetics of their thermal dissociation

reactions. We also prepared DNA-AuNPs with different packing densities, and compared their thermal stabilities.

To monitor the thermal dissociation kinetics of DNA-AuNPs with different anchor groups and packing densities, we designed a simple but sensitive fluorescence-turn on assay (Fig. 2-3A) modified from the literature.<sup>20</sup> Briefly, single stranded DNA molecules were modified with fluorescent dye FAM and conjugated to AuNPs. The fluorescence signals of FAM-labeled DNA molecules were quenched as a result of the close proximity between FAM dyes and AuNPs. Upon dissociating from AuNPs, FAM labeled DNA restored its fluorescence as a result of the increased distance between FAM and AuNPs.

In this study, we first established the fluorescent turn-on assay using **SP-1**. We monitored the thermal dissociation of SP-1 at different temperatures over a period of 20 hours (Figure 2-3B). We then evaluated the rates of the thermal dissociation (Figure 2-3C) by determining the dissociation rate constant **k** from plots of the reaction rate equation:  $\ln([\text{Bound}]/[\text{Total}]) = \mathbf{k}t$ . By determining the dissociation rate constants at different temperatures (Figure 2-3D), we were able to determine the activation energy of the thermal dissociation process by fitting those data into the Arrhenius equation.

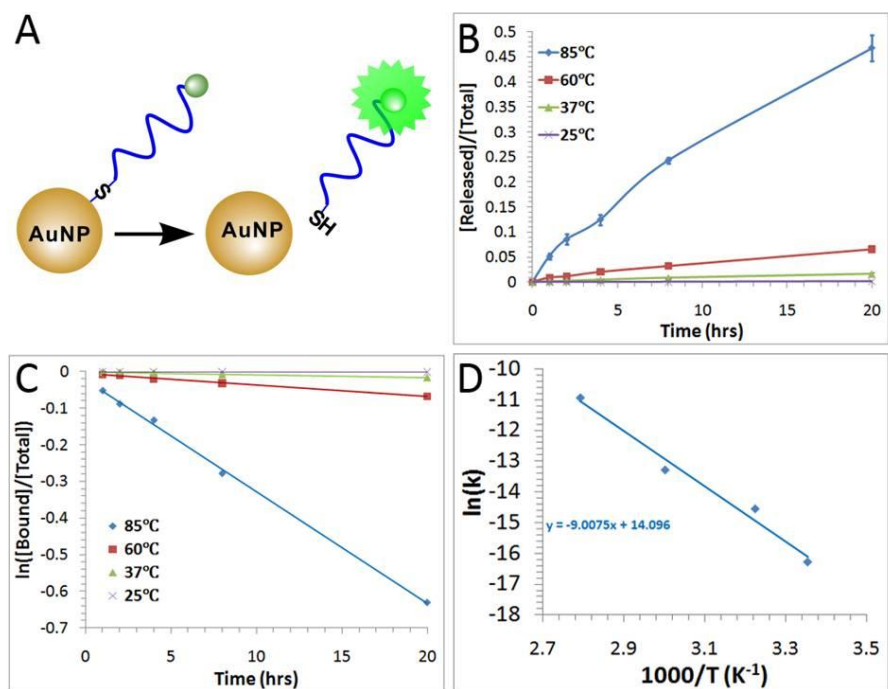


**Figure 2-3.** Thermal dissociation of FAM-labelled DNA from **SP-1**. (A) Schematic illustrating the fluorescent-based measurement of thermal dissociation of FAM-labelled DNA from the DNA-AuNP. (B) Fraction of released DNA from **SP-1** over a period of 20 hours at different temperatures (25, 37, 60, and 85 °C). (C) Plot to determine the thermal dissociation rate constants **k**. (D) Fitting the logarithmic value of rate constants as a function of reciprocal of temperatures to determine the activation energy of the thermal dissociation of **SP-1**. Error bars represent one standard deviation from triplicate sample analyses.

### 2.3.2 Effect of anchor groups on the thermal stability of DNA-AuNPs

After establishing the fluorescence turn-on method with **SP-1**, we studied the effect of anchor groups on the thermal stability of DNA-AuNPs by comparing the thermal dissociation rates of **SP-1**, **SP-2**, and **SP-3** at different temperatures (Figure 2-4). After incubated at 37 °C for 20 hrs, the dissociated amount of FAM-labeled DNA molecules from **SP-1**, **SP-2**, and **SP-3** were 1.6%, 1.7%, and 3.6%, respectively (Table 2-2, Figure 2-4A). The dissociation rate constants were the same for **SP-1** and **SP-2** ( $k = 1.3 \times 10^{-5} \text{ min}^{-1}$ ). However, the rate constant of **SP-3** ( $k = 2.7 \times 10^{-5} \text{ min}^{-1}$ ) was twice as of **SP-1** and **SP-2**. This observed trend in thermal stability was reproducible for at least three independently prepared DNA-AuNPs. To confirm this thermal stability trend, we repeat the experiments at 85 °C. Consistent with the results obtained at 37 °C, experiments conducted at 85 °C also showed that the DNA probes in **SP-1** and **SP-2** were more stable than that from **SP-3**. Furthermore, we observed a strong colloidal aggregation for **SP-3** after heating at 85 °C for 20 hrs (Figure 2-4B inserted photographs), evidenced by changes in color of the solution from red to blue to colorless. No solution color change (stay in red color) was observed for **SP-1** or **SP-2**. These observations confirmed that **SP-3** was thermally less stable than **SP-1** and **SP-2** under the same thermal treatments. To understand the effect of anchor groups on the thermal dissociation kinetics of DNA-AuNPs, we calculated the activation energies for DNA-AuNPs containing different anchor types. The activation energies were determined to be quite similar for **SP-1** (85.3 kJ/mol) and **SP-2** (82.4 kJ/mol). These were 7.6-10.5 KJ/mol higher than the activation energy for **SP-3** ( 74.8

kJ/mol). Since we kept the same conditions for different samples, including DNA sequences, packing densities (Table 2-2), buffer conditions, and incubation temperatures, this activation energy difference should be attributed to the difference in the nature of Au-S bonds.

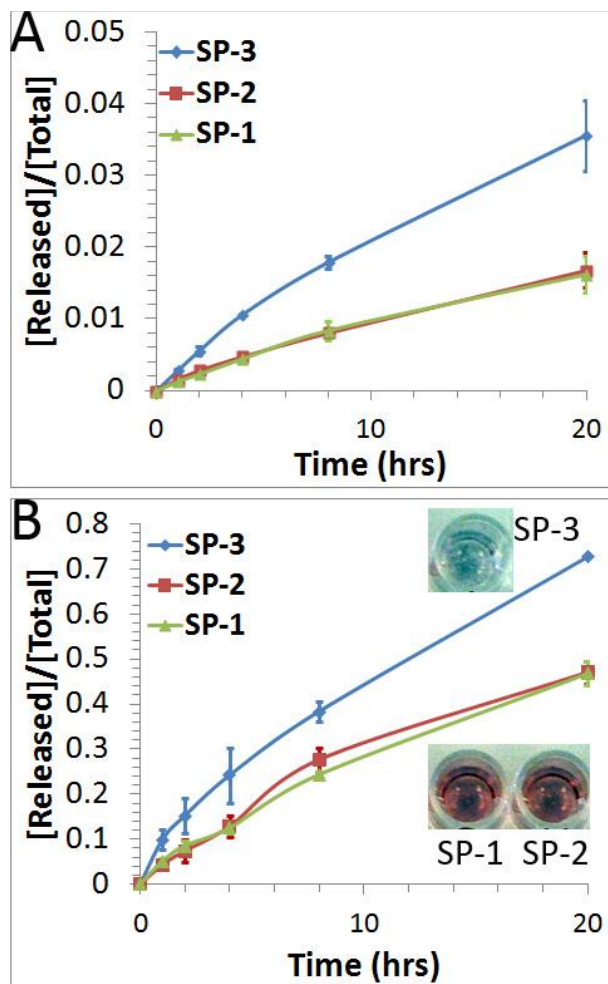


**Figure 2-4.** Fraction of FAM-labeled DNA released from the three DNA-AuNP probes (SP-1, SP-2, and SP3) over a period of 20 hours at 37 °C (A) and 85 °C (B). Inserted photographs in (B) were taken after 20-hour incubation at 85 °C, showing colors of different sample solutions at this time point. Error bars represent one standard deviation from triplicate sample analyses.

**Table 2-2.** Summary of three DNA-AuNP probes (SP-1, SP-2, and SP-3), their packing density, and the dissociation rate constant (**k**) and the fraction released after chemical or thermal treatment.

| Probes      | <sup>1</sup> Packing density | DNA dissociation induced by MCH                        |                                     | DNA dissociation at 37 °C                  |                                    |
|-------------|------------------------------|--|-------------------------------------|--|------------------------------------|
|             |                              | <sup>2</sup> <b>k<sub>i</sub></b> (min <sup>-1</sup> ) | <sup>3</sup> <b>f<sub>MCH</sub></b> | <sup>4</sup> <b>k</b> (min <sup>-1</sup> ) | <sup>3</sup> <b>f<sub>37</sub></b> |
| <b>SP-1</b> | 207±1                        | 1.1×10 <sup>-2</sup>                                   | 53.8%                               | 1.3×10 <sup>-5</sup>                       | 1.6%                               |
| <b>SP-2</b> | 210±9                        | 1.3×10 <sup>-2</sup>                                   | 51.4%                               | 1.3×10 <sup>-5</sup>                       | 1.7%                               |
| <b>SP-3</b> | 223±3                        | 4.0×10 <sup>-3</sup>                                   | 39.6%                               | 2.7×10 <sup>-5</sup>                       | 3.6%                               |

<sup>1</sup>Packing density: defined as number of DNA oligonucleotides per AuNP

<sup>2</sup>For DNA dissociation induced by 50 μM mercaptohexanol (MCH), initial rate constant **k<sub>i</sub>** was determined from equation:  $\ln(1-[\text{Released}]/[\text{Total}]) = \mathbf{k}_i t$ , t=10-30 min.

<sup>3</sup>Final releasing fraction **f**: **f<sub>MCH</sub>** = [Released]/[Total] at 400 min; **f<sub>37</sub>** = [Released]/[Total] at 1200 min

<sup>4</sup>Thermal dissociation rate constant **k** was determined from the first order reaction rate equation:  $\ln(1-[\text{Released}]/[\text{Total}]) = \mathbf{k} t$ , t=60-1200 min.

We also conducted a chemical stability study by treating DNA-AuNPs with mercaptohexanol (MCH) and monitored the chemical dissociation process using a revised fluorescence turn-on method (Figure 2-5A). As shown in Figure 2-5B, upon addition of 50  $\mu\text{M}$  MCH, fluorescence signals for **SP-1** and **SP-2** quickly plateaued within 30 minutes and the signal for **SP-3** increased much slower and gradually plateaued over a period of 400 minutes. The observed initial dissociation rates of **SP-1** ( $k_i = 1.1 \times 10^{-2} \text{ min}^{-1}$ ) and **SP-2** ( $k_i = 1.3 \times 10^{-2} \text{ min}^{-1}$ ) were two times faster than for **SP-3** ( $k_i = 4.0 \times 10^{-3} \text{ min}^{-1}$ ) (Table 2-2). These results are consistent with previous observation that cyclic disulfide was more stable under the treatments with competing thiols, e.g. MCH or DTT.<sup>16</sup> Thus we conclude that the thermal stability and chemical stability of the DNA-AuNPs with different anchor groups follow an opposite trend.

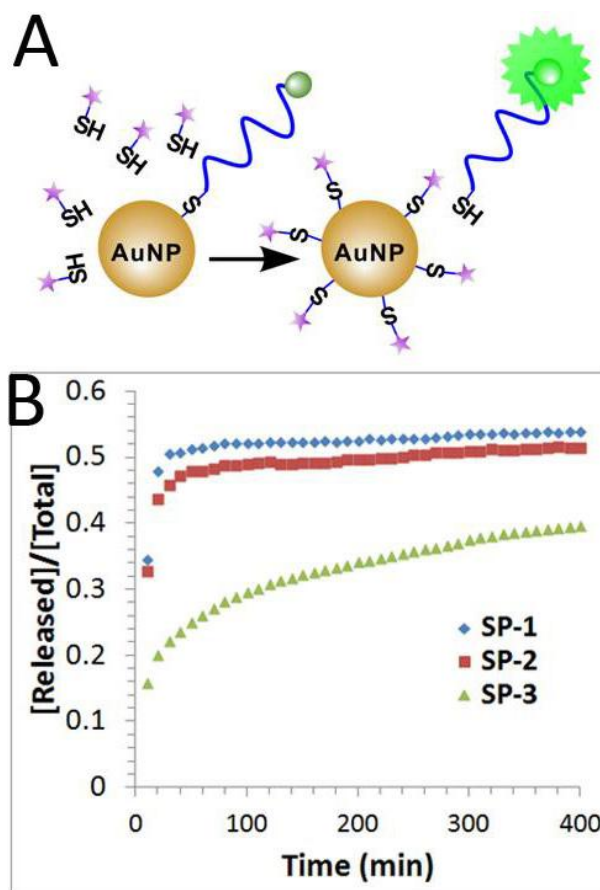


**Figure 2-5.** Dissociation of FAM-labeled DNA from the DNA-AuNPs when the DNA-AuNPs were treated with 50  $\mu$ M Mercaptohexanol (MCH) at 25  $^{\circ}$ C. (A) Schematic illustrating the fluorescence-based measurement of chemical dissociation of FAM-labeled DNA from the DNA-AuNPs. (B) Dissociation of FAM-labeled DNA from three different anchor groups (**SP-1**: thiol, **SP-2**: acyclic disulfide, and **SP-3**: DTPA).

### 2.3.3 Effect of packing densities on the thermal stability of DNA-AuNPs

Packing density is another important factor that can influence the thermal stability of DNA-AuNPs. To study this effect, we prepared a series of thiol modified DNA-AuNPs (the same as **SP-1**) with surface densities varying from 90 to 190 DNA molecules per AuNP. This density range was achieved by controlling the ratio between DNA and AuNPs and adjusting the NaCl concentration during the salt aging steps.

We first examined the thermal stability of DNA-AuNPs as a function of packing densities at 37 °C, using established fluorescence turn-on assay (Figure 2-3A). As shown in Figure 2-6A, DNA-AuNPs with lower packing densities dissociated slower when incubated at 37 °C. The dissociation rate constant for DNA-AuNPs with a packing density of **90/AuNP** was 3.4 fold slower than that of **190/AuNP** (Table 2-3). This kinetic difference is understandable because with the higher packing densities the repulsion among DNA oligonucleotides on the surfaces of DNA-AuNPs increases.<sup>23</sup> As temperature increased, the dissociation process was dominated by the Au-S bond breaking. Thus the effect of packing density is less pronounced at 85 °C, as shown in Figure 2-6B and Table 2-3.

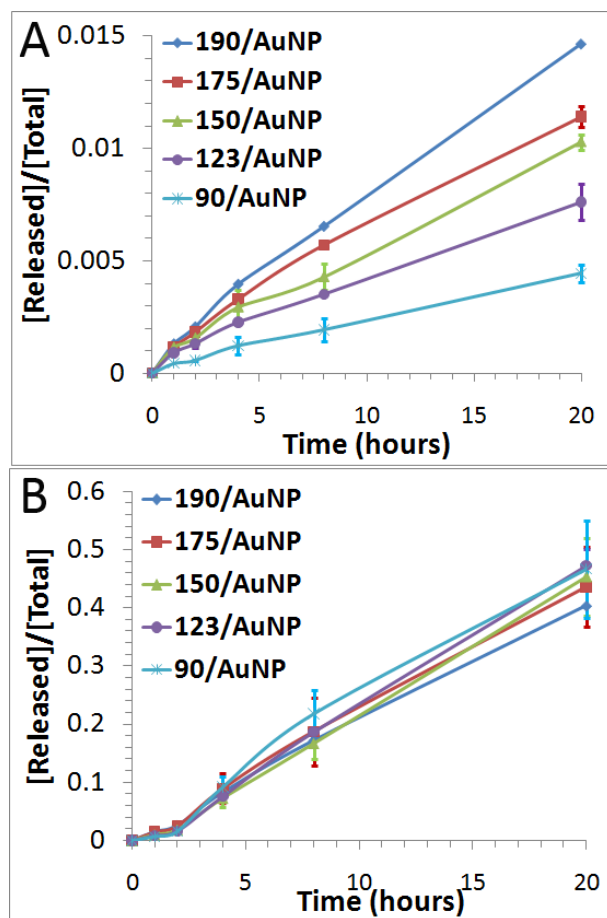


**Figure 2-6.** Effect of packing density on thermal dissociation of DNA-AuNPs at 37 °C (A) and 85 °C (B). The average density ranged from 90 oligonucleotide molecules per AuNP to 190 oligonucleotide molecules per AuNP. Error bars represent one standard deviation from triplicate sample analyses.

**Table 2-3.** Effects of packing density on thermal dissociation kinetics of DNA-AuNPs.

| Packing density | DNA dissociation at 37 °C       |            | DNA dissociation at 85 °C       |            |
|-----------------|---------------------------------|------------|---------------------------------|------------|
|                 | $k_{37}^1$ (min <sup>-1</sup> ) | $f_{37}^2$ | $k_{85}^1$ (min <sup>-1</sup> ) | $F_{85}^2$ |
| <b>190/AuNP</b> | $1.2 \times 10^{-5}$            | 1.5%       | $4.5 \times 10^{-4}$            | 40.4%      |
| <b>175/AuNP</b> | $9.0 \times 10^{-6}$            | 1.1%       | $5.0 \times 10^{-4}$            | 43.6%      |
| <b>150/AuNP</b> | $8.0 \times 10^{-6}$            | 1.0%       | $5.3 \times 10^{-4}$            | 45.3%      |
| <b>123/AuNP</b> | $5.8 \times 10^{-6}$            | 0.8%       | $5.7 \times 10^{-4}$            | 47.2%      |
| <b>90/AuNP</b>  | $3.5 \times 10^{-6}$            | 0.4%       | $5.6 \times 10^{-4}$            | 46.7%      |

<sup>1</sup>Dissociation rate constant **k** was determined from the first order reaction rate equation:  $\ln(1 - [\text{Released}]/[\text{Total}]) = -kt$ ,  $t=60-1200$  min.

<sup>2</sup>Final releasing fraction **f**:  $f = [\text{Released}]/[\text{Total}]$  at 1200 min.

### **2.3.4 Enhancing the thermal stability of DNA-AuNPs containing sicDNA using double-stranded DNA probes**

DNA-AuNPs with a short internal complementary DNA (sicDNA) has been proven to increase the rate of target hybridization and the DNA-mediated AuNP assembling.<sup>28,33,34</sup> However, at the temperature higher than its melting temperature ( $T_m$ ), the sicDNA will dehybridize from DNA-AuNPs and lose its function. To overcome this problem and increase the overall thermal stability of DNA-AuNPs, we designed a series of double-stranded DNA-AuNP probes and studied their potentials to stabilize sicDNA on DNA-AuNPs. As shown in Figure 2-7A (**DP-1**, **DP-2** and **DP-3**), both strands of the double-stranded DNA were modified with different combinations of organosulfur anchor groups. We reasoned that once both strands were conjugated to AuNPs, the DNA hybridization could be stabilized at temperature higher than its  $T_m$  as a result of the increased local concentration. Modifying both complementary strands with anchor groups could also form multiple thiol anchors to each pair of dsDNA and thus could potentially be used to enhance the overall stability of DNA-AuNPs.

To examine the formation of double-stranded DNA-AuNP probes, we first studied their chemical stabilities when they were treated with 2 mM DTT. As shown in Figure 2-7B, all three double-stranded DNA-AuNP probes have improved chemical stability as compared to the probe having a single thiol anchor (SP-1). These results confirmed the success of using DNA hybridization to construct the multiple thiol anchors. The increase numbers of thiol anchors from 2 (**DP-1**) to 4 (**DP-3**) did not result in kinetic differences, suggesting that the two

thiol anchors are sufficient to maintain the chemical stability of the DNA-AuNP probes.

We then studied the thermal stability of this set of DNA-AuNP probes by incubating them at 37 °C for a period of 20 hrs. As shown in Figure 2-7C, **DP-1** showed the best thermal stability, which was consistent with our previous results that the simple thiol anchor was thermally more stable than DTPA anchor on DNA-AuNPs. We further examined the thermal stability of **DP-1** at 60 °C, a temperature higher than the melting temperature of the double stranded DNA ( $T_m = 50$  °C). As can be observed in Figure 2-7D, thermal stability was greatly enhanced for **DP-1** (released less than 10% after 20 hrs) as compared to its control (immediately released of 40%). These results suggest that the construct as shown in **DP-1** has the potential to maintain the sicDNA hybridization at a temperature higher than its  $T_m$ .

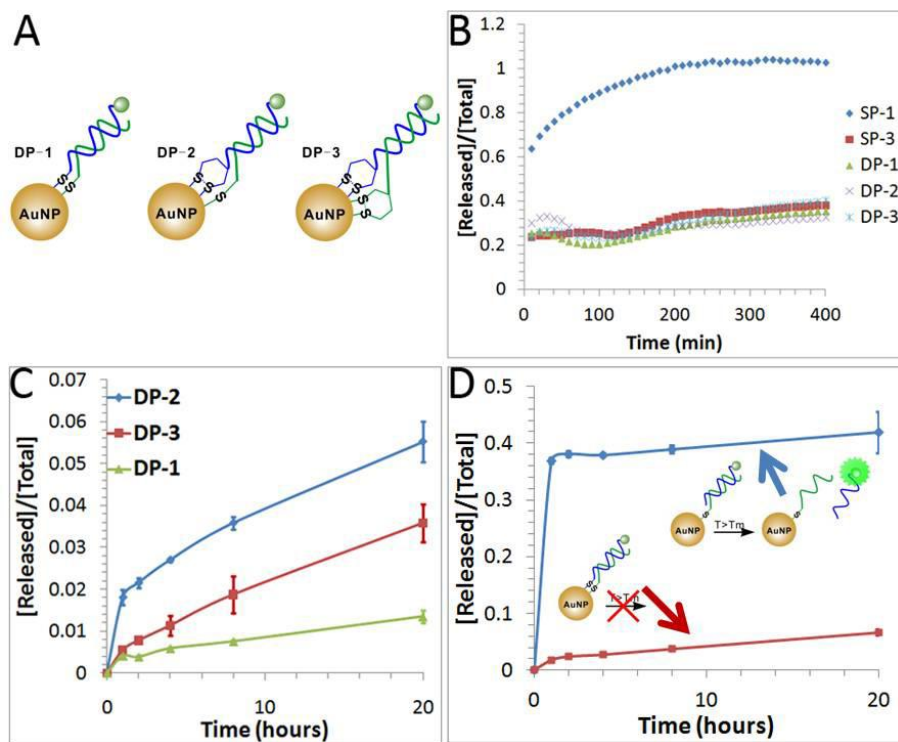


**Figure 2-7.** Designs of double-stranded DNA-AuNP probes to enhance the stability of the short internal complementary DNA (sicDNA). **(A)** Schematic showing the double stranded DNA-AuNP probes constructed by conjugating both of the complementary strands with different combinations of organosulfur anchors. **DP-1** represents DNA-AuNP constructed by conjugating both DNA strands with thiol anchors; **DP-2** represents DNA-AuNP constructed by conjugating one DNA strand with thiol anchor and the other strand with DTPA anchors; **DP-3** represents DNA-AuNP constructed by conjugating both DNA strands with DTPA anchors. **(B)** Chemical dissociation of different types of DNA-AuNPs induced by 2mM DTT at room temperature. **(C)** Thermal dissociation of double-stranded DNA-AuNP probes at temperature (37 °C), which is lower than the melting temperature (50 °C) of the double stranded DNA (dsDNA). **(D)** Comparison of the thermal dissociation of **DP-1** with its control at temperature (60 °C), which is higher than the melting temperature (50 °C) of its dsDNA. Error bars represent one standard deviation from triplicate sample analyses.

## 2.4 Conclusions

We have systematically studied the thermal stability of DNA functionalized gold nanoparticles (DNA-AuNPs) as a function of anchor types and packing densities. By monitoring the thermal dissociation kinetics of DNA-AuNPs that have different designs, we demonstrated that thermal stability of DNA-AuNPs varied with both anchor types and packing densities. Further analyses on the effects of anchor types revealed an opposite trend between the thermal stability and the chemical stability among the DNA-AuNPs that have different anchor types. These results can potentially be used to guide the design of DNA-AuNPs for different therapeutic applications. Finally, we designed a series of double-stranded DNA-AuNP probes by conjugating both DNA strands with organosulfur anchors, and demonstrated their ability to enhance the chemical stability of DNA-AuNPs and thermal stability of sicDNA on DNA-AuNPs.

## 2.5 References

1. Rosi, N. L., Giljohann, D. A., Thaxton, C. S., Lytton-Jean, A. K., Han, M. S., and Mirkin, C. A. *Science* **2006**, *312*, 1027-1030.
2. Giljohann, D. A., Seferos, D. S., Prigodich, A. E., Patel, P. C., and Mirkin, C. A. *J. Am. Chem. Soc.* **2009**, *131*, 2072-2073.
3. Patel, P. C., Giljohann, D. A., Daniel, W. L., Zheng, D., Prigodich, A. E., and Mirkin, C. A. *Bioconjugate Chem.* **2010**, *21*, 2250-2256.
4. Dhar, S., Daniel, W. L., Giljohann, D. A., Mirkin, C. A., and Lippard, S. J. *J. Am. Chem. Soc.* **2009**, *131*, 14652-14653.
5. Seferos, D. S., Giljohann, D. A., Hill, H. D., Prigodich, A. E., and Mirkin, C. A. *J. Am. Chem. Soc.* **2007**, *129*, 15477-15479.
6. Zheng, D., Seferos, D. S., Giljohann, D. A., Patel, P. C., and Mirkin, C. A. *Nano Lett.* **2009**, *9*, 3258-3261.
7. Prigodich, A. E., Seferos, D. S., Massich, M. D., Giljohann, D. A., Lane, B. C., and Mirkin, C. A. *ACS Nano* **2009**, *3*, 2147-2152.
8. Barhoumi, A., Huschka, R., Bardhan, R., and Knight, M. W., and Halas, N. J. *Chem. Phys. Lett.* **2009**, *482*, 171-179.
9. Braun, G. B., Pallaoro, A., Wu, G. H., Missirlis, D., Zasadzinski, J. A., and Tirrell, M. Reich, N. O. *ACS Nano* **2009**, *3*, 2007-2015.
10. Poon, L., Zandberg, W., Hsiao, D., Erno, Z., Sen, D., Gates, B. D., and Branda, N. R. *ACS Nano* **2010**, *4*, 6395-6403.
11. Jain, P. K., Qian, W., and El-Sayed, M. A. *J. Am. Chem. Soc.* **2006**, *128*, 2426-2433.

12. Huschka, R., Neumann, O., Barhoumi, A., and Halas, N. J. *Nano Lett.* **2010**, *10*, 4117-4122.
13. Huschka, R., Zuloaga, J., Knight, M. W., Brown, L. V., Nordlander, P., and Halas, N. J. *J. Am. Chem. Soc.* **2011**, *133*, 12247-12255.
14. (a) Boisselier, E., and Astruc, D. *Chem. Soc. Rev.* **2009**, *38*, 1759-1782; Hakkinen, H. *Nat. Chem.* **2012**, *4*, 443-455.
15. Herdt, A. R., Drawz, S. M., Kang, Y. J., and Taton, T. A. *Colloid Surface B* **2006**, *51*, 130-139.
16. Letsinger, R. L., Elghanian, R., Viswanadham, G., and Mirkin, C. A. *Bioconjugate Chem.* **2000**, *11*, 289-291.
17. Li, Z., Jin, R. C., Mirkin, C. A., and Letsinger, R. L. *Nucleic Acids Res.* **2002**, *30*, 1558-1562.
18. Dougan, J. A., Karlsson, C., Smith, W. E., and Graham, D. *Nucleic Acids Res.* **2007**, *35*, 3668-3675.
19. Seela, F., Ding, P., and Budow, S. *Bioconjug Chem.* **2011**, *22*, 794-807.
20. Bhatt, N., Huang, P. J. J., Dave, N., and Liu, J. W. *Langmuir* **2011**, *27*, 6132-6137.
21. Heinz, H., Vaia, R. A., and Farmer, B. L. *Langmuir* **2008**, *24*, 3727-3733.
22. Mei, B. C., Oh, E., Susumu, K., Farrell, D., Mountziaris, T. J., and Mattoussi, H. *Langmuir* **2009**, *25*, 10604-10611.
23. Cederquist, K. B., and Keating, C. D. *ACS Nano* **2009**, *3*, 256-260.
24. Hurst, S. J., Lytton-Jean, A. K. R., and Mirkin, C. A. *Anal. Chem.* **2006**, *78*, 8313-8318.

25. (a) Demers, L. M., Mirkin, C. A., Mucic, R. C., Reynolds, R. A., Letsinger, R. L., Elghanian, R., and Viswanadham, G. *Anal. Chem.* **2000**, *72*, 5535-5541;  
(b) Li, F.; Li, J.; Wang, C.; Zhang, J.; Li, X-F.; Le, X. C. *Anal. Chem.* **2011**, *83*, 6464-6467.
26. Wen, Y. Q., McLaughlin, C. K., Lo, P. K., Yang, H., and Sleiman, H. F. *Bioconjugate Chem.* **2010**, *21*, 1413-1416.
27. Lee, J. S., Lytton-Jean, A. K. R., Hurst, S. J., and Mirkin, C. A. *Nano Lett.* **2007**, *7*, 2112-2115.
28. Zhang, T., Chen, P., Sun, Y. W., Xing, Y. Z., Yang, Y., Dong, Y. C., Xu, L. J., Yang, Z. Q., and Liu, D. S. *Chem. Commun.* **2011**, *47*, 5774-5776.
29. Fenter, P., Eberhardt, A., and Eisenberger, P. *Science* **1994**, *266*, 1216-1218.
30. Kluth, G. J., Carraro, C., and Maboudian, R. *Phys. Rev. B* **1999**, *59*, 10449-10452.
31. Parak, W. J., Pellegrino, T., Micheel, C. M., Gerion, D., Williams, S. C., and Alivisatos, A. P. *Nano Lett.* **2003**, *3*, 33-36.
32. Dulkeith, E., Ringler, M., Klar, T. A., and Feldmann, J. *Nano Lett.* *5*, **2005**, 585-589.
33. Prigodich, A. E., Lee, O. S., Daniel, W. L., Seferos, D. S., Schatz, G. C. and Mirkin C. A. *J. Am. Chem. Soc.* **2010**, *132*, 10638-10641.
34. Maye, M. M., Nykypanchuk, D., Lelie, D. V., and Gang, O. *J. Am. Chem. Soc.* **2006**, *128*, 14020-14021.

# Chapter Three: Dynamic DNA Assembly on Aptamer Functionalized Gold Nanoparticles for Bioassays<sup>2</sup>

## 3.1 Introduction

Nanoparticles (NPs) have shown great potential and exciting opportunities for diverse applications. Unique size and surface properties of NPs are critical to their desired functions.<sup>1-4</sup> Surfaces of many NPs are known to cause nonspecific binding via electrostatic<sup>5</sup> and hydrophobic interactions.<sup>6-7</sup> Reduction of nonspecific binding is essential when applying NPs for integrated cancer imaging, therapy, or in vitro diagnostics.<sup>8-9</sup> Several surface modification strategies, including the use of polyethylene glycol,<sup>10</sup> monolayer/mixed-monolayer protection,<sup>11-12</sup> site-directed labeling,<sup>13</sup> and amphiphilic triblock copolymer labeling,<sup>14-15</sup> have been developed, aiming at reducing non-specific interactions. Conversely, nonspecific adsorption has been demonstrated to enhance the efficiency of in vitro translation of proteins,<sup>16</sup> and the uptake of antisense oligonucleotide-modified gold NPs.<sup>17</sup> Therefore, it is desirable to control and tune nonspecific binding ability of NPs for different applications.

In this chapter, I will describe a simple but effective strategy to dynamically control the nonspecific binding of DNA functionalized gold nanoparticles (DNA-AuNPs) through directed DNA assembling on surfaces of AuNPs. The strategy is illustrated in Figure 3-1, through a practical application of protecting aptamer functionalized AuNPs (Apt-AuNPs) from nonspecific binding to interference proteins and sample matrix. We incubate Apt-AuNP probe with rationally

---

<sup>2</sup> A portion of this chapter has been published in Li, F.; Li, J.; Wang, C.; Zhang, J.; Li, X.-F.; Le, X.C. *Anal. Chem.* **2011**, *83*, 6464-6467.

designed protection oligonucleotide that is composed of a hybridization sequence and an overhang component. When this protection oligo is incubated with the AuNP that is conjugated to the aptamer, hybridization with the aptamer assembled the protection oligonucleotide on the AuNP. This protection restricted the access of interfering molecules to the AuNP surface, thereby eliminating nonspecific interactions. In the presence of target molecules, competitive binding of the target molecules to the aptamer result in dynamic substitution of the protection oligonucleotide (Figure 3-1). Non target molecules (e.g. serum proteins) could not replace the protection oligonucleotide because their binding to aptamers was much weaker than the hybridization between the protection oligo and aptamer sequence. As a result, the strategy was capable of effectively eliminating the nonspecific binding while maintaining the affinity binding to the target molecule.

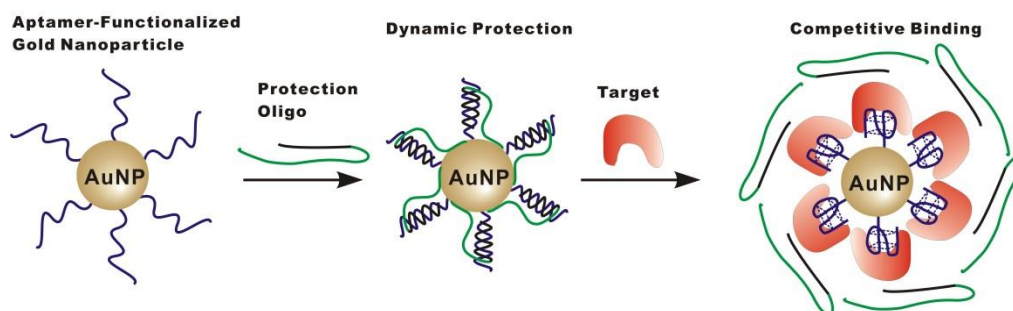


**Figure 3-1.** Schematic illustrating the principle of competitive protection. Aptamer (blue) functionalized gold nanoparticle (Apt-AuNP) probe was incubated with a protection oligonucleotide composed of a hybridization sequence (black) and an overhang component (green). Hybridization with the aptamer assembled the protection oligonucleotide on the AuNP. This protection resulted in elimination of non-specific interactions, because of the restricted access to the AuNP surface. In the presence of the target molecule, binding of the target molecules to the aptamer resulted in competitive substitution of the protection oligonucleotide. Non-target molecules (e.g. serum proteins) could not compete on the protection oligonucleotide because their binding to aptamers was much weaker than the hybridization between the aptamer and the protection oligo sequence. As a result, the strategy was capable of effectively eliminating the non-specific binding while maintaining the affinity binding with the target protein.

## 3.2 Experimental

### 3.2.1 Materials and reagents

Solution of gold nanoparticles (AuNPs) (10 nm in diameter,  $5.4 \times 10^{12}$  AuNPs per mL, G1527), Bovine serum albumin (BSA), human serum (product number, P2918) and tris (2-carboxyethyl) phosphine hydrochloride (TCEP) were purchased from Sigma. All DNA samples were purchased from Integrated DNA Technologies (Coralville, IA) and purified by HPLC. The DNA sequences and modifications were listed in Table 3-1. Human  $\alpha$ -thrombin and human prothrombin were purchased from Haematologic Technologies Inc. (Essex Junction, VT). Reagents for SDS-PAGE gel electrophoresis and western blot, including 40% acrylamide mix solution, ammonium persulfate, prestained SDS-PAGE molecular weight standards (low range),  $10 \times$  Tris-glycine buffer, Coomassie Brilliant Blue R-250, and polyvinylidene fluoride (PVDF) membrane, were purchased from BioRad Laboratories (Mississauga, ON, Canada). Tween 20 and 1,2-bis (dimethylamino)-ethane (TEMED) were purchased from Fisher Scientific (Nepean, ON, Canada). The binding buffer contained 100 mM NaCl, 20 mM Tris-HCl, 2 mM MgCl, 5 mM KCl, 1 mM CaCl<sub>2</sub>, and 0.02% Tween 20. The washing buffer contained  $1 \times$  PBS, and 0.1% Tween 20, pH 7.4. The protein loading buffer (10 mL) was made of 800 mg SDS, 4.0 mL glycerol, 0.4 mL 2-mercaptoethanol, 2.0 mL Tris-HCl at pH 6.8, and 8 mg bromophenol blue.

**Table 3-1.** DNA sequences and calculated melting temperature (T<sub>m</sub>) for the four oligo sequences when hybridized with the 15mer aptamer sequence.

| Probe                | DNA Sequence  | T <sub>m</sub> (°C)* |
|----------------------|---|----------------------|
| <b>15mer Apt</b>     | 5'-SH-(CH <sub>2</sub> ) <sub>6</sub> -GGT TGG TGT GGT TGG-3' |                      |
| <b>Oligo8</b>        | 5'-CCAACCAC-3'  | 27.7                 |
| <b>Oligo9</b>        | 5'-CCAACCACA-3'   | 34.2                 |
| <b>Oligo10</b>       | 5'-CCAACCACAC-3'  | 39.9                 |
| <b>Oligo11</b>       | 5'-CCAACCACACC-3'   | 46.0                 |
| <b>PolyA-oligo10</b> | 5'-AAA AAA AAA AAA AAA AAA<br>AA CCA ACC ACA C-3'             |                      |
| <b>PolyT-oligo10</b> | 5'- TTT TTT TTT TTT TTT TTT TT<br>CCA ACC AC AC-3'            |                      |
| <b>OligoA20</b>      | 5'-AAA AAA AAA AAA AAA AAA<br>AA-3'                           |                      |

\*T<sub>m</sub> was calculated using OligoAnalyzer 3.1 (free software from IDT). Settings were 250 nM oligo, 140 mM Na<sup>+</sup>, 1 mM Mg<sup>2+</sup>.

### 3.2.2 Preparation of Apt-AuNPs

A thiolated aptamer probe (15-mer Apt, 1 nmol) was received in a disulfide form. Prior to use, it was activated by 50  $\mu\text{L}$  of 5 mM TCEP in 100 mM Tris-HCl for 1 hr at room temperature. This solution was then added to 1 mL AuNPs solution, and the mixture was placed at 4  $^{\circ}\text{C}$  for 16 hrs. To this mixture was slowly added 100  $\mu\text{L}$  of 2 M NaCl, and followed by 10 seconds sonication. This process was repeated for 5 times with 20 minutes interval to maximize the aptamer loading amounts. The final solution was stored at 4  $^{\circ}\text{C}$  for 24 hrs. Then it was centrifuged at 17,000 g for 1 hr to separate the AuNPs from the unreacted reagents. The AuNPs were washed twice with 10 mM Tris-HCl (pH 7.4), and then redispersed in 1 mL of 10 mM Tris-HCl (pH 7.4). The Apt-AuNP solution was stored at 4  $^{\circ}\text{C}$  when not in use and was found to be stable for more than two weeks (no color change). It was estimated from fluorescence measurement that about 80 aptamer molecules were attached to each AuNP.

Immediately before use, Apt-AuNPs were treated using the following protocol to protect the AuNP surfaces. Protection oligonucleotides (PolyA-oligo10, PolyT-oligo10, or one of the other 5 oligos shown in Table S1) were added to the Apt-AuNP solution, the final concentrations of both the aptamer and the protection oligo were 1  $\mu\text{M}$ . The aptamer and protection oligo in the mixture were allowed to hybridize for 1.5 hrs at room temperature. The solution was then diluted 10 times with binding buffer for western blot applications.

### 3.2.3 Characterization of Apt-AuNPs

The modified and unmodified gold nanoparticles were characterized using transmission electron microscopy (TEM) and UV/visible absorption spectrometry.

A JEOL JEM-2100 transmission electron microscope was used to take images of bare AuNPs, Apt-AuNPs, and protected Apt-AuNPs (Figure 3-2). The commercially available AuNPs, dissolved in deionized water, were well dispersed (Figure 3-2, left panel). The AuNPs functionalized with a G-rich aptamer was known to be prone to aggregation under high salt conditions. So we stored apt-AuNPs in 10 mM Tris-HCl buffer to avoid aggregation. (Figure 3-2, middle panel). Protection with PolyA-oligo10 do not cause any change in stability. (Figure 3-2, right panel).

Nanoparticles were also characterized using UV/Visible absorption spectrometry. A Lambda 35 UV/Vis absorption spectrophotometer (Perkin Elmer) was used. Figure 3-3 shows absorption spectra of AuNPs, Apt-AuNPs, and oligo protected Apt-AuNPs. Unmodified AuNPs was dissolved in deionized water, and the solution showed a maximum absorption at 518 nm. The aptamer functionalized gold nanoparticles (Apt-AuNPs) were dissolved in Tris-HCl buffer. The protected Apt-AuNPs were dissolved in PBS buffer. A small red shift of 6 nm was observed when Apt-AuNPs were dissolved in Tris-HCl buffer, and there was no aggregation. When hybridized to the protection oligos (polyA-oligo10, Oligo10, and polyT-oligo10), and dissolved in PBS buffer, Apt-AuNPs showed the same spectra as the Apt-AuNPs in Tris-HCl buffer.

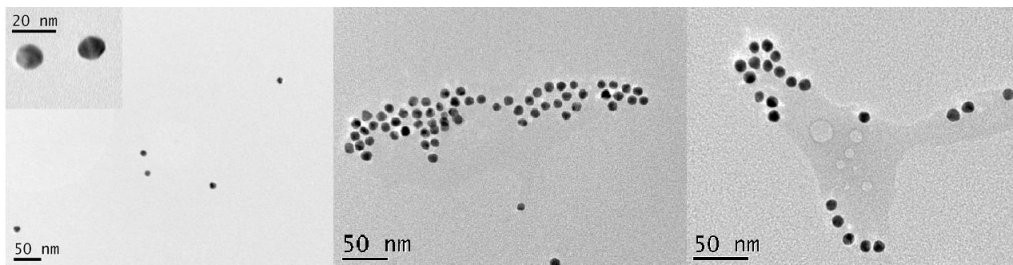


**Figure 3-2.** Transmission electron microscopy (TEM) images of the modified and unmodified gold nanoparticles. A JEOL JEM-2100 transmission electron microscope was used to take images of the gold nanoparticles. The commercially available AuNPs, when dissolved in deionized water, were well dispersed (left panel). The AuNPs functionalized with the aptamer were well dispersed in 10mM Tris-HCl buffer (middle panel). PolyA-oligo10 protected Apt-AuNPs were well dispersed in 1×PBS buffer (right panel).

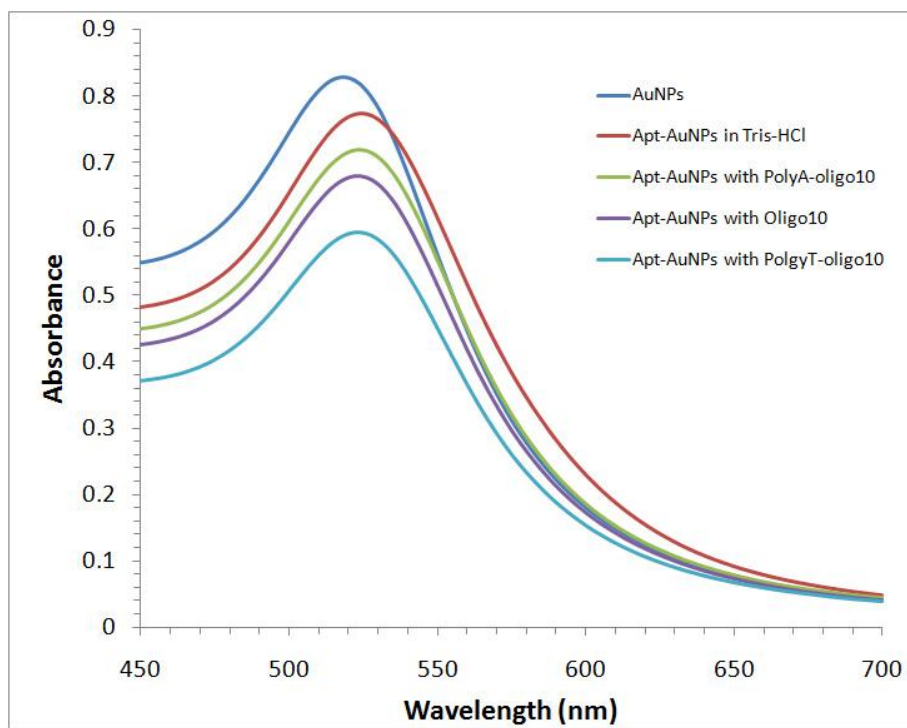


**Figure 3-3.** UV/Vis absorption spectra of gold nanoparticles (AuNPs) and aptamer functionalized gold nanoparticles (Apt-AuNPs) before and after incubating with protection oligos. The scanning rate was 120 nm/min and the resolution was 1 nm.

### **3.2.4 Gel electrophoresis, protein transfer, and membrane blotting**

SDS-PAGE separation of proteins was performed with 5% stacking gel and 12% resolving gel. All the gels were freshly prepared in house. Before loading, protein samples were mixed with protein loading buffer on a volume ratio of 3:1 and then heated at 95 °C for 5 min. A potential of 12 V/cm was applied for gel electrophoresis separation. The proteins on the gel were then transferred to the PVDF membrane with a constant voltage of 120 V for 1 hr. During this procedure, the temperature was kept at 4 °C. The blotting buffer (1000 mL) consisted of 200 mL methanol, 100 mL 10×Tris-glycine buffer, and 700 mL deionized water. After transferring, the gel was stained with Coomassie Brilliant Blue R-250 to estimate the efficiency of protein transferring (~60% in our experiment). The membrane was immediately blocked with 3% BSA for 1 hour to prevent nonspecific binding. Other blocking reagents, such as 1% tween 20, were also tested. After blocking, the membrane was washed twice with washing buffer for 10 min each and once with binding buffer. For serum samples, the total protein amount was determined by measuring absorbance at 280 nm.

### **3.2.5 Protein detection using competitive protected Apt-AuNPs**

After gel electrophoresis, transferring and membrane blocking steps, competitive protected Apt-AuNPs were added and incubated for 1 hr at room temperature. After incubation, the membrane was washed 3 times with washing buffer (10 min each time) and dried at room temperature. The dried membrane was imaged by ImageQuant 350 (IQ 350) digital imaging system (GE Healthcare). The intensities of the protein band and the background near the target band

(approximately 5 mm away from the edge of the band) were measured as the darkness in grey scale values and were used to obtain signal-to-background ratios.

### **3.2.6 Signal amplification using layer-by-layer assembly of Apt-AuNPs**

Similar procedures as described above were used in the layer by layer signal amplification experiments, except PolyA-oligo10 protected apt-AuNP and PolyT-oligo10 protected Apt-AuNP were used alternately to build the subsequent AuNP layers. Briefly, PolyA-oligo10 protected Apt-AuNP probe was used to incubate with membrane the same way as mentioned above. After incubation, the membrane was washed twice with washing buffer and once with binding buffer. Then PolyT-oligo10 protected apt-AuNP probe was added to the membrane to form the second layer of AuNP. The same washing and incubation with PolyA-oligo10 protected or PolyT-oligo10 protected Apt-AuNP probes were repeated to form the subsequent layers of AuNP. Images of the membrane after building each layer were captured by IQ 350, to observe the signal enhancement.

### **3.2.7 Signal amplification using targeted growth of Apt-AuNPs**

For further signal enhancement, commercial silver or gold enhancement kits were used, following the recommended protocols for immuno-membranes. Briefly, the membrane containing target protein and Apt-AuNPs was soaked in silver enhancement or gold enhancement solution for 5 min, washed for 3 times with deionized water, and left to dry. The dried membrane was imaged by desktop flatbed scanner (hp scanjet 4400c) and analyzed by imaging software (adobe photoshop CS3).

### 3.3 Results and discussion

#### 3.3.1 Competitive protection strategy for Aptamer-AuNPs

To demonstrate the competitive protection strategy, we chose human  $\alpha$ -thrombin as the target protein because of the importance of this protein in blood clotting process. A 15-mer DNA aptamer binding to the fibrinogen site of thrombin was used as the affinity ligand.<sup>18</sup> To evaluate the method on individual target, we used western blot analysis to separate the target protein from other components in sample matrix (Figure 3-4). In a typical experiment, proteins (e.g.  $\alpha$ -thrombin and prothrombin) in a sample (e.g. human serum) were separated by sodium dodecyl sulfate polyacrylamide gel electrophoresis (SDS-PAGE). The proteins on the gel were then transferred onto a polyvinylidene difluoride (PVDF) membrane, and detected by visualizing Apt-AuNPs.

Figure 3-5 shows typical images from western blot analyses of human  $\alpha$ -thrombin in diluted human serum. In the absence of the protection oligo, Apt-AuNP probe was able to detect thrombin on the membrane (Figure 3-5a). However, there is strong background resulting from sample matrix present in human serum. By incorporating the competitive protection approach into the Apt-AuNP detection system, we were able to improve signal-to-background ratio by a factor of 9 and to detect the target protein without the background interference from the serum matrix (Figure 3-5b).

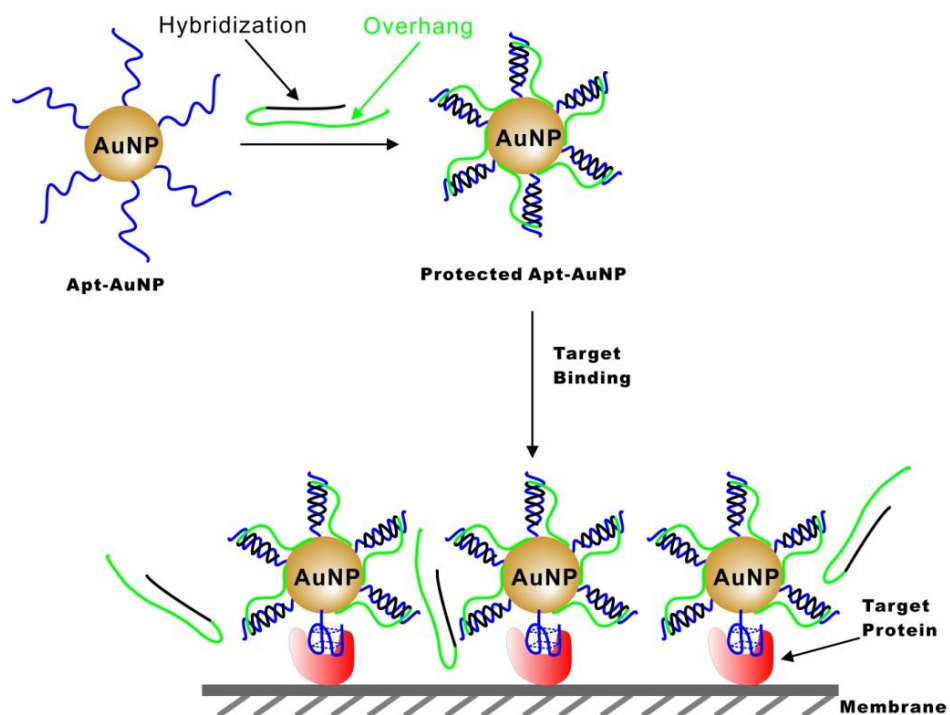


**Figure 3-4.** Schematic showing the application of competitive protected Apt-AuNPs to protein analysis on western blot membrane. Aptamer (blue) functionalized gold nanoparticle (Apt-AuNP) probe was incubated with a protection oligonucleotide composed of a hybridization sequence (black) and an overhang component (green). Hybridization with the aptamer assembled the protection oligonucleotide on the AuNP. This protection resulted in elimination of non-specific interactions, because of the restricted access to the AuNP surface. In detecting the specific proteins on western blot membranes, binding of the target molecules to the aptamer resulted in competitive substitution of the protection oligonucleotide. Non-target molecules (e.g. serum proteins) could not compete on the protection oligonucleotide because their binding to aptamers was much weaker than the hybridization between the aptamer and the protection oligo sequence. As a result, the strategy was capable of effectively eliminating the non-specific binding while maintaining the affinity binding with the target protein. Once bound to the target proteins, Apt-AuNPs can be visualized directly on the membranes.

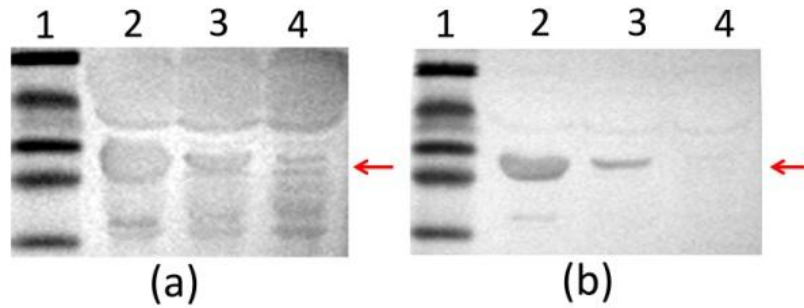


**Figure 3-5.** Western blot analysis of human  $\alpha$ -thrombin in 10-time diluted human serum. (a): detection using Apt-AuNP probes without the protection approach; (b): detection with PolyA-oligo10 protected Apt-AuNP probe. Lane 1 contained the pre-stained protein standards. Lanes 2-4 contained varying amounts of human  $\alpha$ -thrombin: 3.75  $\mu$ g (lane 2), 750 ng (lane 3), and 150 ng (lane 4). The arrows indicate human  $\alpha$ -thrombin. The intensities of the target signal and the background were measured on the basis of darkness (grey scale) of the target band and the background approximately 5 mm around the band.

### 3.3.2 Design and characterization of the protection oligonucleotide

Our success in achieving a 9-fold signal-to-background increase was due to a rational design of the protection oligonucleotide that incorporated a hybridization sequence and an overhang component. We reasoned that the hybridization sequence complementary to the aptamer sequence would enhance the selectivity for the target molecules because of their affinity binding to the aptamer. The use of an overhang was to restrict access of nonspecific molecules to the surface of AuNP.

We first studied the use of the competitive hybridization strategy to discriminate the target molecule from closely related molecules that may cross-react with the aptamer. We chose prothrombin as a potential interfering molecule for this test, because it has cross-reaction with the thrombin aptamers.<sup>19</sup> In designing the hybridization oligonucleotides, we considered the melting temperature of these oligos when hybridized to the aptamer sequence. The rationale was to facilitate competition between the target binding and the oligo hybridization to the same aptamer molecule on the AuNP, thereby achieving competitive protection of the AuNP. Considering that the single melting transition temperature of the 15mer thrombin aptamer is 38 °C,<sup>20</sup> we tested four protection oligo sequences, ranging from 8 to 11 nucleotides in length (Table 3-1), whose hybridization duplex with the aptamer have melting temperature of 27.7 °C to 46 °C. Figure 3-6 shows typical images from the analysis of human  $\alpha$ -thrombin and prothrombin when applying no protection (Figure 3-6a), or Oligo8 (Figure 3-6b), Oligo9 (Figure 3-6c), Oligo10 (Figure 3-6d), Oligo11 (Figure 3-6e) as the protection oligo. In the absence of competitive protection (Figure 3-6a),

prothrombin presented a potential interference. The use of protection oligos with increasing length resulted in decrease/elimination of prothrombin interference. With the protection oligo having a length of 10 n.t. (Oligo10), optimum detection of thrombin was free from the prothrombin interference.

We then tested the hybridization oligos on a more complex matrix, 10-time diluted human serum. Results are shown in Figure 3-7. The Apt-AuNP protected with Oligo8 (Figure 3-7b) resulted in a similar background as compared to Apt-AuNP detection without protection (Figure 3-7a). With the other three protection oligos (Oligo9, Oligo10, and Oligo11), both the background as well as the signals from the target molecule were reduced, suggesting that this approach is not sufficient to control the background arising from nonspecific binding to Apt-AuNPs.

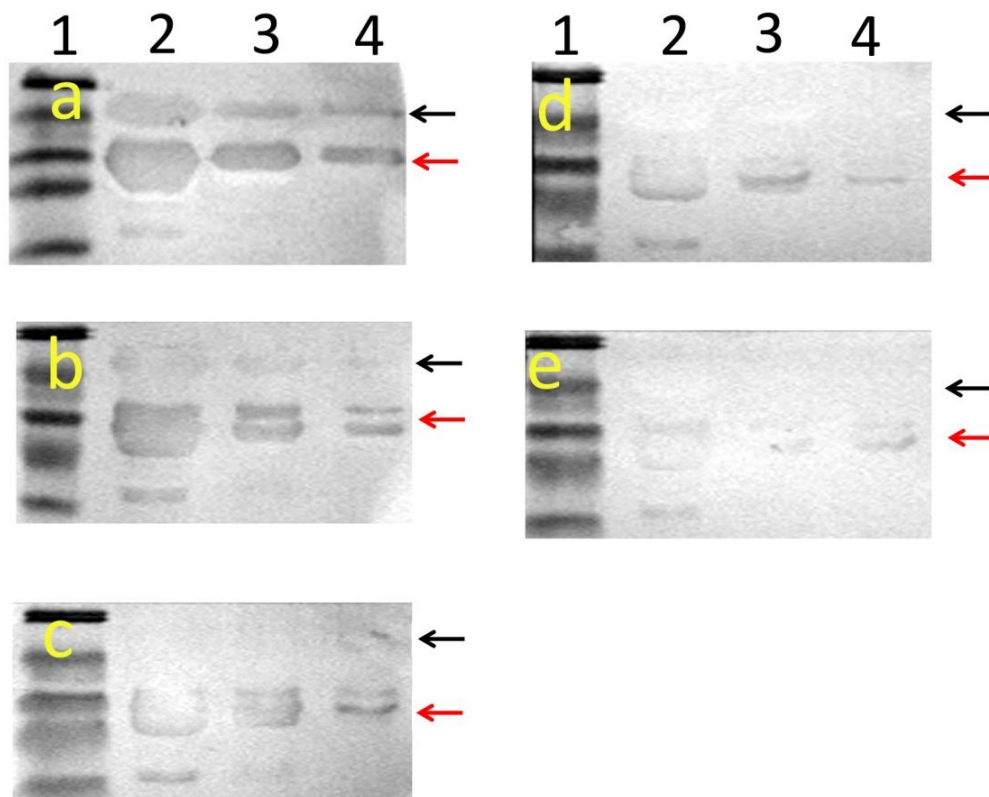


**Figure 3-6.** Membrane images from the western blot analysis of human  $\alpha$ -thrombin and human prothrombin. Equal amount of both proteins were loaded. The different hybridization oligos used for the protection of the Apt-AuNP were no protection (panel a), Oligo8 (b), Oligo9 (c), Oligo10 (d), Oligo11 (e). All other conditions for western blotting were the same. Lane 1 contained pre-stained low-range protein standard. Lanes 2-4 were from the analyses of 3.75  $\mu\text{g}$  (lane 2), 0.75  $\mu\text{g}$  (lane 3), and 0.15  $\mu\text{g}$  (lane 4) of human  $\alpha$ -thrombin and human prothrombin. The black arrows indicate human prothrombin, and the red arrows indicate human  $\alpha$ -thrombin.

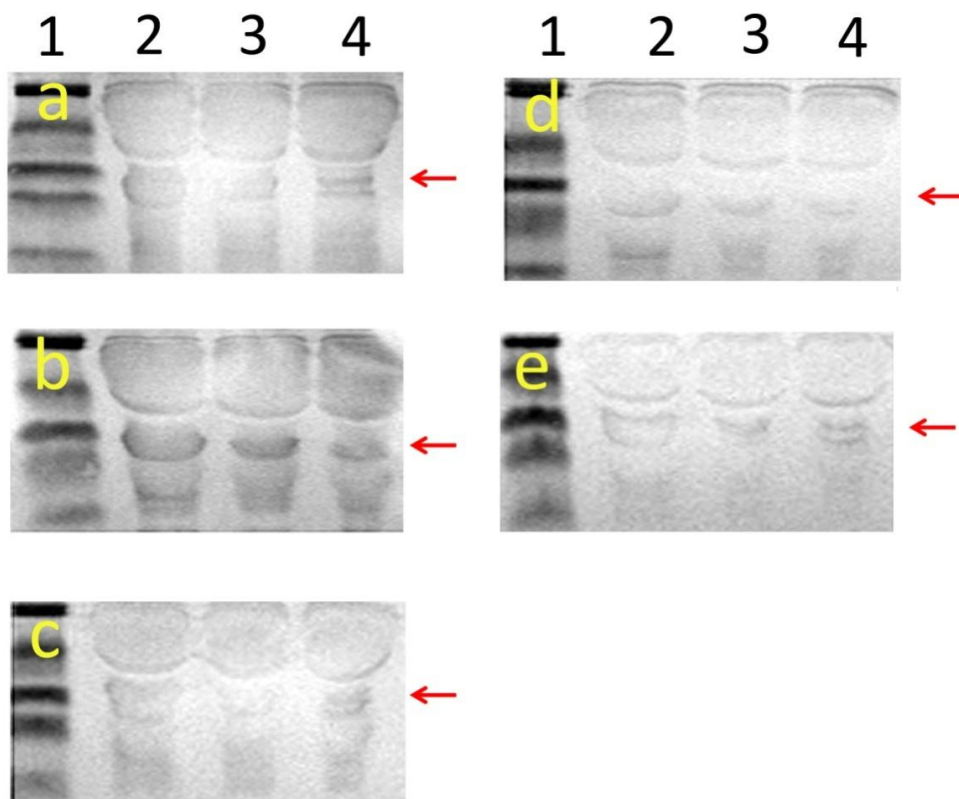


**Figure 3-7.** Membrane images from the western blot analysis of human  $\alpha$ -thrombin in 10-time diluted human serum. The different hybridization oligos used for the protection of the Apt-AuNP were: no protection (panel a), Oligo8 (b), Oligo9 (c), Oligo10 (d), Oligo11 (e). All other conditions for western blotting were the same. Lane 1 was from pre-stained low-range protein standard. Lanes 2-4 were from the analyses of 3.75  $\mu\text{g}$  (lane 2), 0.75  $\mu\text{g}$  (lane 3), and 0.15  $\mu\text{g}$  (lane 4) of human  $\alpha$ -thrombin in 10-time diluted human serum. The arrows indicate human  $\alpha$ -thrombin.

The above results from testing the cross-reaction molecules (prothrombin) and the complex matrix (serum) suggest that the competitive hybridization alone is not sufficient to eliminate the nonspecific binding from large amount of sample matrix. To further protect the AuNP surface and to prevent nonspecific adsorption, we extended the protection oligo by adding an overhang component, which was designed to restrict the access of nonspecific molecules to the surface of AuNP. We constructed two longer protection oligos by extending Oligo10 with either a polyA or a polyT sequence. As shown in Figure 3-8, the oligo with the polyA overhang was able to eliminate the background (Figure 3-8a), while the oligo with the polyT overhang reduced the background substantially (Figure 3-8b). Recognizing that the relative affinity of nucleotides to gold surface is  $A > C \geq G > T$ ,<sup>21-22</sup> one could potentially further fine-tune the sequences of the protection oligo to control the surface of AuNP. The use of the polyA oligo only (OligoA20) without the hybridization sequence did not reduce the background (Figure 3-8c), confirming the necessity of both hybridization and overhang sequences in the protection oligo.

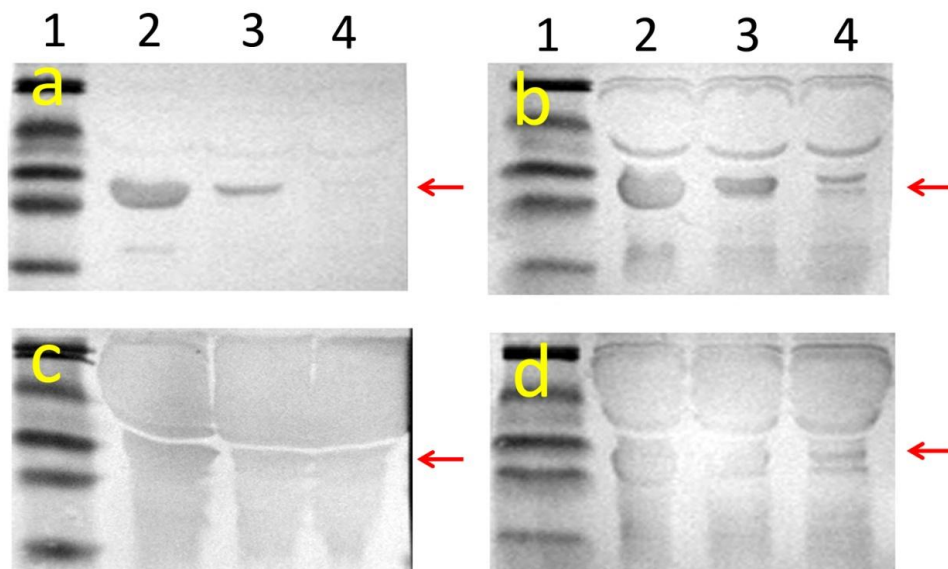


**Figure 3-8.** Membrane images from the western blot analysis of human  $\alpha$ -thrombin in 10-time diluted human serum. The different protection oligos used for the protection of the Apt-AuNP were polyA (panel a), polyT (b), OligoA20 (c), and no protection (d). All other conditions for western blotting were the same. Lane 1 contained pre-stained low-range protein standard. Lanes 2-4 were from the analyses of 3.75  $\mu\text{g}$  (lane 2), 0.75  $\mu\text{g}$  (lane 3), and 0.15  $\mu\text{g}$  (lane 4) of human  $\alpha$ -thrombin in 10-time diluted human serum. The arrows indicate human  $\alpha$ -thrombin.

### **3.3.3 Layer-by-layer assembly of Apt-AuNPs for signal amplification**

Another novel feature that we have built in the sequences of the protein oligos (PolyA-oligo10 and PolyT-oligo10) was their function as building blocks to generate supermolecular structures, with the end outcome of amplifying the detection signal.<sup>24-26</sup> Specifically, we took advantage of the hybridization sequence and the polyA or polyT overhang in the oligonucleotide to assemble extra layers of AuNP in a controlled manner to the surface of western blot membrane. The layers of AuNP resulted in enhancement in detection sensitivity (Figure 3-9). The first layer of AuNP was formed by bringing the Apt-AuNPs to the target protein on the membrane. The AuNP was protected with the oligo that has a polyA overhang. After washing, the membrane was treated with Apt-AuNP that was protected with the oligo having the polyT overhang. The polyT overhang hybridized with the polyA to form the second layer of AuNP. The subsequent layers of AuNP were assembled in the same manner by applying alternately the Apt-AuNP with protection oligos containing either polyA or polyT overhangs. With the assembly of each additional layer of AuNP, the intensity of the protein-AuNP band became stronger (Figure 3-9, right panels). Due to the enhancement of signal intensity, a detection limit of 6 ng thrombin could be achieved from the image of 5 layers of AuNP. This detection limit was based on the signal intensity (a grey scale measure of 52) from 6 ng thrombin, equivalent to the background plus three times standard deviation deviation of six background measures (a total grey scale measure of 45).

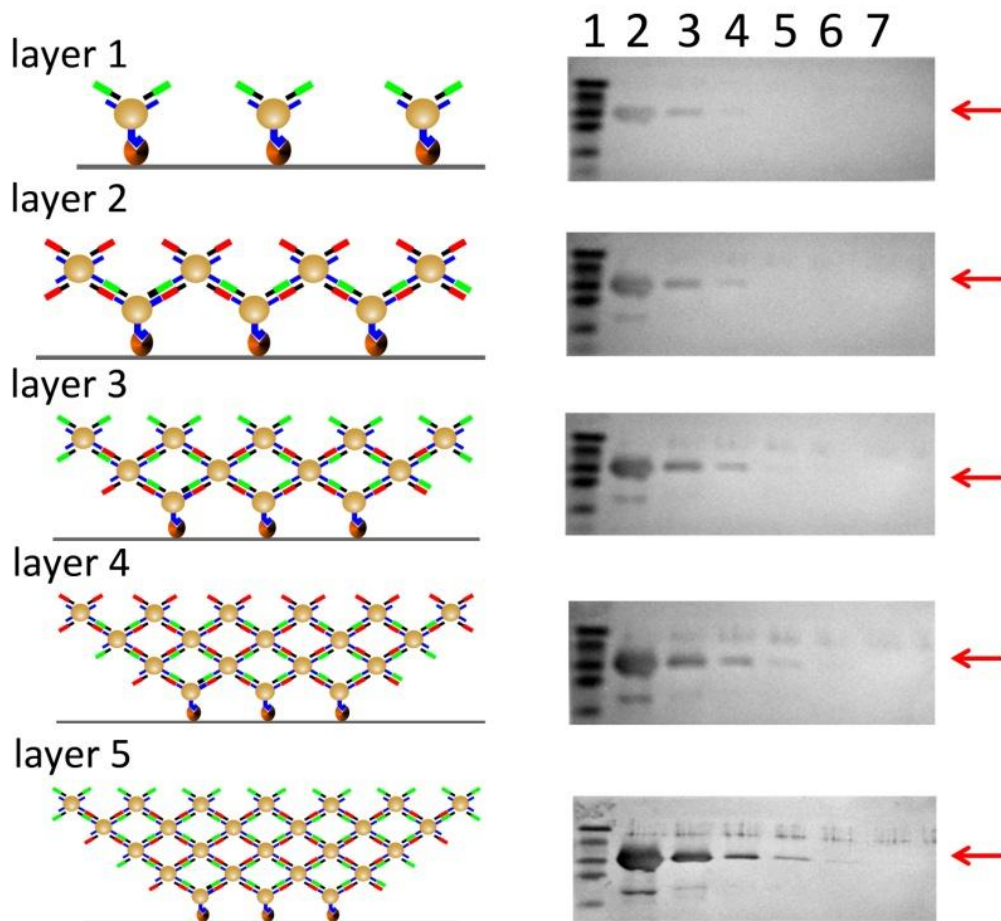


**Figure 3-9.** Schematic showing the layer-by-layer assembly of Apt-AuNPs for signal amplification. AuNPs were conjugated with specific aptamers for human  $\alpha$ -thrombin. Binding of the aptamer to  $\alpha$ -thrombin resulted in the formation of the first layer of AuNPs on the membrane. The subsequent layers of AuNPs were assembled by the hybridization of two oligonucleotides (red and green). Formation of the multiple layers of AuNPs enhanced the sensitivity of visualizing proteins. Lane 1 contained the pre-stained protein standards. Lanes 2-7 contained varying amounts of human  $\alpha$ -thrombin: 3.75  $\mu$ g (lane 2), 750 ng (lane 3), 150 ng (lane 4), 30 ng (lane 5), 6 ng (lane 6), and 1.2 ng (lane 7). The arrows indicate human  $\alpha$ -thrombin.

### 3.3.4 Targeted growth of Apt-AuNPs for signal amplification

To amplify the detection signal rapidly for detecting Apt-AuNP bounded proteins on western blot membrane, we also developed a targeted growth strategy using silver or gold enhancement. As shown in Figure 3-10, a layer of AuNP was first formed by bringing the AuNP-conjugated aptamer to the target protein on the membrane (Figure 3-10A). After washing away the unbound Apt-AuNPs, silver enhancement solutions containing silver ions and reducing reagents was then mixed and applied to the membrane. Silver ions were reduced rapidly to metallic silvers and deposited on Apt-AuNPs, enlarging the sizes of AuNPs (Figure 3-10B, left panel). As a result, intensities of protein bands on the membrane were enhanced, improving the detection limit for the target protein, human  $\alpha$ -thrombin, by 10 times from 500 ng (Figure 3-10A, right panel) to 50 ng (Figure 3-10B, right panel). Gold enhancement solution was also used to amplify the detection signal, and the detection limit for thrombin was further improved to 5 ng (Figure 3-10C).

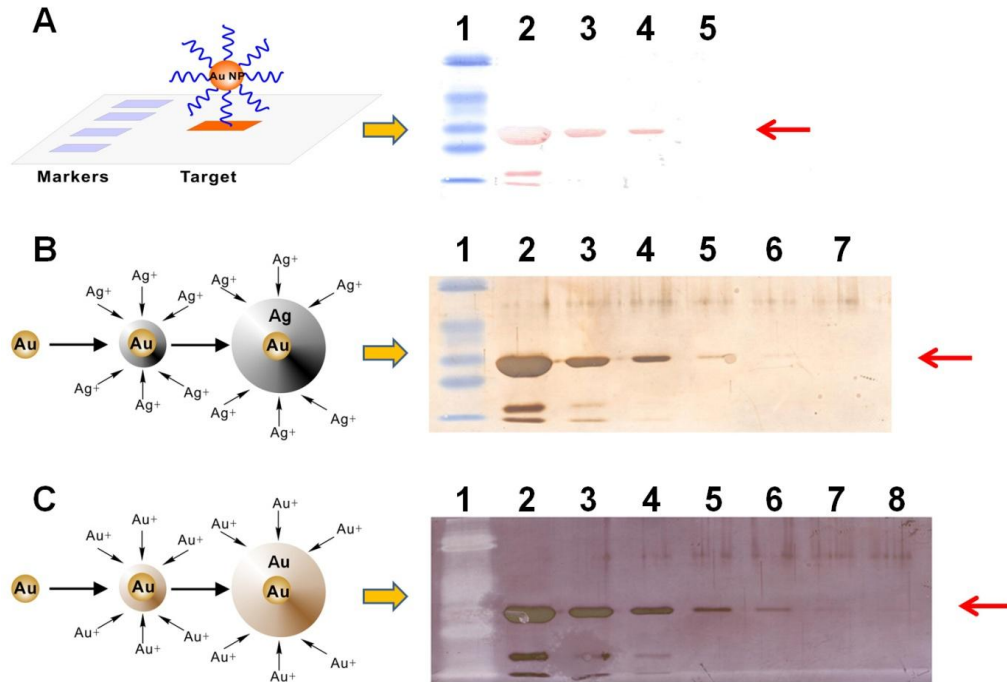


**Figure 3-10.** Signal enhancement strategies for detecting human  $\alpha$ -thrombin on the western blot membrane with Apt-AuNPs. **A:** detection with Apt-AuNP probe; **B:** detection with Apt-AuNP probe followed by silver enhancement; **C:** detection with Apt-AuNP probe followed by gold enhancement. Lane 1 contained pre-stained low-range protein standards. Lanes 2-8 contained varying amounts of human  $\alpha$ -thrombin: 5  $\mu$ g (lane 2), 1  $\mu$ g (lane 3), 500 ng (lane 4), 100 ng (lane 5), 50 ng (lane 6), 10 ng (lane 7), and 5 ng (lane 8). The red arrows indicate  $\alpha$ -thrombin.

After establishing the signal amplification with silver or gold enhancement, we further applied gold enhancement strategy to the detection of human  $\alpha$ -thrombin spiked in diluted human serum samples. As shown in Figure 3-11a, intensities of thrombin bands were amplified by the gold enhancement, however, bands of nonspecific serum proteins were also enhanced during this process, resulting severe background signals. To enhance assay specificity and eliminate the strong background interferences, we combined our competitive protection strategy with the gold enhancement to achieve the targeted growth of Apt-AuNPs for target proteins on the membrane. Briefly, we first protected Apt-AuNPs with protection oligo PolyA-oligo10, and then applied them to the western blot membrane containing the target protein and serum proteins. After washing away the unbound Apt-AuNPs, gold enhancement solution was applied to amplify the detection signal. As shown in Figure 3-11b, the targeted growth strategy effectively eliminated the background signals from interference proteins, enabling a quantitative analysis of the target protein (Figure 3-11c). A detection limit of 50 ng was achieved for human  $\alpha$ -thrombin in diluted serum samples.

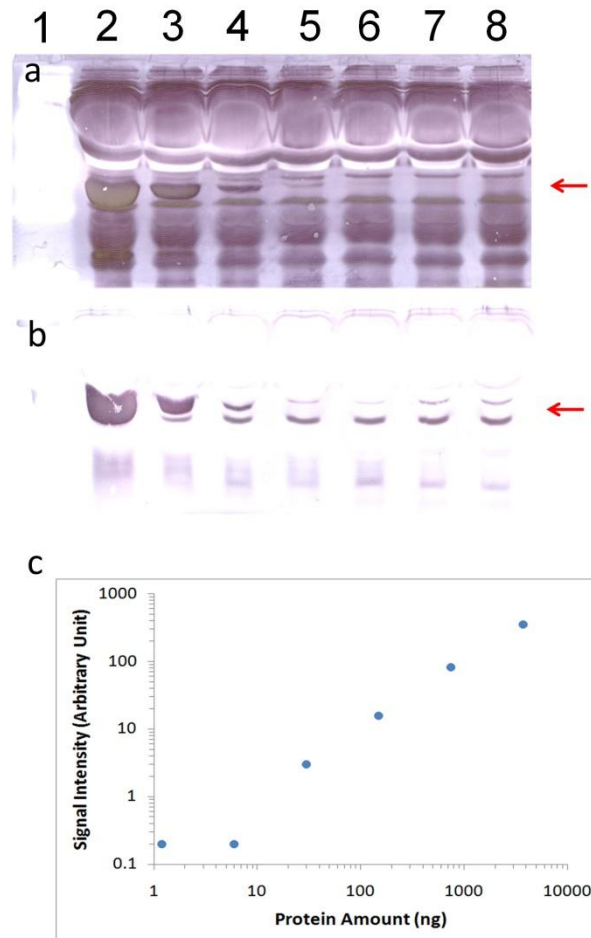


**Figure 3-11.** Targeted growth strategy for detecting human  $\alpha$ -thrombin in 10-time diluted human serum. (a) detection with Apt-AuNPs followed by gold enhancement (non-targeted growth strategy); (b) detection with PolyA-oligo10 protected Apt-AuNPs followed by gold enhancement (targeted-growth strategy); (c) quantification of proteins from (b) by measuring gray scales of each bands. Lane 1 contained pre-stained low-range protein standards. Lanes 2-8 contained varying amounts of human  $\alpha$ -thrombin: 5  $\mu$ g (lane 2), 1  $\mu$ g (lane 3), 500 ng (lane 4), 100 ng (lane 5), 50 ng (lane 6), 10 ng (lane 7), and 5 ng (lane 8). The red arrows indicate  $\alpha$ -thrombin.

### **3.4 Conclusions**

We have demonstrated that assembling protection DNA on Apt-AuNP was able to effectively control its nonspecific binding and enhance detection sensitivity. By incorporating appropriate hybridization and overhang sequences, we can potentially apply this method to different oligonucleotide-functionalized NP systems to control selectivity. The strategies of the directed growth of AuNP layers through controlled assembly and the targeted growth of AuNPs with gold enhancement can be used to enhance signals for detection of many other targets of clinical and prognostic significance. The simplicity of directed visualization makes this detection method attractive for potential personalized and point-of-care analysis.

### 3.5 References

1. Rosi, N. L.; Mirkin, C. A. *Chem. Rev.* **2005**, *105*, 1547-1562.
2. Giljohann, D. A.; Mirkin, C. A. *Nature* **2009**, *462*, 461-464.
3. Zhao, Q.; Lu, X.; Yuan, C. G.; Li, X. F.; Le, X. C. *Anal. Chem.* **2009**, *81*, 7484-7489.
4. Xie, C.; Xu, F.; Huang, X.; Dong, C.; Ren, J. *J. Am. Chem. Soc.* **2009**, *131*, 12763-12770.
5. Xu, H.; Mao, X.; Zeng, Q.; Wang, S.; Kawde, A. N.; Liu, G. *Anal. Chem.* **2009**, *81*, 669-675.
6. Huang, C. C.; Huang, Y. F.; Cao, Z.; Tan, W.; Chang, H. T. *Anal. Chem.* **2005**, *77*, 5735-5741.
7. Liu, G.; Mao, X.; Phillips, J. A.; Xu, H.; Tan, W.; Zeng, L. *Anal. Chem.* **2009**, *81*, 10013-10018.
8. Kim, D.; Jeong, Y. Y.; Jon, S. *ACS Nano* **2010**, *4*, 3689-3696.
9. Zhao, W.; Chiuman, W.; Brook, M. A.; Li, Y. *ChemBiochem* **2007**, *8*, 727-731.
10. Zheng, D.; Seferos, D. S.; Giljohann, D. A.; Patel, P. C.; Mirkin, C. A. *Nano. Lett.* **2009**, *9*, 3258-3261.
11. Liu, J.; Lu, Y. *J. Am. Chem. Soc.* **2007**, *129*, 8634-8643.
12. Liu, J.; Lu, Y. *Nat. Protoc.* **2006**, *1*, 246-252.
13. Zhang, J.; Wang, L.; Zhang, H.; Boey, F.; Song, S.; Fan, C. *Small.* **2010**, *6*, 201-204.
14. Burnette, W. N. *Anal. Biochem.* **1981**, *112*, 195-203.
15. Bakalova, R.; Zhelev, Z.; Ohba, H.; Baba, Y. *J. Am. Chem. Soc.* **2005**, *127*, 9328-9329.

16. Scholl, B.; Liu, H. Y.; Long, B. R.; McCarty, O. J. T.; O'Hare, T.; Druker, B. J.; Vu, T. Q. *ACS Nano* **2009**, *3*, 1318-1328.
17. Chen, W.; Xu, D.; Liu, L.; Peng, C.; Zhu, Y.; Ma, W.; Bian, A.; Li, Z.; Yuanyuan; Jin, Z.; Zhu, S.; Xu, C.; Wang, L. *Anal. Chem.* **2009**, *81*, 9194-9198.
18. Gilroy, K. L.; Cumming, S. A.; Pitt, A. R. *Anal. Bioanal. Chem.* **2010**, *398*, 547-554.
19. Li, Y. Y.; Zhang, C.; Li, B. S.; Zhao, L. F.; Li, X. B.; Yang, W. J.; Xu, S. Q. *Clin. Chem.* **2007**, *53*, 1061-1066.
20. Wang, Y. L.; Li, D.; Ren, W.; Liu, Z. J.; Dong, S. J.; Wang, E. K. *Chem. Commun.* **2008**, 2520-2522.
21. Jana, N. R.; Ying, J. Y. *Adv. Mater.* **2008**, *20*, 430-434.
22. Bock, L. C.; Griffin, L. C.; Latham, J. A.; Vermaas, E. H.; Toole, J. J. *Nature* **1992**, *355*, 564-566.
23. Kim, D.; Daniel, W. L.; Mirkin, C. A. *Anal. Chem.* **2009**, *81*, 9183-9187.
24. Taton, T. A.; Mirkin, C. A.; Letsinger, R. L. *Science* **2000**, *289*, 1757-1760.

# Chapter Four: Dynamic DNA Assemblies Mediated by Binding-Induced DNA Strand-Displacement Reactions<sup>3</sup>

## 4.1 Introduction

Over the past 30 years, tremendous effort has contributed to the successful development of DNA nanostructures and nanodevices.<sup>1</sup> Attention has recently shifted from designing DNA nanostructures/devices to exploring their potential functions in biological systems, including regulating cell function,<sup>2</sup> delivering therapeutic reagents,<sup>3</sup> and amplifying detection signals for molecular diagnostic and imaging.<sup>4</sup> Successful applications of DNA assembly systems have been limited to nucleic acids and a few small molecules.<sup>4b, 4h, 5</sup> It remains a challenge to apply DNA assembly systems to respond to specific proteins. In this chapter, I describe a binding-induced DNA strand displacement strategy that uses proteins to initiate the process of diverse dynamic DNA assembly systems.

Different from the toehold-mediated dynamic DNA displacement which is currently the most widely used strategy to direct dynamic DNA assemblies,<sup>1-5</sup> the binding-induced DNA strand displacement strategy relies on protein bindings to accelerate the rates of strand displacement reactions. In principle, by incorporating DNA toehold and functional domain into the output DNA from the binding-induced strand displacement, we shall be able to construct dynamic DNA assemblies that can respond to a specific protein binding. Thus, I first show an isothermal binding-induced DNA strand displacement strategy that is able to release the pre-designed output DNA at room temperature with high conversion

---

<sup>3</sup> This chapter has been accepted as Li, F.; Zhang, H.; Wang, Z.; Li, X.; Li, X.-F.; Le, X. C. *J. Am. Chem. Soc.* **2013**, *135*, 2443-2446.

efficiency and low background. I then apply this strategy to design two dynamic DNA assembly systems that are triggered by protein binding, including a binding-induced DNA strand displacement beacon and a binding-induced DNA circuit.

The strategy is illustrated in Figure 4-1. The binding-induced strand displacement is designed to have target recognition and signal output elements. Target recognition is achieved by two specific affinity ligands binding to the same target molecule. One affinity ligand is conjugated to the output DNA motif (**OT**) that is formed by pre-hybridizing the output DNA (**O**) and the supporting DNA (**T**), and the other is conjugated to the competing DNA motif (**C**). The complementary sequence of **OT** was designed to have the same length as **C**. Thus, in the absence of the target molecule, the rate of the strand exchange reaction between **OT** and **C** is extremely slow.<sup>6</sup> However, in the presence of the target molecule, the binding of the target molecule to the two affinity ligands that are linked to **OT** and **C** brings **C** to close proximity to **OT**. This process greatly increases the local concentration of **C** and accelerates the strand displacement reaction between **OT** and **C**. As a consequence, the output **O** is released from its support **T**. The subsequent dynamic DNA assembly can then be triggered by **O** using the principle of toehold-mediated strand displacement. To be more specific, the toehold part of **O** is designed to be embedded in the complementary part of **OT** (black color in Figure 4-1), so no dynamic DNA assembly can be triggered until the presence of the target molecule and the release of the toehold part of the output DNA.

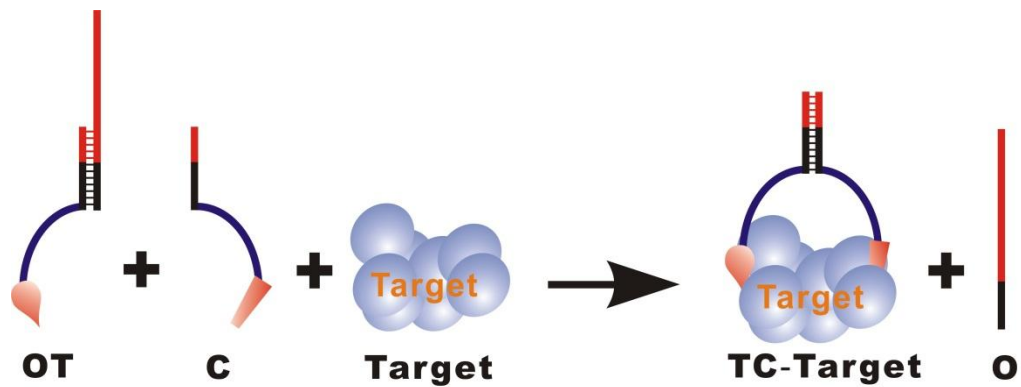


**Figure 4-1.** Schematic illustrating the principle of the binding-induced DNA strand displacement. To trigger the strand displacement, two DNA motifs (**OT** and **C**) are designed to be able to bind to the same target molecule through specific affinity ligand that is conjugated to the end of both motifs. The **OT** motif is formed by pre-hybridizing the output DNA **O** with the supporting DNA **T**. Binding of the two affinity ligands to the same target molecule assembles two DNA motifs together, and thus triggers an internal DNA strand displacement reaction between **OT** and **C**. As a result, the output DNA **O** is released from **T**, and a following toehold-mediated dynamic DNA assembly can then be initiated by the released **O**.

## **4.2 Experimental**

### **4.2.1 Materials and reagents**

Streptavidin from *Streptomyces avidinii* (product number, S4762), biotin (product number, B4501), bovine serum albumin (BSA), magnesium chloride hexahydrate ( $\text{MgCl}_2 \cdot 6\text{H}_2\text{O}$ ), and 100× Tris-EDTA (TE, pH 7.4) buffer were purchased from Sigma. SYBR Gold and ROX Reference Dye (ROX) were purchased from Invitrogen. Reagents for polyacrylamide gel electrophoresis (PAGE), including 40% acrylamide mix solution and ammonium persulfate were purchased from BioRad Laboratories (Mississauga, ON, Canada). Low molecular DNA ladder was purchased from New England Biolabs. Tween 20 and 1, 2-bis (dimethylamino)-ethane (TEMED) were purchased from Fisher Scientific (Nepean, ON, Canada). NANOpure  $\text{H}_2\text{O}$  ( $>18.0 \text{ M}\Omega$ ), purified using an Ultrapure Milli-Q water system, was used for all experiments. All DNA samples were purchased from Integrated DNA Technologies (Coralville, IA) and purified by HPLC. The DNA sequences and modifications are listed in Table 4-1.

**Table 4-1.** DNA sequences and modifications.

|   | DNA name         | Sequences   |
|---|------------------|---|
| For binding-induced DNA strand displacement and displacement beacon | <b>O</b>         | 5'-ATA GAT CCT CAT AGC GAG ACC TAG CAA-3'                                       |
|   | <b>L</b>         | 5'-TT AGT CCT ACA GCA GTA ACG ACT ATA GAT CCT CAT AGC GAG ACC TAG CAA-3'        |
|   | <b>T (12 nt)</b> | 5'-biotin-TTT TTT TTT TTT TTT TTG CTA GGT CTC-3'                                |
|   | <b>T (14 nt)</b> | 5'-biotin-TTT TTT TTT TTT TTT TTG CTA GGT CTC GC-3'                             |
|   | <b>T (16 nt)</b> | 5'-biotin-TTT TTT TTT TTT TTT TTG CTA GGT CTC GCT A-3'                          |
|   | <b>T (18 nt)</b> | 5'-biotin-TTT TTT TTT TTT TTT TTG CTA GGT CTC GCT ATG-3'                        |
|   | <b>T (20 nt)</b> | 5'-biotin-TTT TTT TTT TTT TTT TTG CTA GGT CTC GCT ATG AG-3'                     |
|   | <b>C (12 nt)</b> | 5'-GAG ACC TAG CAA TTT TTT TTT TTT TTT-biotin-3'                                |
|   | <b>C (14 nt)</b> | 5'-GC GAG ACC TAG CAA TTT TTT TTT TTT TTT-biotin-3'                             |
|   | <b>C (16 nt)</b> | 5'-T AGC GAG ACC TAG CAA TTT TTT TTT TTT TTT-biotin-3'                          |
|   |                  | <b>F</b>  |
|   | <b>Q</b>         | 5'-TTG CTA GGT CTC GCT ATG AGG ATC TAT-Dabcyl-3'                                |
| For binding-induced catalytic DNA circuit                           | <b>O</b>         | 5'-A TAGATCCT CATAGCGA GACCTAG CAA  |
|   | <b>H1</b>        | 5'-CTAGGTC TCGCTATG AGGATCTA CCATCGTGTAC TAGATCCT CATAGCGA AAGAGCAC CCTTGTCA-3' |
|   | <b>H2</b>        | 5'-AGGATCTA GTACACGATGG TAGATCCT CATAGCGA CCATCGTGTAC-3'                        |
|   | <b>F'</b>        | 5'-FAM-TGACAAGG GTGCTCTT TCGCTATG-3'  |
|   | <b>Q'</b>        | 5'-AAGAGCAC CCTTGTCA-Dabcyl-3'  |
|   | <b>P</b>         | 5'-CATAGCGA AAGAGCAC CCTTGTCA-3'  |

#### **4.2.2 Probe preparation for binding-induced DNA strand displacement**

DNA probe (**OT**) for binding-induced strand displacement was prepared at a final concentration of 5  $\mu\text{M}$  by mixing 20  $\mu\text{L}$  50  $\mu\text{M}$  supporting DNA (**T**) with 13.3  $\mu\text{L}$  50  $\mu\text{M}$  Output DNA (**O**) in 166.7  $\mu\text{M}$  TE-Mg (1 $\times$  TE, 10 mM  $\text{MgCl}_2$ , 0.05% Tween20) buffer, heating to 90  $^\circ\text{C}$  for 5 min, and allowing solution to cool down to 25  $^\circ\text{C}$  slowly in a period of 3 hours. Probe (**FQ**) for displacement beacon was also prepared at a final concentration of 5  $\mu\text{M}$  by mixing 20  $\mu\text{L}$  50  $\mu\text{M}$  FAM labeled DNA (**F**) with 20  $\mu\text{L}$  50  $\mu\text{M}$  dark quencher labeled DNA (**Q**) in 160  $\mu\text{M}$  TE-Mg buffer, heating to 90  $^\circ\text{C}$  for 5 min, and allowing solution to cool down to 25  $^\circ\text{C}$  slowly in a period of 3 hours. Reporter (**F'Q'**) for catalytic DNA circuit was prepared the same way as **FQ**, except that the ratio between **F'** and **Q'** was kept to 1:2 to minimize the background fluorescence.

#### **4.2.3 Monitoring the binding-induced DNA strand displacement using gel electrophoresis**

For a typical binding-induced DNA strand displacement reaction, the reaction mixture contained 2  $\mu\text{M}$  probe **OT**, 2  $\mu\text{M}$  competing DNA (**C**), 1  $\mu\text{M}$  target protein, and TE-Mg buffer. The reaction mixture was incubated at 25  $^\circ\text{C}$  for 45 min. After incubation, the performance of binding-induced DNA strand displacement was then assessed using 15% native polyacrylamide gel electrophoresis (PAGE). All the gels were freshly prepared in house. Before loading, DNA samples were mixed with DNA loading buffer on a volume ratio of 5:1. A potential of 12 V/cm was applied for gel electrophoresis separation. After

separation, PAGE gels containing DNA were stained using SYBR gold, and imaged by ImageQuant 350 (IQ 350) digital imaging system (GE Healthcare).

#### **4.2.4 Binding-induced DNA strand-displacement beacon**

For a typical binding-induced DNA strand displacement beacon, the reaction mixture contained 10 nM probe **OT**, 10 nM competing DNA (**C**), 20 nM displacement beacon **FQ**, 50 nM ROX, 1  $\mu$ M polyT oligo, varying concentrations of the target protein, and TE-Mg buffer. The reaction mixture was incubated at 25  $^{\circ}$ C for 45 min in a 96-well plate. Fluorescence was measured directly from the microplate using a multi-mode microplate reader (DX880, Beckman Coulter) with both excitation/emission at 485/515 nm for displacement beacon and excitation/emission at 535/595 nm for ROX as a reference dye. The measured fluorescent signal was normalized so that 1 n.u. of fluorescence corresponded to fluorescent signal generated by 1 nM **O**. This normalization was achieved using a positive control containing 10 nM **O**, 20 nM **FQ**, 1  $\mu$ M polyT oligo, and 50 nM Rox in TE-Mg buffer, and a negative control containing identical reagents in positive control except that there was no **O** added .

To monitor the kinetic process of binding-induced DNA strand-displacement, fluorescence of the reaction mixture was collected every 1.5 minutes for the first 30 minutes and then every 5 minutes for another 2 hours.

#### 4.2.5 Binding-induced catalytic DNA circuit

For a typical binding-induced catalytic DNA circuit, the reaction mixture contained 125 nM **H1**, 200 nM **H2**, 125 nM **F'Q'**, 20 nM **OT**, 20 nM **C**, 1  $\mu$ M polyT oligo, 50 nM ROX, varying concentrations of target protein, and TE-Mg buffer. The reaction mixture was incubated at 25  $^{\circ}$ C in 96-microplate well, and fluorescence was monitored directly from the multimode microplate reader. To monitor the reaction at real-time, fluorescent signal was collected every 1.5 minutes for the first 30 minutes and then every 5 minutes for another 3.5 hours. To normalize the fluorescent signal, both positive and negative controls were used. A positive DNA (**P**) was designed to be able to trigger the reporter (**F'Q'**) independently from the catalytic DNA circuit, and thus could be used to serve as a positive control to normalize the fluorescence intensities generated by the binding-induced catalytic DNA circuit. The positive control contained 50 nM **P** for reporter **F'Q'**, 125 nM **H1**, 200 nM **H2**, 125 nM **F'Q'**, 1  $\mu$ M polyT oligo, 50 nM ROX, and TE-Mg buffer. The negative control contained the identical reagents in the positive control, except that there was no **P** added.

## 4.3 Results and discussion

### 4.3.1 Binding-induced DNA strand displacement for streptavidin

To test the feasibility of our strategy, we designed a binding-induced strand displacement strategy for streptavidin using biotin as affinity ligands (Figure 4-2). The streptavidin was selected due to its extremely high binding affinity to biotin ( $K_d = 10^{-14}$  M). This strong interaction ensures that the target binding process will not limit the performance of the binding-induced strand displacement. **T** and **C** were each conjugated with a biotin molecule. The output **O** was designed to hybridize to **T** with a complementary length of 12 nt. **O** was extended with another 15 nt oligonucleotide to help direct further DNA assemblies. We first characterized this binding-induced strand displacement strategy using polyacrylamide gel electrophoresis (PAGE). By mixing equal amounts of **OT** and **C** without streptavidin for over 45 minutes, we could barely observe the released output **O** (Figure 4-3, Lane 4), indicating that the rate of strand exchange between **OT** and **C** was extremely slow. However, in the presence of streptavidin, a very strong band of **O** appeared in the gel, confirming that the binding between streptavidin and biotin did accelerate the kinetics of strand displacement reaction between **OT** and **C**. As many dynamic DNA assembly systems, e.g. DNA catalytic circuits, or nanomachines, make use of DNA with lengths over 50 nt, we further test the versatility of our strategy to output DNA with a length of 50 nt (**L**). As shown in Figure 4-4, a strong band of **L** appeared in lane 5 upon target binding, indicating that our strategy is versatile enough to release diverse output DNA molecules.

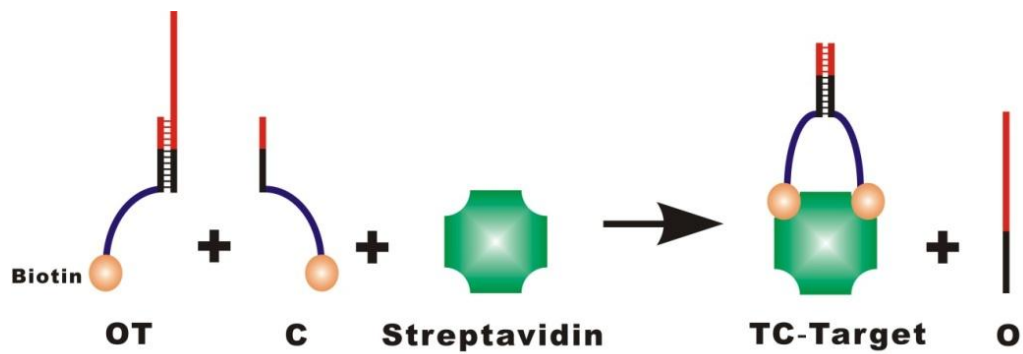


**Figure 4-2.** Schematic illustrating that the binding of streptavidin to biotinylated DNA results in binding-induced DNA assembly and strand displacement of the output DNA **O**. The supporting DNA **T** and the competing **C** were each conjugated with a biotin molecule. **T** was initially hybridized to the output DNA **O**, forming the **OT** motif. Binding of the two biotinylated DNA with the same target streptavidin molecule brought **C** in close proximity to **OT**. This process increased the local concentration of **C** drastically, and thus accelerated the strand displacement between **C** and **OT**. As a result, **O** was released from **T** as an output to trigger a following DNA assembly using the principle of toehold-mediated DNA strand displacement.

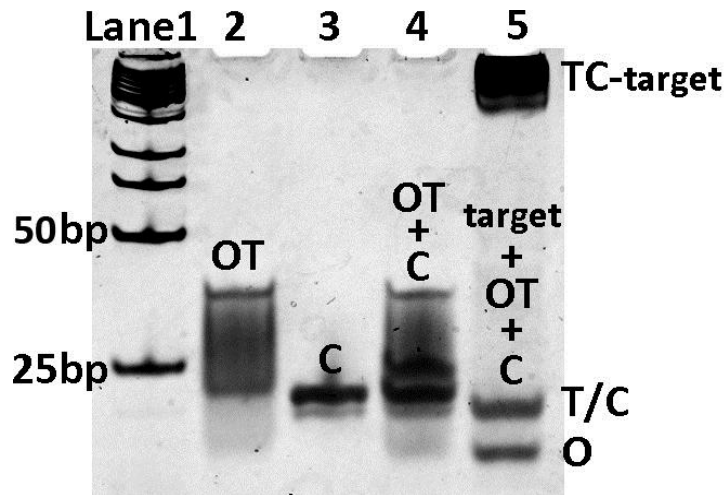


**Figure 4-3.** Native PAGE analysis of the binding-induced DNA strand displacement that release the output DNA **O** (27 n.t. in length). Lane 1 contained low molecular DNA ladder. Lane 2 contained 2  $\mu\text{M}$  **OT**. Lane 3 contained 2  $\mu\text{M}$  **C**. Lane 4 was from the analysis of a mixture containing 2  $\mu\text{M}$  **OT** and 2  $\mu\text{M}$  **C**. Lane 5 was from the analysis of a mixture containing 2  $\mu\text{M}$  **OT**, 2  $\mu\text{M}$  **C**, and 1  $\mu\text{M}$  streptavidin.

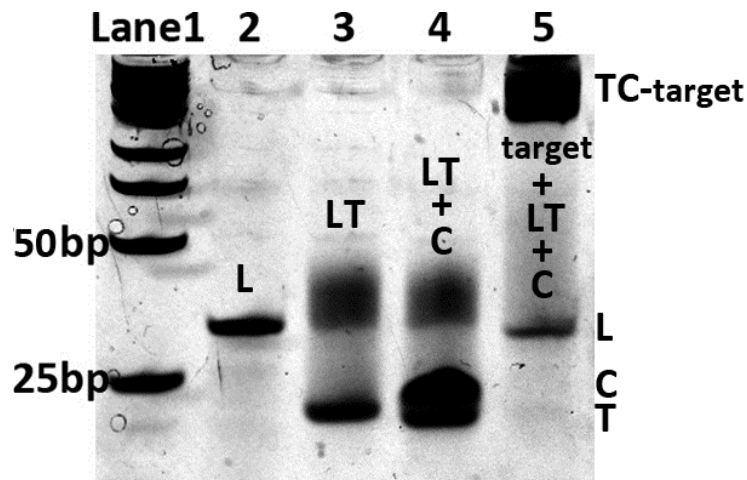


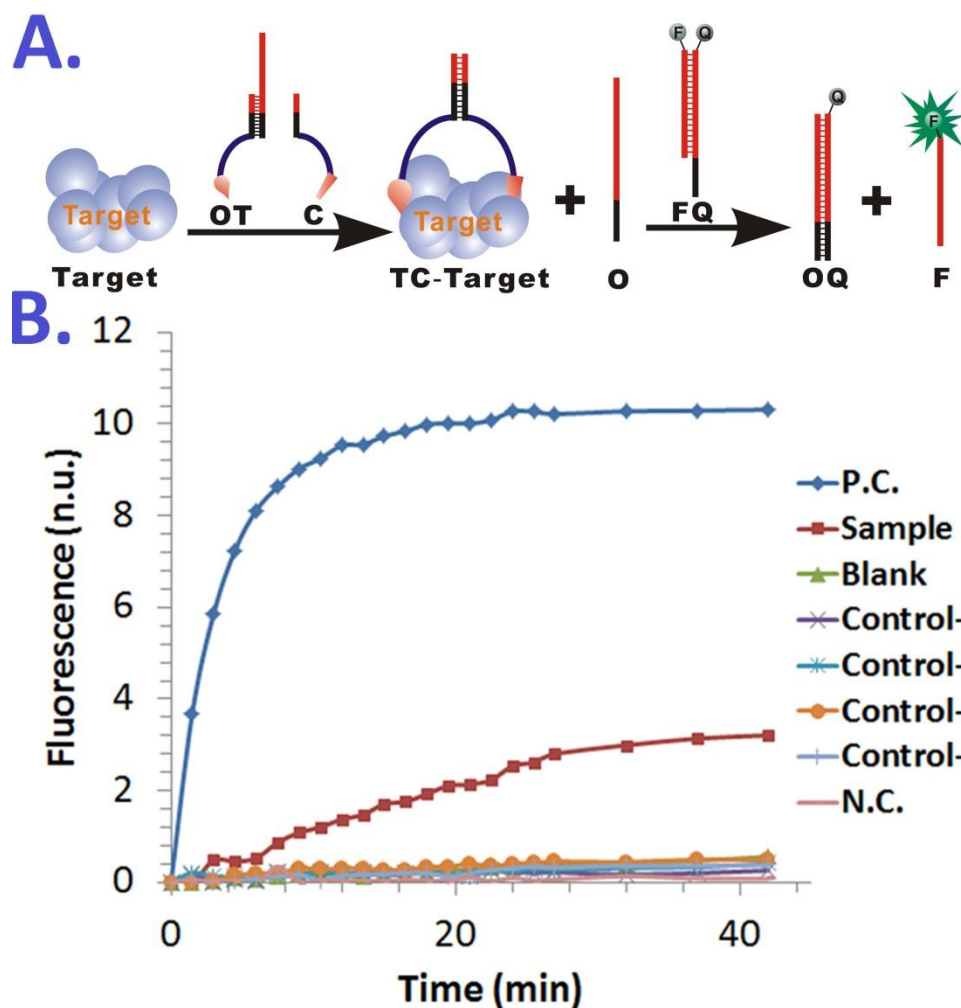
**Figure 4-4.** Native PAGE analysis of the binding-induced DNA strand displacement that release the output DNA **L** (50 n.t. in length). Lane 1 contained low molecular DNA ladder. Lane 2 contained 2  $\mu\text{M}$  **L**. Lane 3 contained 2  $\mu\text{M}$  **LT**. Lane 4 was from the analysis of a mixture containing 2  $\mu\text{M}$  **LT** and 2  $\mu\text{M}$  **C**. Lane 5 was from the analysis of a mixture containing 2  $\mu\text{M}$  **LT**, 2  $\mu\text{M}$  **C**, and 1  $\mu\text{M}$  streptavidin.

### 4.3.2 Binding-induced strand-displacement beacon

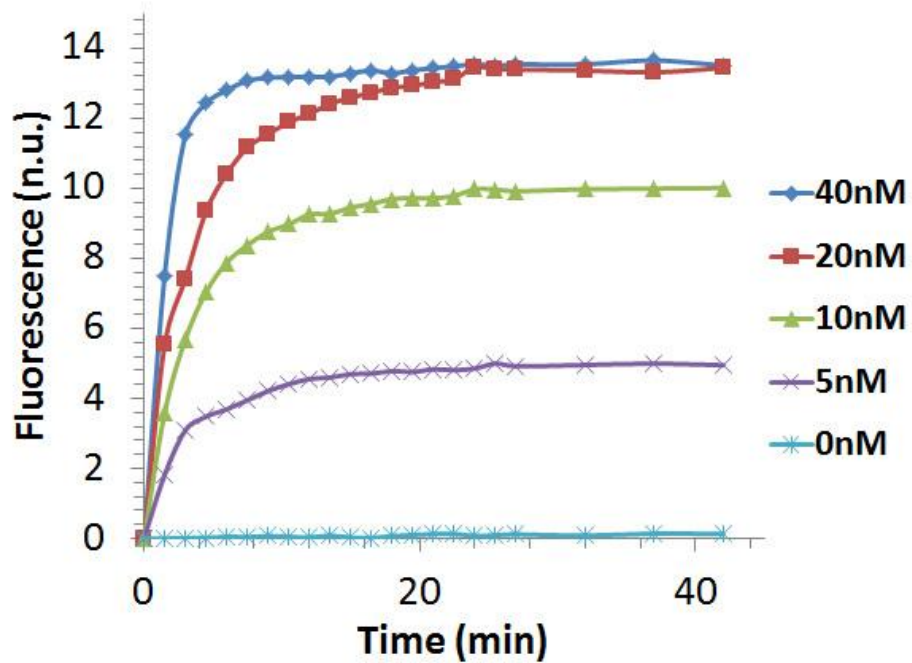
After establishing the binding-induced strand displacement strategy, we aim to demonstrate its ability to direct dynamic DNA assemblies using two examples: a strand displacement beacon<sup>4d, 7, 8</sup> and a catalytic DNA circuit.<sup>4a-4c</sup> We first combined our strategy with the toehold-mediated strand displacement beacon to construct a binding-induced DNA strand displacement beacon (binding-induced displacement beacon for short). We first designed a toehold-mediated strand displacement beacon that was able to respond to the output DNA **O** (Figure 4-5A). Briefly, two complementary DNA strands are labeled with a fluorophore (**F**) and a quencher (**Q**) respectively. **Q** is designed to have 7 nucleotides longer than **F** as a toehold part for the binding of the output DNA **O**. In the absence of **O**, stable DNA duplex is formed between **F** and **Q**, and fluorescence signal is quenched. However, in the presence of **O**, the toehold-mediated strand displacement reaction is initiated and **F** is released from **Q**, turning-on the fluorescence signal quantitatively (Figure 4-6). We further reason that if we monitor **O** instantly using the toehold-mediated strand displacement beacon, we shall be able to monitor protein bindings quantitatively by forming binding-induced displacement beacons (Figure 4-5B).

Figure 4-5B shows the fluorescence signal increase of the binding-induced displacement beacon for streptavidin as a function of time. Within a period of 45 minutes, fluorescence intensities from 10 nM streptavidin (red curve) are readily distinguishable from the blank (green curve) that contained all reagents but not the target streptavidin. To confirm that the binding-induced displacement beacon

is target specific, we tested our system using the same 10 nM streptavidin that was fully saturated with 500  $\mu\text{M}$  of free biotin (Control-1). The results are similar to those of the blank. Likewise, the absence of other components, e.g. **O** (Control-2), **C** (Control-3), or **OT** (Control-4), all give similar background fluorescence intensities to the blank. These results suggest that specific binding is the key triggering process for the binding-induced displacement beacon.



**Figure 4-5.** (A) Schematic illustrating the principle of the binding-induced strand-displacement beacon. (B) Evaluation of the binding-induced strand-displacement beacon. The fluorescence intensity was normalized in such a way that 1 normalized unit (n.u.) corresponds to 1 nM output DNA **O**. The control-1 contained the same amount of streptavidin and reagents, except that 500  $\mu$ M biotin was used to saturate all the binding sites of streptavidin. The control-2 was carried out using the same amount of streptavidin and reagents with the streptavidin sample solution, but no output DNA **O**. Similarly, the control-3 was carried out without competing DNA **C**, and the control-4 was carried out without **OT**. In the blank, all reagents were the same as streptavidin sample solution, except there was no streptavidin added. The positive control (P.C.) contained 10 nM **O** and 20 nM **FQ** in TE-Mg buffer.



**Figure 4-6.** Characterization of the toehold-mediated strand-displacement beacon that was able to respond to the output DNA **O**. The reaction mixture contained 20 nM FQ and varying concentrations of the output DNA **O**.

### 4.3.3 Estimating the conversion efficiency of the binding-induced strand-displacement beacon

After establishing the binding-induced displacement beacon, we further estimated its efficiency to quantify the target streptavidin in terms of converting target streptavidin to the output DNA **O** (conversion efficiency) at different target concentrations. Here, the conversion efficiency was calculated as ratios of the experimentally determined concentrations of **O** over their theoretical values. The experimentally determined concentrations of **O** were achieved by normalizing fluorescence intensities against the positive control. The theoretical concentrations of **O** were calculated based on the probability of each streptavidin to form the **OTC-Target** binding complex (Figure 4-7). Briefly, as the probability for each streptavidin molecule to form an effective **OTC-Target** complex is 1.25 (Figure 4-7), and each **OTC-Target** complex yields 2/3 output DNA **O** on average ( $[O] / [T]$  was optimized to be 2/3, Figure 4-8), thus the theoretical concentration of **O** equal to  $[\text{target}] \times 1.25 \times 2/3$ . By comparing the experimentally determined concentrations of **O** with their theoretical concentrations, we discovered that our binding-induced displacement beacon maintained extremely high converting efficiencies in the target concentration range of 160 pM and 10 nM (Figure 4-9). The averaged converting efficiency was calculated to be  $99.3\% \pm 7.6\%$ .

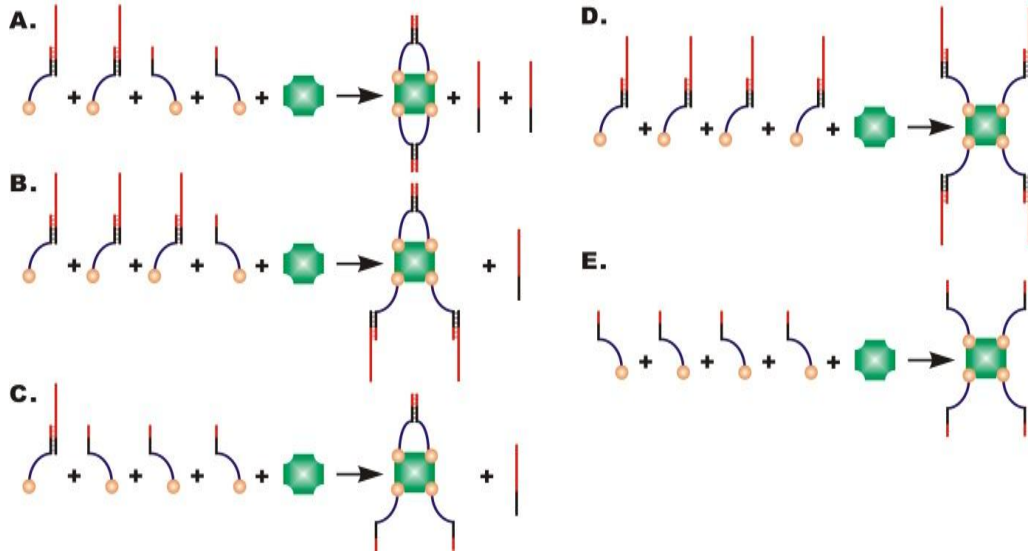


**Figure 4-7.** Schematic showing the model for calculating the theoretical concentrations of the released output DNA **O**. As each streptavidin molecule contain 4 binding sites for biotin, a maximum of 2 output DNA molecules can be released from 1 streptavidin molecule. This is achieved by having 2 **OT** duplexes and 2 **C** molecules binding to the same streptavidin molecule (e.g. shown in **A**). When 3 **OT** duplexes and 1 **C** molecule bind to the same streptavidin molecule, only 1 output DNA molecule can be released (e.g. shown in **B**). Similarly, 1 output DNA molecule can be released when 3 **C** molecules and 1 **OT** duplex bind to the same streptavidin molecule (e.g. shown in **C**). When 4 **OT** duplexes (**D**) or 4 **C** molecules (**E**) bind to the same streptavidin molecule, no output DNA can be released. As each streptavidin have 4 binding sites, so there are 16 possible binding complexes in total. Based on the frequencies of each type of binding structures shown in A to E, the determined possibility for each streptavidin molecule to form one effective binding complex that can result in the release of one output DNA molecule is 1.25.

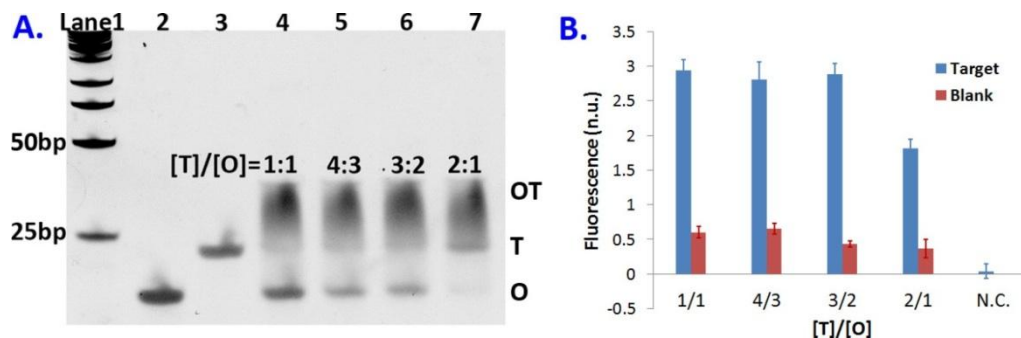


**Figure 4-8.** Optimization of the ratio between **T** and **O**. (A) Characterization of **OT** using PAGE. Lane 1 contained low molecular DNA ladder. Lane 2 contained 2  $\mu\text{M}$  **O**. Lane 3 contained 2  $\mu\text{M}$  **T**. Lane 4 contained a mixture of 2  $\mu\text{M}$  **T** and 2  $\mu\text{M}$  **O**. Lane 5 contained a mixture of 2  $\mu\text{M}$  **T**, 1.5  $\mu\text{M}$  **O**. Lane 6 contained a mixture of 2  $\mu\text{M}$  **T** and 1.3  $\mu\text{M}$  **O**. Lane 7 contained a mixture of 2  $\mu\text{M}$  **T** and 1  $\mu\text{M}$  **O**. (B) Characterization of **OT** using binding-induced displacement beacon. The streptavidin test solutions contained 10 nM streptavidin, 10 nM **C**, 10 nM **QF**, and **OT** with varying ratios. Different ratios between **T** and **O** were achieved by fixing the concentration of **T** at 10 nM and tuning the concentrations of **O**. Error bars represent one standard deviation from duplicated analyses.

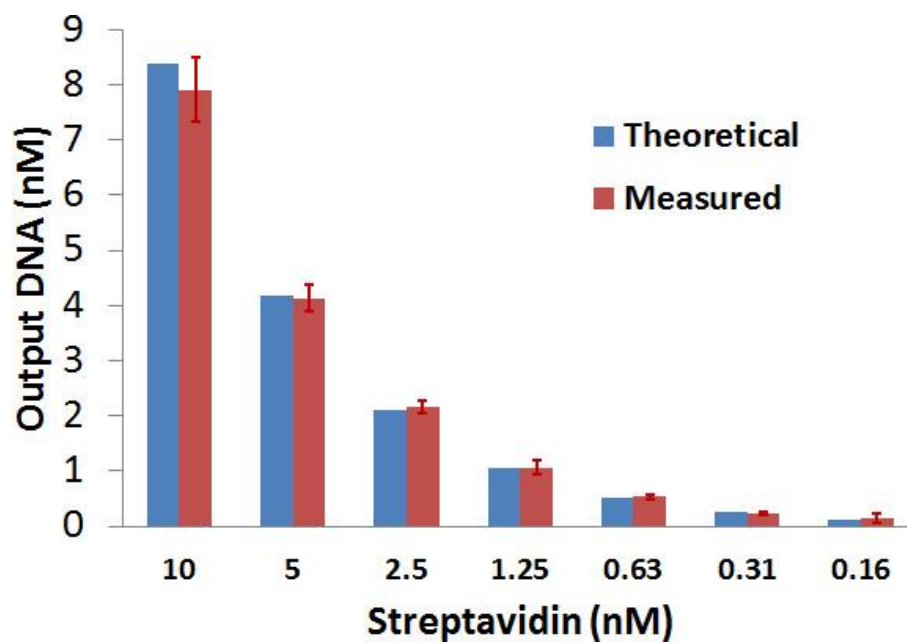


**Figure 4-9.** Estimation of the conversion efficiency from the target streptavidin to the output DNA **O** at different streptavidin concentrations through the binding-induced strand-displacement beacon. The streptavidin test solutions contained 20 nM **OT**, 20 nM **C**, 20 nM **QF**, and varying concentrations of streptavidin. Error bars represent one standard deviation from duplicate analyses.

#### 4.3.4 Minimizing the target-independent displacement by tuning the length of DNA probes

The success of designing binding-induced displacement beacon shows the potential of our binding-induced DNA strand displacement strategy to direct dynamic DNA assemblies. However, we noticed an increasing background fluorescence signal from the blank after long time incubation (Figure 4-10B), indicating the nonspecific release of the output DNA from the target-independent strand displacement. Elimination of the nonspecific release of the output DNA is of great importance to direct many dynamic DNA assemblies with high structural complexities, e.g. catalytic DNA circuit,<sup>4a-4c</sup> because long time incubation steps are commonly involved in those assemblies. Thus to meet those requirements and expand our binding-induced strand displacement strategy to more dynamic DNA assembly systems, we optimized our strategy by tuning the length of complementary part of **OT** and **C**. This optimization is based on the previous discovery that increasing the length of DNA duplex could slow down the rate of strand exchange reactions drastically,<sup>6</sup> which can potentially be used here to minimize target independent displacement. We then monitored the performance of different designs using the binding-induced displacement beacon.

As shown in Figure 4-10A and 4-10B, in the presence of 10 nM streptavidin, the fluorescence intensities did decrease as we increased the length of **OT** and **C** correspondingly from 12 nt to 16 nt. For example, at  $t = 45$  min, negligible background fluorescence was observed for **OT** and **C** with lengths of 14 nt and 16 nt (Figure 4-10A). However, after incubating the reaction mixture for 150 minutes, background was still noticeable for all three designs (Figure 4-10B),

indicating that nonspecific release of output DNA **O** from the target-independent binding-induced strand displacement could not be ignored after a long incubation time. To eliminate the target-independent displacement completely, we fixed the competing DNA **C** to be 12 nt in length, and increased duplex length of **OT** from 12 nt to 20 nt. In principle, shorter competing DNA is thermodynamically unfavored to displace a longer DNA strand, and thus should be able to suppress nonspecific release of **O** even after a long incubation time. Indeed, we found in Figure 4-10C and 4-10D that the nonspecific displacement was eliminated completely even after 150 minutes as soon as we increased duplex length by 2 nt. However, longer duplexes also lead to lower specific signal intensities. To maximize signal-to-background, we chose a 2-nt difference between **OT** (14 nt) and **C** (12 nt). We also examined this optimized condition with PAGE (Figure 4-11), and found that no output DNA **O** band appeared on the gel without target molecule (Lane 4), while strong **O** band appeared with target (Lane 5). This result further confirmed that we were able to completely eliminate the nonspecific release of **O** by this design.

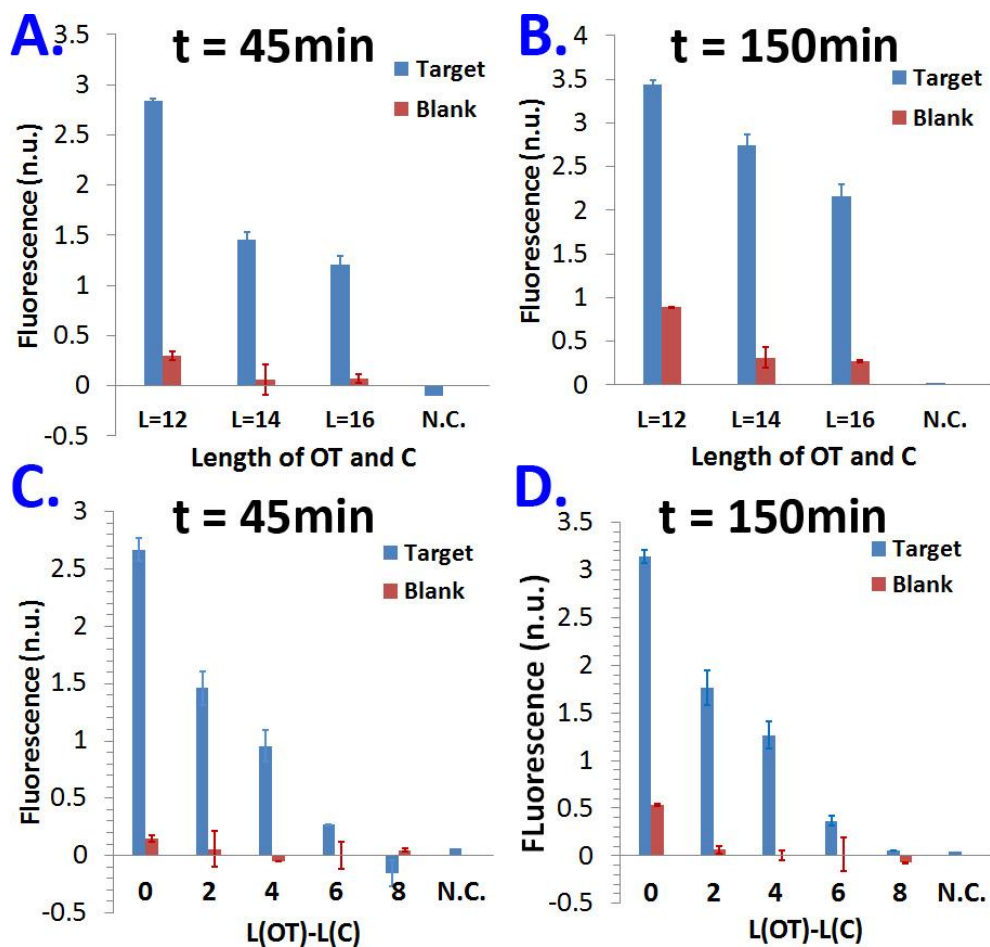


**Figure 4-10.** Optimization of the binding-induced DNA strand-displacement strategy to minimize the target-independent strand displacement. Streptavidin test solutions contained 5 nM streptavidin, 10 nM OT, 10 nM C, and 20 nM FQ. In the blank, all reagents were the same as streptavidin sample solution, except there was no streptavidin added. Effects of simultaneous increases in the length of both OT and C on the performance of the binding-induced strand displacement were monitored at 45 min (A) and 150 min (B). Effects of the length difference between OT and C were also monitored at 45 min (C) and 150 min (D). Error bars represent one standard deviation from duplicated analyses.

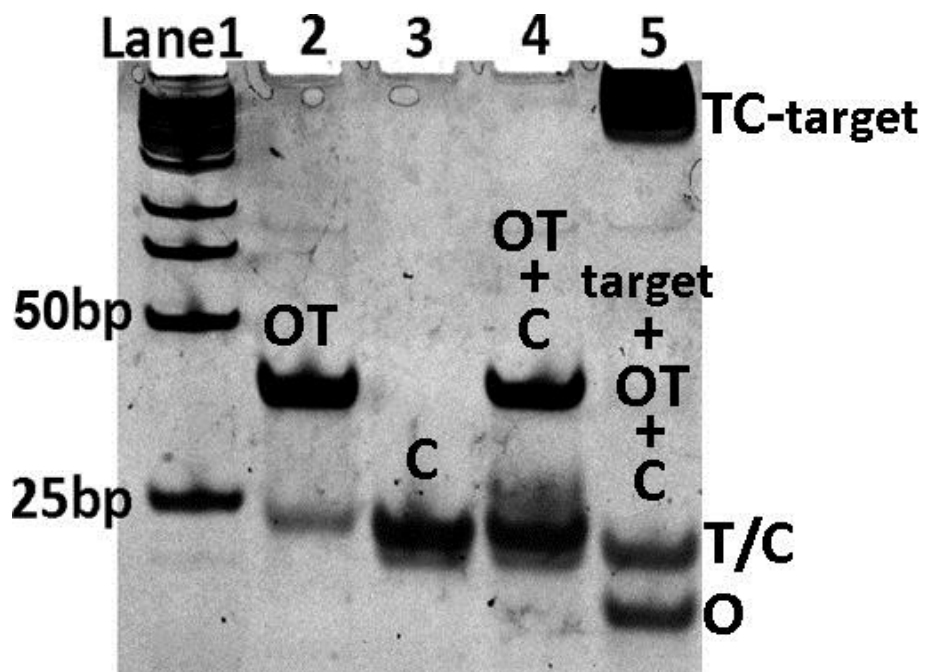


**Figure 4-11.** Native PAGE characterization of the binding-induced DNA strand-displacement strategy that is able to eliminate the target-independent displacement. The **OT** probe used in this experiment was 14 bp in length, and competing DNA **C** was 12 nt in length. Lane 1 contained low molecular DNA ladder. Lane 2 contained 2  $\mu\text{M}$  **OT**. Lane 3 contained 2  $\mu\text{M}$  **C**. Lane 4 was from the analysis of a mixture containing 2  $\mu\text{M}$  **OT** and 2  $\mu\text{M}$  **C**. Lane 5 was from the analysis of a mixture containing 2  $\mu\text{M}$  **OT**, 2  $\mu\text{M}$  **C**, and 1  $\mu\text{M}$  streptavidin.

#### 4.3.5 Binding-induced catalytic DNA circuit

Upon eliminating the target-independent displacement, we design here a binding-induced catalytic DNA circuit to demonstrate the ability of our strategy to direct dynamic DNA assemblies with high structural complexity. To achieve this goal, we combined our strategy to the double hairpin based toehold-mediated catalytic DNA circuit (toehold-mediated catalytic DNA circuit for short). The principle of our binding-induced catalytic DNA circuit strategy is shown in Figure 4-12A: a pair of DNA hairpins (**H1** and **H2**) is designed to be potentially able to partially hybridize to each other. However, the spontaneous hybridization between **H1** and **H2** is kinetically hindered by caging complementary regions in the stem parts of the hairpins. In the presence of the target molecule, the output DNA **O** is released by the binding-induced strand displacement reaction, and opens the stem part of **H1** by the principle of the toehold-mediated activation. The newly exposed sticky end of **H1** nucleates at the sticky end of **H2** and triggered another strand-displacement reaction to release **O**. Thus **O** is able to act as a catalyst to trigger the formation of other **H1-H2** complexes. By coupling to a toehold-mediated displacement beacon, the detection signal can be amplified during the process.

To test the signal amplification ability of our binding-induced DNA circuit, we monitored the fluorescence intensity increase as a function of time over a period of 4 hours. As shown in Figure 4-12B, the final fluorescence intensity generated from 10 nM streptavidin is close to 100 normalized units, which corresponds to 100 nM positive DNA (**P**), and almost no background fluorescence signal was observed for the blank. Comparing to toehold-mediated catalytic DNA circuit triggered directly by the output DNA **O** (the red curve in Figure 4-12B),

the binding-induced catalytic DNA circuit (the green curve in Figure 4-12B) demonstrated comparable signal amplification capability. Furthermore, the measured fluorescence intensities are responsive to the concentrations of streptavidin in the range of 10 pM to 10 nM, providing the quantification capability (Figure 4-12C). We estimated from the standard curve in Figure 6C that the final fluorescence signal has been amplified over 10-fold throughout this concentration range.

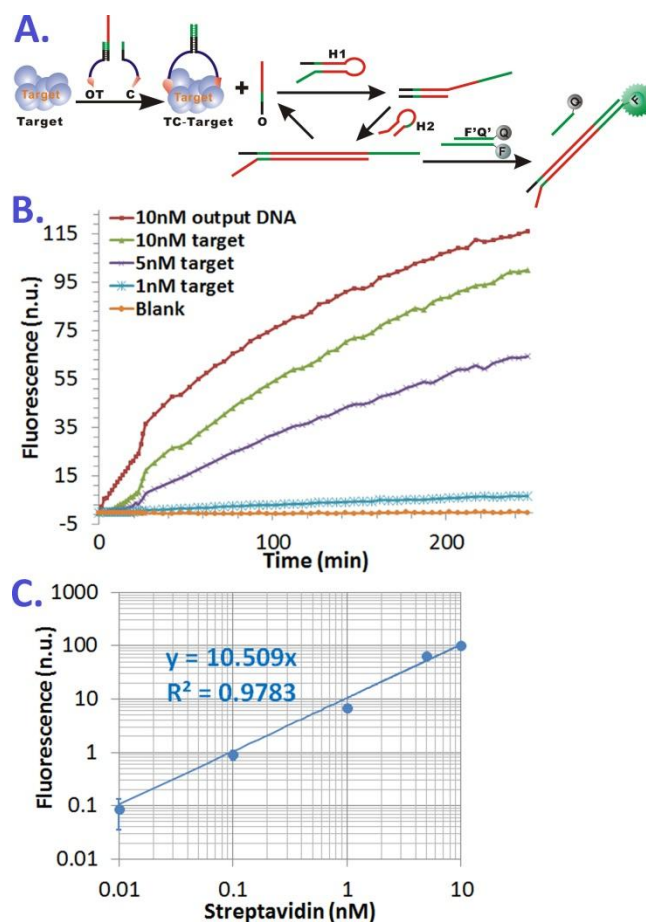


**Figure 4-12.** (A) Schematic illustrating the principle of the binding-induced catalytic DNA circuit. (B) Evaluation of the binding-induced catalytic DNA circuit. The fluorescence intensity was normalized in such a way that 1 normalized unit (n.u.) corresponds to 1 nM positive DNA **P**. An output DNA test solution contained 10 nM output DNA **O**, 125 nM **H1**, 200 nM **H2**, and 125 nM **F'Q'**. Streptavidin test solutions contained 20 nM **OT**, 20 nM **C**, 125 nM **H1**, 200 nM **H2**, 125 nM **F'Q'**, and varying concentrations of streptavidin. In the blank, all reagents were the same with streptavidin test solutions, except there was no streptavidin added. (C) Increases in fluorescence intensity reflect increasing concentrations of streptavidin that converts to positive DNA **P** by the binding-induced catalytic DNA circuit. The magnitude of amplification was determined by the linearly fitting between fluorescence intensity and concentration of streptavidin. Error bars represent one standard deviation from duplicated analyses.

## **4.4 Conclusions**

We have successfully developed a binding-induced DNA strand-displacement strategy that can work at room temperature with high conversion efficiency and low background. Our success in constructing the binding-induced displacement beacon and binding-induced catalytic DNA circuit demonstrated the power and potential of our strategy to direct dynamic DNA assemblies that are able to respond to the protein bindings. The concept and strategies we developed in this work show their potentials to further expand the existing dynamic nanotechnology to proteins for different applications. For example, both systems we developed here can potentially be applied as point-of-care diagnostic tools for proteins with unique enzyme-free and room-temperature signal generation or amplification capabilities.

## 4.5 References

1. (a) Seeman, N. C. *J. Theor. Biol.* **1982**, *99*, 237-247. (b) Winfree, E.; Liu, F.; Wenzler, L. A.; Seeman, N. C. *Nature* **1998**, *394*, 539-544; (c) Aldaye, F. A.; Palmer, A. L.; Sleiman, H. F. *Science* **2008**, *321*, 1795-1799; (d) Douglas S. M.; Dietz, H.; Liedl, T.; Hogberg, B.; Graf, F.; Shih, W. M. *Nature* **2009**, *459*, 414-418; (e) Wei, B.; Dai, M.; Yin P. *Nature* **2012**, *485*, 623-627. (f) Zhang, D. Y.; Seelig, G. *Nat. Chem.* **2011**, *3*, 103-113; (g) Pinheiro, A. V.; Han D.; Shih, W. M.; Yan, H. *Nat. Nanotech.* **2011**, *6*, 763-772.
2. Venkataraman, S.; Dirks, R. M.; Ueda, C. T.; Pierce, N. A. *Proc. Natl. Acad. Sci. U. S. A.* **2010**, *107*, 16777-16782.
3. (a) Douglas, S. M.; Bachelet, I.; Church, G. M. *Science* **2012**, *335*, 831-834; (b) Jiang, Q.; Song C.; Nangreave, J.; Liu, X.; Lin, L.; Qiu, D.; Wang, Z-G.; Zou, G.; Liang, X.; Yan, H.; Ding, B. *J. Am. Chem. Soc.* **2012**, *134*, 13396-13403.
4. (a) Yin, P.; Choi, H. M. T.; Calvert, C. R.; Pierce, N. A. *Nature* **2008**, *451*, 318-323; (b) Li, B.; Ellington, A. D.; Chen, X. *Nucleic Acids Res.* **2011**, *39*, e110; (c) Qian, L.; Winfree, E. *Science* **2011**, *332*, 1196-1200; (d) Picuri, J. M.; Frezz, B. M.; Ghadiri, M. R. *J. Am. Chem. Soc.* **2009**, *131*, 9368-9377; (e) Liao, S.; Seeman, N. C. *Science* **2004**, *306*, 2072-2074; (f) Surana, S.; Bhat, J. M.; Koushika, S. P.; Krishnan, Y. *Nature Commun.* **2011**, *2*, 340; (g) Modi, S.; Swetha, M. G.; Goswami, D., Gupta, G. D., Mayor, S., Krishnan, Y. *Nat. Nanotechnol.* **2009**, *4*, 325-330; (h) Seferos, D. S.; Giljohann, D. A.; Hill, H. D.; Prigodich, A. E.; Mrikin, C. A. *J. Am. Chem. Soc.* **2007**, *129*, 15477-15479; (i) Lin, C.; Liu, Y.; Yan, H. *Nano Lett.* **2007**, *7*, 507-512; (j)

- Pei, H.; Liang, L.; Yao, G.; Li, J.; Huang, Q.; Fan, C. *Angew. Chem. Int. Ed.* **2012**, *51*, 9020-9024.
5. (a) Xing, Y.; Yang, Z.; Liu, D. *Angew. Chem. Int. Ed.* **2011**, *50*, 11934-11936;  
(b) Dirks, R. M.; Pierce, N. A. *Proc. Natl. Acad. Sci. U. S. A.* 2004, *101*, 15275-15278; (c) Zhang, D.; Seferos, D. S.; Giljohann, D. A.; Patel, P. C.; Mirkin, C. A. *Nano Lett.* **2009**, *9*, 3258-3261.
6. Reynaldo, L. P.; Vologodskii, A. V.; Neri, B. P. *J. Mol. Biol.* **2000**, *297*, 511-520.
7. Li, Q.; Luan, G.; Guo, Q.; Liang, J. *Nucleic Acids Res.* **2002**, *30*, e5.
8. Zhang, D. Y.; Chen, S. X.; Yin, P. *Nat. Chem.* **2012**, *4*, 208-214.

# Chapter Five: Binding-Induced Molecular Translator for Homogeneous Protein Assays<sup>4</sup>

## 5.1 Introduction

Having established the binding-induced DNA strand-displacement strategy to expand the dynamic DNA assembly systems to proteins, I aimed to apply this technique to construct a binding-induced molecular translator that could be directly used for homogeneous bioassays.

Molecular translation of the input target molecule into a unique output DNA to trigger the subsequent DNA assembly is one of the key steps to achieve the specific detection of the target molecule with the assembled DNA nanostructures/devices.<sup>1</sup> Many efforts have been made to design and improve the molecular translators based on nucleic acids.<sup>1,2</sup> For example, Ghadiri and co-workers have designed universal molecular translators that were able to convert any target nucleic acids to a pre-designed output DNA for signal generation.<sup>3</sup> This was based on the previous discovery that DNA strand exchange reactions can be accelerated by  $10^6$  fold using toehold-mediated strand-displacement.<sup>4</sup> Turberfield and co-workers have shown that DNA toehold placed a few nucleotides away from the displaced strand could also be used to accelerate the strand-displacement reaction, suggesting its potential to be used as control for molecular translators.<sup>5</sup> By incorporating structure-switching aptamers to such molecular translators, Liu and co-workers were able to use small molecules e.g. adenosine, to trigger changes in DNA structures.<sup>6</sup> Until now, applications of such molecular translators

---

<sup>4</sup> This chapter has been published in Li, F.; Zhang, H.; Lai, C.; Li, X.-F.; Le, X. C. *Angew. Chem. Int. Ed.* **2012**, *51*, 9317-9320.

have been limited to nucleic acids and a few small molecules. It remains a challenge to apply the technique to proteins. In this chapter, I will describe a binding-induced molecular translator that is constructed based on the principle of the binding-induced strand displacement and demonstrate its application to assay for proteins.

## **5.2 Experimental**

### **5.2.1 Materials and reagents**

Solution of gold nanoparticles (AuNPs) (20 nm in diameter,  $7.0 \times 10^{11}$  AuNPs per mL) was obtained from Ted Pella (Redding, CA). Streptavidin from *Streptomyces avidinii* (product number, S4762), biotin (product number, B4501), bovine serum albumin (BSA), human serum albumin (HSA), human lysozyme, human IgG, o-(2-carboxyethyl)-o'-(2-mercaptoethyl) heptaethylene glycol (SH-PEG), and tris (2-carboxyethyl) phosphine hydrochloride (TCEP) were obtained from Sigma. Recombinant human platelet derived growth factor BB (PDGF-BB) was purchased from R&D Systems (Minneapolis, MN). Human  $\alpha$ -thrombin was purchased from Haematologic Technologies Inc. (Essex Junction, VT). All DNA samples were purchased from Integrated DNA Technologies (Coralville, IA) and purified by HPLC. The DNA sequences and modifications are listed in Table 5-1 and Table 5-2. Phosphate buffered saline (PBS) 10 $\times$  solution and Tween20 were purchased from Fisher Scientific. NANOpure H<sub>2</sub>O (>18.0 M $\Omega$ ), purified using an Ultrapure Milli-Q water system, was used for all experiments.

**Table 5-1.** DNA sequences for constructing the binding-induced molecular translator for streptavidin.

| DNA name       |     | Sequences  |
|----------------|-----|--|
| DNA-1          |     | 5'-SH-TTT TTT TTT TTT TTT <b>GTC GTG GGT CTT</b> TTT TTT<br>TTT TTT TTT TTT TTT TT-Biotin-3' |
| DNA-3          |     | 5'- <b>AGA CCC ACG ACT</b> TTT T-TAMRA-3'  |
| DNA-2          | L9  | 5'-Biotin-TTT TTT TTT TTT TTT TTT TTT TTT TTT TTA<br><b>CCC ACG AC-3'</b>                    |
|                | L8  | 5'-Biotin-TTT TTT TTT TTT TTT TTT TTT TTT TTT TTA<br><b>CCC ACG A-3'</b>                     |
|                | L7  | 5'-Biotin-TTT TTT TTT TTT TTT TTT TTT TTT TTT TTA<br><b>CCC ACG-3'</b>                       |
| Blocking oligo | B10 | 5'-GGG TAA AAA A-3'  |
|                | B11 | 5'-GGG TAA AAA AA-3'   |
|                | B12 | 5'-GGG TAA AAA AAA-3'  |

**Table 5-2.** DNA sequences for constructing the binding-induced molecular translator for PDGF-BB. The sequence highlighted in orange color is aptamer known to bind PDGF-BB.

|                 | DNA name            | Sequences  |
|-----------------|---------------------|--|
| <b>Design-1</b> | DNA-1               | 5'-SH-TTT TT <b>GTC GTG GGT CTT TTT TTT TTT TTT</b><br><b>TTT TTT TT <u>ACT CAG GGC ACT GCA AGC AAT TGT</u></b><br><u>GGT CCC AAT GGG CTG AGT A-3'</u>       |
|                 | DNA-2               | 5'-TTT <u>ACT CAG GGC ACT GCA AGC AAT TGT GGT</u><br><u>CCC AAT GGG CTG AGT ATT TTT TTT TTT TTT</u><br><b>TTT TTT TTA CCC ACG ACT TT-3'</b>                  |
|                 | DNA-3               | 5'-AGA CCC ACG ACT TTT T-TAMRA-3'  |
| <b>Design-2</b> | DNA-1               | 5'-SH-TTT TT <b>GTC GTG GGT CTT TTT-3'</b>   |
|                 | DNA-2               | 5'-TTT <u>ACT CAG GGC ACT GCA AGC AAT TGT GGT</u><br><u>CCC AAT GGG CTG AGT ATT TTT TTT TTT TTT</u><br><b>TTT TTT TTA CCC ACG ACT TT-3'</b>                  |
|                 | DNA-3               | 5'-AGA CCC ACG ACT TTT T/36-TAMSp/-3'  |
|                 | Immobilized aptamer | 5'-SH-TTT TTT <u>ACT CAG GGC ACT GCA AGC AAT</u><br><u>TGT GGT CCC AAT GGG CTG AGT A-3'</u>  |
| <b>Design-3</b> | DNA-1               | 5'-Quencher-TTT TT <b>GTC GTG GGT CTT TTT TTT</b><br><b>TTT TTT TTT TTT TT <u>ACT CAG GGC ACT GCA AGC</u></b><br><u>AAT TGT GGT CCC AAT GGG CTG AGT A-3'</u> |
|                 | DNA-2               | 5'-TTT <u>ACT CAG GGC ACT GCA AGC AAT TGT GGT</u><br><u>CCC AAT GGG CTG AGT ATT TTT TTT TTT TTT</u><br><b>TTT TTT TTA CCC ACG ACT TT-3'</b>                  |
|                 | DNA-3               | 5'-AGA CCC ACG ACT TTT T-TAMRA-3'  |

### 5.2.2 Construction of binding-induced molecular translator

To construct the binding-induced molecular translator, functional DNA oligonucleotides were conjugated to AuNPs through thiolated gold bond. Briefly, the thiolated DNA-1 was annealed to the output DNA-3 at 1: 1 ratio first by heating at 70 °C for 5 min and then slowly cooling down to room temperature over 2 hours. Then the duplex was treated with 100 μM TCEP for 1 hr at room temperature to reduce the disulfide bond. This solution was then added to 1 mL of 1 nM AuNP solution, and the mixture was placed at room temperature for 12 hrs. To this mixture was slowly added 20 μL of 3 M NaCl, and followed by 10 seconds of sonication. This process of addition of NaCl and sonication was repeated for 5 times with 1 hour interval, to maximize the oligonucleotide loading amounts. The solution was then incubated at room temperature for 24 hrs. To yield a more stable conjugate, DNA-AuNPs were further treated with 120 μM of SH-PEG for 2 hrs to passivate the active surface of AuNPs. Then the final solution was centrifuged at 13,500 rpm for 30 min to separate the AuNPs from the unreacted reagents. The DNA-AuNPs were washed 3 times with 0.5 × PBS buffer (pH 7.4) containing 0.01% Tween20, and finally redispersed in this PBS buffer.

Absorption spectra (from 400 nm to 700 nm) of DNA-AuNPs were obtained using a Lambda 35 UV/Vis absorption spectrophotometer (Perkin Elmer). The number of fluorescently labelled output DNA loaded on each AuNP was established by measuring the concentrations of AuNPs and fluorescent DNA duplex in each sample. For their typical uses as binding-induced molecular translators, DNA duplexes were loaded maximally on AuNPs, and this loading amount was measured to be 80 DNA molecules per AuNP on average.

### 5.2.3 Monitoring binding-induced molecular translator by a fluorescence turn-on assay

The performance of binding-induced molecular translator was assessed by using a fluorescence turn-on assay. For a typical assay, the reaction mixture contained 500 pM DNA-AuNPs (final output DNA-3 concentration was adjusted to be 40 nM), 40 nM competing DNA-2, 1  $\mu$ M blocking oligo, varying concentrations of the target protein, and 1  $\times$  PBS buffer containing 1 mM MgCl<sub>2</sub> and 0.05% BSA (pH 7.4). The reaction mixture was incubated at 37  $^{\circ}$ C for 30 min and then 25  $^{\circ}$ C for one hour in a 384 microplate. Fluorescence was measured directly from the microplate using a multi-mode microplate reader with excitation at 535 nm and emission at 595 nm. Fluorescence measurements were taken before and after the incubation. Relative fluorescent intensity  $I_R$  was defined as  $I_R = (F - F_0)/F_0$ , where  $F$  is the fluorescent intensity of each sample after incubation,  $F_0$  is the background fluorescent intensity measured before incubation.

To monitor the kinetic process of molecular translation, the reaction mixtures were placed in a real-time PCR instrument and the temperature program was 25  $^{\circ}$ C for the initial 30 min, followed by 37  $^{\circ}$ C for another 30 min, and finally 25  $^{\circ}$ C for 60 min. Fluorescence of reaction mixtures were detected at the following time points with respect to incubation: 0 min, 30 min, 45 min, 60 min, 65 min, 90 min and 120 min, corresponding to the incubation temperature of 25  $^{\circ}$ C, 25  $^{\circ}$ C, 37  $^{\circ}$ C, 37  $^{\circ}$ C, 25  $^{\circ}$ C, 25  $^{\circ}$ C, and 25  $^{\circ}$ C, respectively.

#### **5.2.4 Detection of PDGF-BB using binding-induced molecular translator**

To assay for PDGF-BB, a sample (or standard solution of PDGF-BB) was incubated in a 50-  $\mu$ L reaction mixture containing 500 pM DNA-AuNP probes, 50 nM competing DNA-2 probes, 1  $\mu$ M blocking DNA and 1 $\times$  PBS buffer containing 1mM MgCl<sub>2</sub> and 0.05% BSA (pH 7.4). The reaction mixtures were held in a 384 microplate, and the incubation temperatures were 37  $^{\circ}$ C for the initial 30 min and then 25  $^{\circ}$ C for one hour. Fluorescence was detected with a multi-mode microplate reader directly from the 384 microplate, before and after the incubation.

To test the specificity of the assay for PDGF-BB, four other human proteins were analyzed separately, using the same procedure as for the PDGF-BB (Figure S10). The test proteins included human serum albumin (HSA), IgG, lysozyme, and  $\alpha$ -thrombin. Their concentrations were 1  $\mu$ M, 40 times higher than the concentration of PDGF-BB used in the test (25nM).

#### **5.2.5 Estimation of melting temperatures for designing binding-induced molecular translator**

Melting temperatures ( $T_m$ ) of the designed duplexes were estimated using Oligo Analyzer (free software from IDT). Under our experimental conditions,  $T_m$  of the DNA-1/DNA-3 duplex was 40.2  $^{\circ}$ C.  $T_m$  of the duplex between DNA-2 (e.g. L9) and DNA-1 was 32.4  $^{\circ}$ C. However, upon the target binding that assembled DNA-2 and DNA-1 to form a loop (Figure S1),  $T_m$  of the DNA-2/ DNA-1 duplex in the assembly form was increased to 56.4  $^{\circ}$ C. This  $T_m$  value was estimated by considering the binding-induced DNA assembly as a DNA hairpin structure with

9 complementary base pairs as the stem and 100 dNTP as the loop. This loop length (100 dNTP) was chosen for  $T_m$  estimation because of its similar size to that of the affinity complex. The blocking oligos were designed to partially hybridize on competing DNA-2, with  $T_m$  of 30.8 °C for block B10, 34.6 °C for B11, and 37.8 °C for B12.

## **5.3 Results and discussion**

### **5.3.1 Experimental Design**

Our strategy is illustrated in Figure 5-1. The binding-induced molecular translator is composed of target recognition and signal output elements. Target recognition was achieved by two specific affinity ligands binding to the target protein. One affinity ligand is linked to DNA-1 (blue color in Figure 5-1) and is conjugated to a gold nanoparticle (AuNP) that serves as the scaffold for the molecular translator. The second affinity ligand is conjugated to DNA-2 (red) that serves as the competing DNA. An output DNA (DNA-3, green) is initially hybridized to DNA-1 to form a stable DNA-1/DNA-3 duplex. The three DNA sequences are designed in such a way that the complementary sequences between DNA-1 and DNA-3 are 2-4 n.t. longer than the complementary sequences between DNA-1 and DNA-2. Thus, in the absence of the molecular target and the absence of affinity binding, displacement of output DNA-3 by competing DNA-2 is minimum. However, in the presence of the target molecule, the binding of the target molecule to the two affinity ligands that are linked to DNA-1 and DNA-2 brings DNA-2 to close proximity to DNA-1/DNA-3 duplex. This binding-induced assembly of DNA-2 around the AuNP scaffold greatly increases the local

concentration of DNA-2 and accelerates the strand displacement reaction between DNA-2 and DNA-3. As a consequence, the output DNA-3 is released from the scaffold. The subsequent detection signal can be generated by directly monitoring the displaced output DNA-3 or by using the output DNA to trigger further DNA assembly.

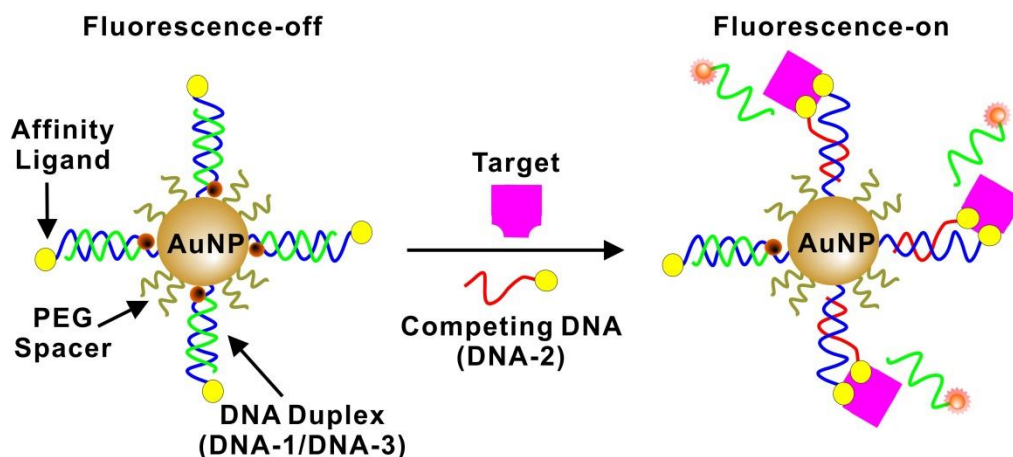


**Figure 5-1.** Schematic illustrating the principle of the binding-induced molecular translator. The molecular translator is composed of a DNA-1 (blue) functionalized gold nanoparticle scaffold and a competing DNA (DNA-2, red), both of which are conjugated to a specific affinity ligand for the target recognition. A fluorescently labelled output DNA-3 (green) is initially hybridized to DNA-1 and is assembled on the AuNP scaffold, resulting in fluorescence being quenched by AuNP. Binding of the two affinity ligands to the same target assembles DNA-2 onto the AuNP scaffold, and thus triggers an internal strand displacement between DNA-2 and DNA-3. Release of the output DNA-3 from the duplex and from AuNP scaffold turns on fluorescence.

### 5.3.2 Binding-induced molecular translator for streptavidin

To test the feasibility of our strategy, we first designed a molecular translator for streptavidin using biotin as the affinity ligand (Figure 5-2). DNA-1 and DNA-2 are each conjugated to a biotin molecule. Output DNA-3 is labelled with a fluorescent dye, tetramethylrodamine (TAMRA), and its 11 n.t. sequence is complementary to DNA-1. Hybridization of DNA-3 to DNA-1 results in fluorescence quenching of the dye by AuNP. Thus, in the absence of the target molecule, the fluorescence of the system is “off”. In the presence of the target molecule (streptavidin), binding of streptavidin to the biotinylated DNA-1 and DNA-2 brings competing DNA-2 onto the AuNP scaffold, enhancing competition of DNA-2 with DNA-3. The binding-induced assembly increases the local concentration of DNA-2 and accelerates the strand displacement kinetics. The displaced output DNA-3 is released from the AuNP scaffold and the fluorescence is turned “on”. By measuring the fluorescent signal from the output DNA-3, we are able to assess the performance of the binding-induced molecular translator.

Figure 5-3 shows fluorescence intensities of the output DNA-3 as a result of the binding-induced molecular translation process. Fluorescence intensities from 10 nM streptavidin are readily distinguishable from the blank that contained all reagents but not the target streptavidin (Figure 5-3A). The measured fluorescence intensities are responsive to the concentration of streptavidin in the range of 100 pM and 25 nM (Figure 5-3B), providing quantitative capability.

To confirm that the binding-induced translation is a target specific process, we tested our system using the same 10 nM concentration of streptavidin that was fully saturated with 500  $\mu$ M biotin (Control 1 in Figure 5-3A). The results are

similar to those of the blank. Likewise, the absence of the competing DNA-2 (Control 2 in Figure 5-3A) gives rise to background fluorescence intensity similar to blank. These results suggest that specific binding is the key triggering process for the successful binding-induced molecular translation strategy.

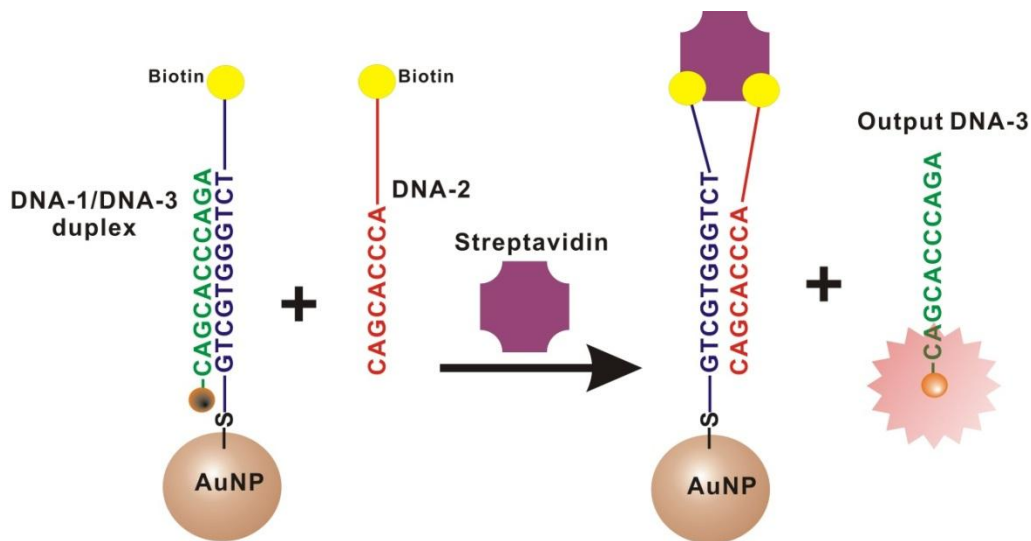


**Figure 5-2.** Schematic showing that the binding of streptavidin to biotinylated DNA results in a stable binding-induced DNA assembly and strand displacement of fluorescent output DNA. DNA-1 and DNA-2 were each conjugated to a biotin molecule. DNA-1 was initially hybridized to the output DNA-3 that was labelled with a fluorescent dye, tetramethylrodamine (TAMRA). The fluorescence from the TAMRA was initially quenched by AuNP. Binding of the two biotinylated DNA (DNA-1 and DNA-2) to the same streptavidin assembled DNA-2 onto the AuNP scaffold, and thus triggered an internal strand displacement between DNA-2 and DNA-3. As a result, TAMRA-labelled output DNA-3 was released from AuNP scaffold and the fluorescent signal was turned on.

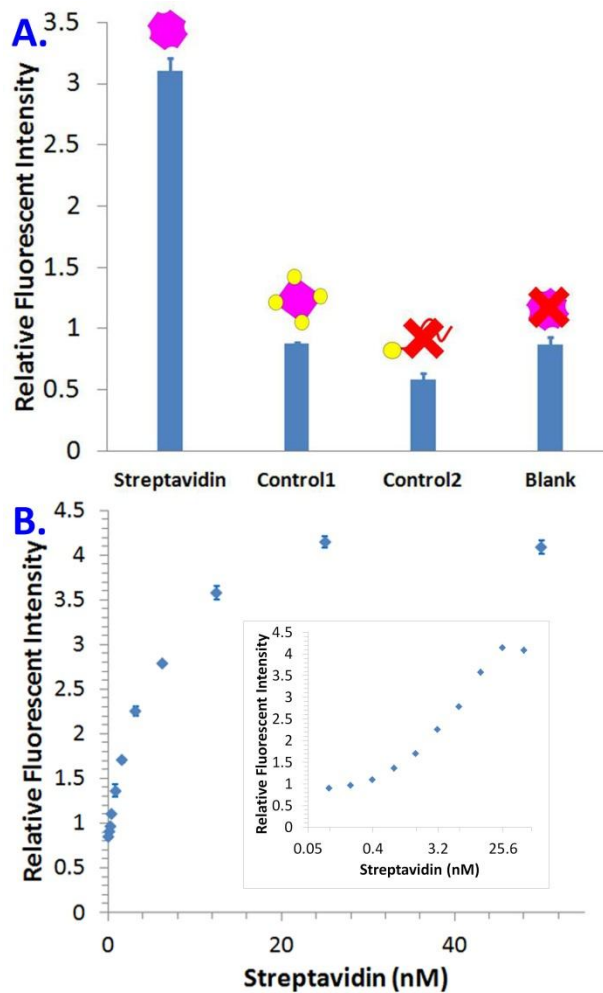


**Figure 5-3.** Evaluation of the binding-induced molecular translator for streptavidin using a fluorescence turn-on assay. (A) The streptavidin test solution contained 0.5 nM DNA-1 AuNP conjugates, 40 nM competing DNA-2, and 10 nM streptavidin. Control 1 contained the same amount of reagents as in streptavidin test solution except that 500  $\mu$ M biotin was used to saturate the binding with streptavidin. Control 2 was carried out using same concentrations of DNA-1 AuNP conjugates and streptavidin, but no competing DNA-2. In the blank, all reagents and probes were identical to the streptavidin test solution, except there was no streptavidin added. (B) Increases in relative fluorescence intensity reflect increasing concentrations of streptavidin that translates to corresponding amounts of detectable output DNA.

A key concept to our success in the efficient molecular translation of streptavidin into a pre-designed output DNA is the binding-induced DNA strand displacement that is accelerated upon the target binding and that is minimized in the absence of target binding. Among the factors that can potentially alter the rate of the DNA strand displacement reaction, the length of the DNA-1/DNA-3 duplex, the concentration and length of the competing DNA-2, and temperature play major roles in DNA displacement kinetics.<sup>8</sup> With rational design, the primary driving force of the binding-induced strand displacement reaction was the dramatic increase of the local concentration of the competing DNA upon the binding-induced DNA assembly.<sup>7</sup> We designed the DNA-1/DNA-3 duplex to have 11 base pair complementary sequences that have a melting temperature ( $T_m$ ) of 40 °C under the experimental conditions. The selection of these DNA sequences was based on two considerations: (i) the  $T_m$  is suitable to maintain stable DNA-1/DNA-3 duplex at room temperature; and (ii) DNA-3 can be displaced quickly by the competing DNA-2 upon the target binding.

### **5.3.3 Effect of competing oligo length on binding-induced molecular translator**

The strand displacement can potentially be tuned by designing the competing DNA-2 with different lengths (e.g., 7, 8, or 9 n.t. as shown in Figure 5-4A). In principle, a shorter competing DNA-2 sequence could reduce the nonspecific strand displacement. However, shorter competing DNA sequences also lead to lower specific signal intensities (Figure 5-4B). We chose a competing DNA-2 that has 9 n.t. complementary to DNA-1.  $T_m$  of the 9 n.t. DNA-2/DNA-1 duplex is



#### **5.3.4 Effect of blocking oligo on binding-induced molecular translator**

To further reduce the random (non-specific) strand displacement, we introduced a blocking oligo (B10 to B12) to partially hybridize with DNA-2 (Figure 5-5). The blocking oligo (10-12 n.t.) was designed to hybridize to 6-8 poly-T and 4 n.t. of the competing sequence of DNA-2 (Figure 5-6A). Hybridized to this blocking oligo, DNA-2 is left with a competing sequence of only 5 n.t., making it unfavourable to compete and displace DNA-3 from DNA-1/DNA-3 duplex. The duplex between the blocking oligo and DNA-2 (estimated  $T_m$  30.8 °C) can be stable under the annealing temperature of 25 °C. The use of blocking oligo (e.g., B10) resulted in a reduction of background fluorescence without adversely affecting the fluorescence signal of the target (Figure 5-6B).

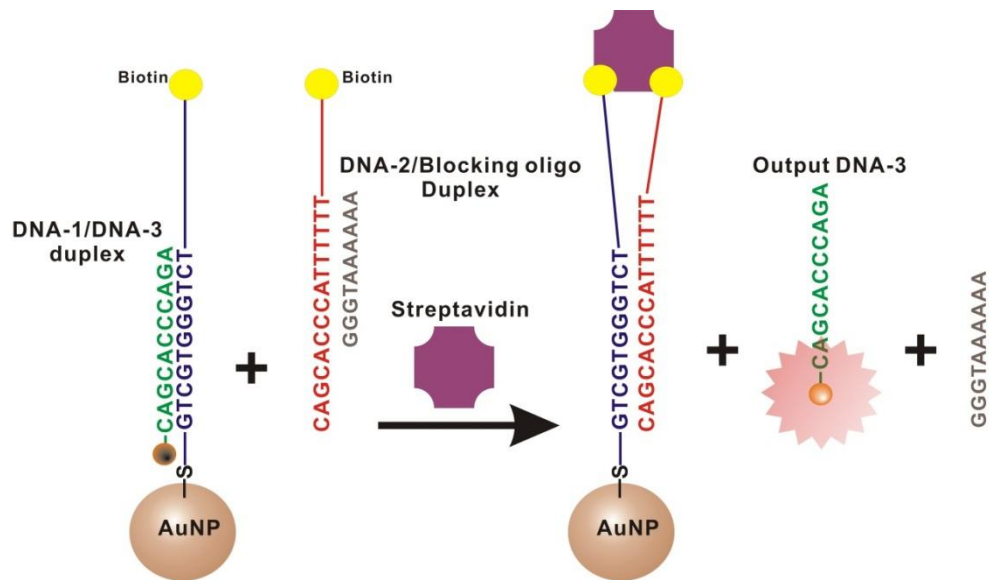


**Figure 5-5.** Schematic illustrating the effect of the blocking oligo on the binding-induced molecular translator for streptavidin. The blocking oligo initially hybridizes to the competing DNA-2, minimizing the random hybridization of DNA-2 to DNA-1. The binding of streptavidin to the biotinylated DNA-1 and DNA-2 induces the strand displacement and releases output DNA-3 and the blocking oligo.

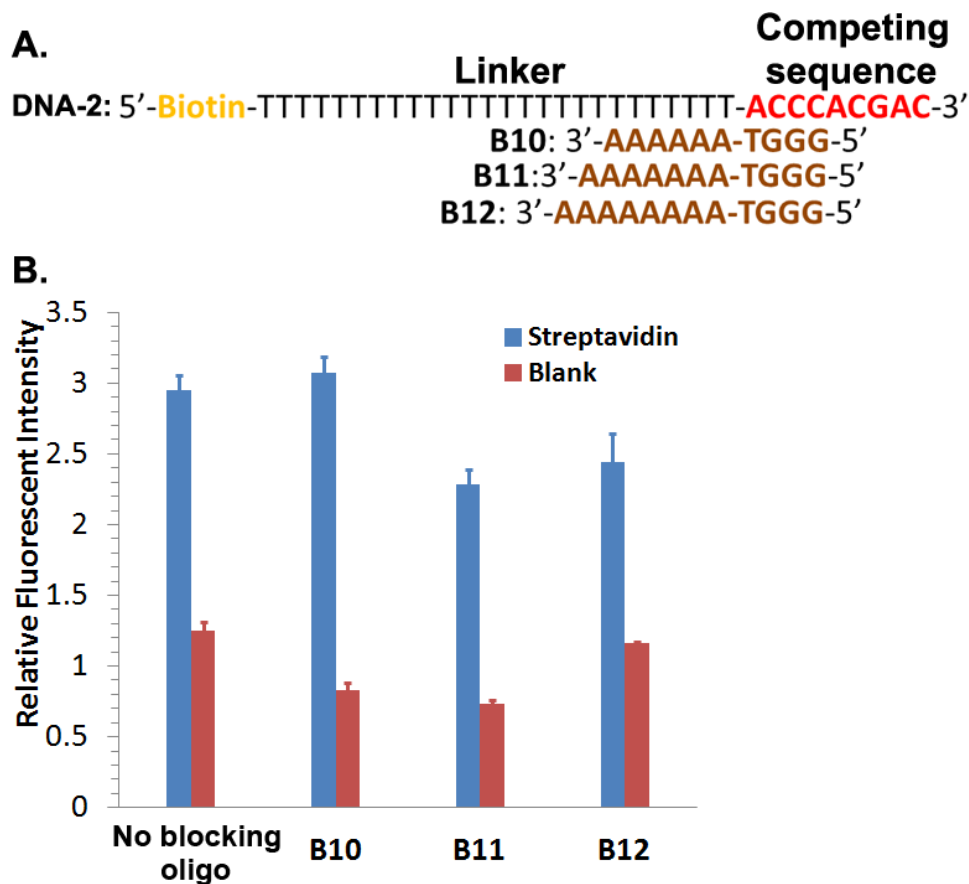


**Figure 5-6.** (A) Three designs of blocking oligo, showing blocking sequences of 10, 11, and 12 n.t. (brown) that are complementary to competing DNA-2. (B) Comparing three designs of the blocking oligo on the performance of the binding-induced molecular translator. The concentration of streptavidin is 10 nM. Error bars represent one standard deviation from triplicate analyses.

### 5.3.5 Temperature effect on binding-induced molecular translator

Because the kinetics of strand displacement is dependent on the temperature,<sup>3</sup> we have examined the effect of temperature on the performance of the binding-induced molecular translator (Figure 5-7). The rate of the binding-induced strand displacement process can be accelerated by increasing the incubation temperature (e.g. 37 °C) to be near the  $T_m$  of the DNA-1/DNA-3 duplex.

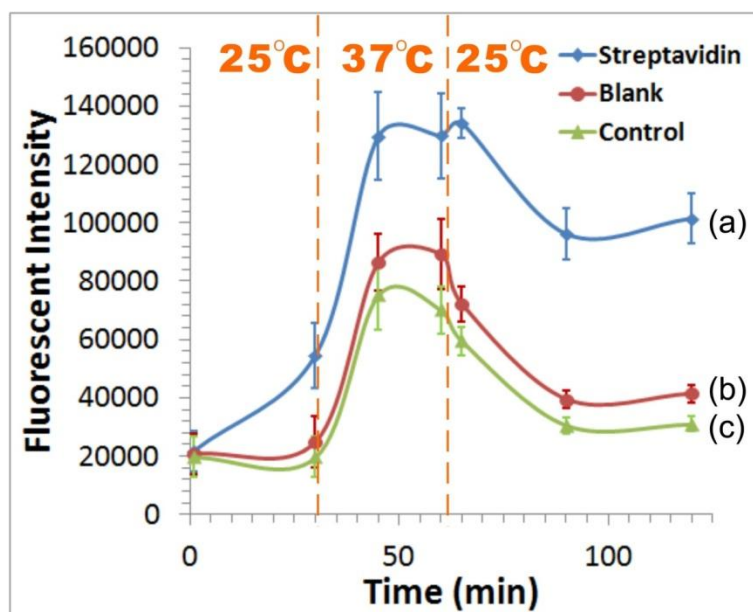


**Figure 5-7.** Effect of temperature on the performance of the binding-induced molecular translator. The test solution (a) contained 0.5 nM DNA-1/DNA-3 gold nanoparticle conjugates, 40 nM DNA-2, and 10 nM streptavidin. In blank (b), all reagents and probes were identical to the test solution for streptavidin, except there was no streptavidin added. In the second control experiment (c), the same concentration of DNA-1/DNA-3 gold nanoparticle conjugates as in (a) was used, but no DNA-2 or streptavidin was added. Error bars represent one standard deviation from triplicate analyses.

### 5.3.6 Binding-induced molecular translator for PDGF-BB

The AuNP scaffold integrated in our binding-induced molecular translator serves two primary functions: (i) to quench fluorescence of the hybridized DNA-3 probe, and (ii) to increase the local concentration of the assembled DNA in a small volume.<sup>9</sup> To demonstrate the general applicability of this strategy and to confirm the importance of increasing the local concentrations, we designed three types of molecular translators for a clinically relevant protein: platelet-derived growth factor BB (PDGF-BB). An aptamer was used as the affinity ligand to bind to PDGF-BB. The molecular translator in design-1 (Figure 5-8A) was constructed the same way as for the streptavidin-biotin system. Both DNA-1 and DNA-2 were extended by including a 44-n.t. PDGF aptamer (Table 5-2). The extended DNA-1 was then conjugated to AuNP and hybridized with DNA-3. Thus binding of PDGF-BB to two aptamers resulted in the binding-induced strand displacement of the output DNA-3. Detection of the displaced DNA-3 showed quantitative relationship between the signal output and the concentrations of PDGF-BB (red curve in Figure 5-8D).

We further examined the influence of the density of the DNA-1/DNA-3 duplex on AuNP (Figure 5-9). The observed increases in fluorescent intensity with the increase of DNA density on AuNP are consistent with the role of the increased local concentration on the performance of the binding-induced molecular translator.

In design-2 (Figure 5-8B), the PDGF aptamer and DNA-1 were each directly conjugated to AuNP, at an equal ratio. AuNP served as a scaffold to facilitate

binding of PDGF-BB to two aptamers and the binding-induced strand displacement. As compared to design-1 in which DNA-1 was extended by an addition of the 44-n.t. aptamer, DNA-1 in design-2 was not extended. Therefore, the volume of the DNA-1-AuNP in design-2 is smaller than that in design-1. A higher local concentration is expected for the binding-induced assembly in a smaller volume. Results from testing PDGF-BB using design-2 (blue curve in Figure 5-8D) showed indeed improved signal intensities than those obtained using design-1 (red curve in Figure 5-8D).

As a comparison to the AuNP-based molecular translator, we also constructed a third molecular translator using a dark quencher instead of AuNP (Figure 5-8C). The signal intensity of the output DNA was as much as 4 fold lower than the other two designs making use of AuNP scaffold (Figure 5-8D). These results are consistent with the notion that the local concentrations of the DNA assembly are substantially increased on AuNP scaffold.

After comparing the performance of binding-induced molecular translator with different designs, we chose design-2 to test its specificity to PDGF-BB against 4 other human serum proteins, including human serum albumin, human IgG, human  $\alpha$ -thrombin, and human lysozyme. As shown in Figure 5-10, the PDGF aptamer functionalized binding-induced molecular translator shows good signal response to PDGF-BB, but only background level signal response (comparing to the blank) to the other 4 serum proteins with concentrations 40 times higher than the tested PDGF-BB, suggesting the high specificity of the binding-induced molecular translator.

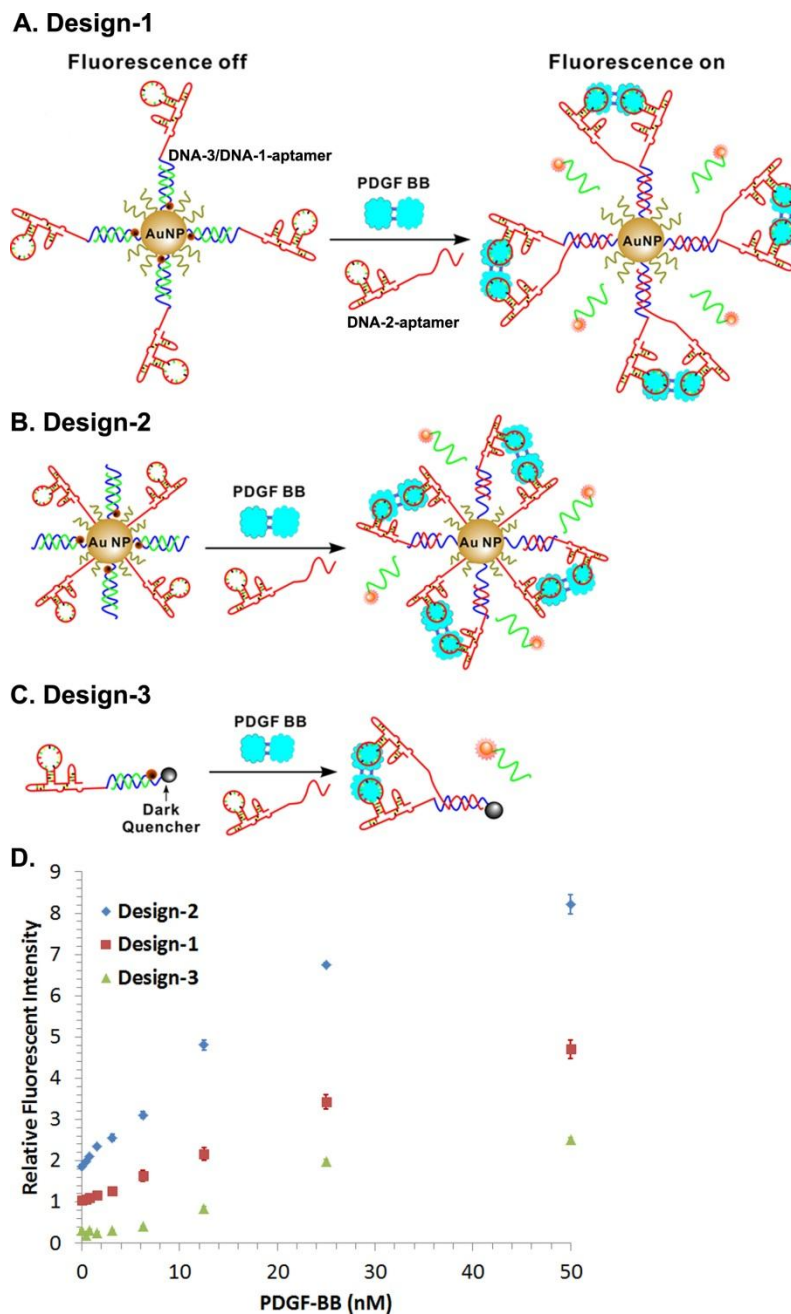


**Figure 5-8.** (A-C) Schematic illustrations of three design strategies to construct the molecular translators for PDGF-BB. (D) Performance of the three molecular translator design strategies, as assessed by detecting PDGF-BB (0-50 nM). The total concentration of the fluorescently labelled output DNA was kept at 40 nM for all samples. Error bars represent one standard deviation from triplicate analyses.

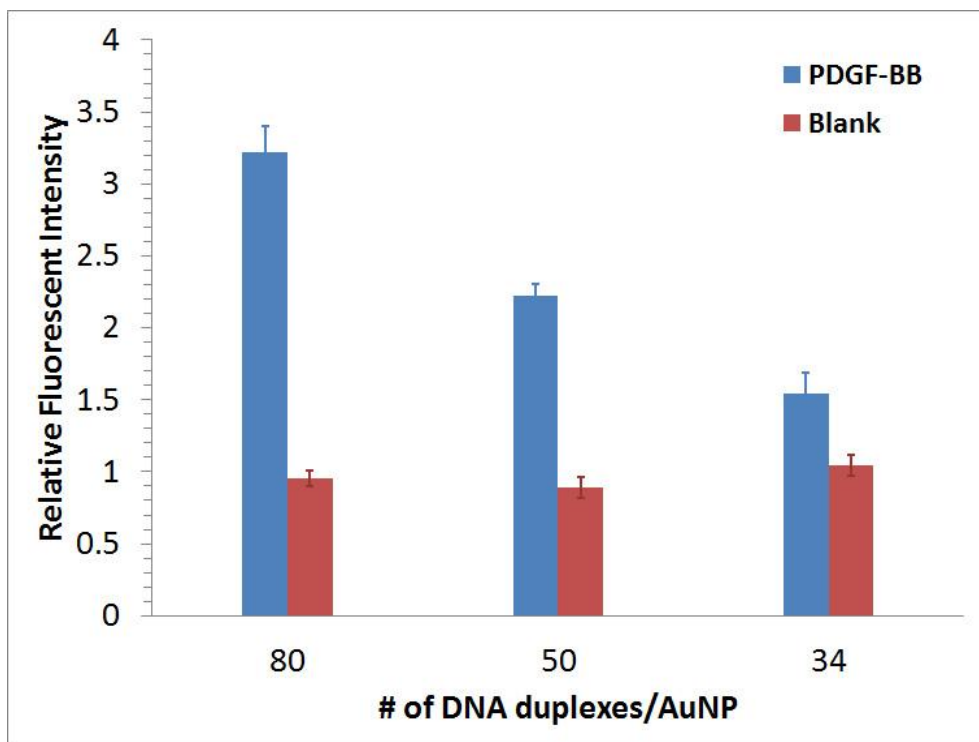


**Figure 5-9.** Effect of DNA-1/DNA-3 duplex density on the performance of the binding-induced molecular translator Design-1 for PDGF-BB detection. The PDGF-BB test solutions (blue bars) contained 25 nM PDGF-BB, 40 nM competing DNA-2, 1  $\mu$ M blocking oligo, and varying density of DNA-1/DNA-3 duplexes on AuNP (duplex concentration was fixed at 40 nM). The varying number of DNA duplexes per AuNP was achieved by using different densities of DNA-1 conjugates on AuNP. In the blank (red bars), all reagents and probes were identical to the PDGF-BB test solution, except that there was no PDGF-BB added. Error bars represent one standard deviation from triplicate analyses.

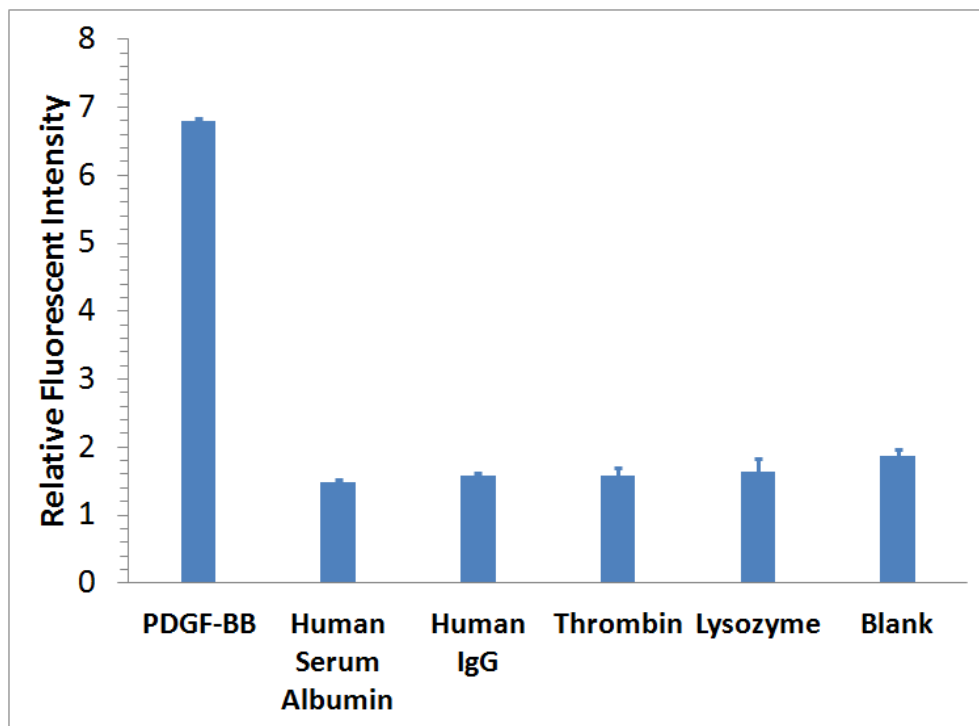


**Figure 5-10.** Results of specificity test. Samples contain either 25 nM PDGF-BB or 1  $\mu$ M nonspecific proteins (human serum albumin, human IgG, human  $\alpha$ -thrombin, and human lysozyme). Error bars represent one standard deviation from triplicate analyses.

## 5.4 Conclusions

We have successfully constructed a binding-induced molecular translator that is able to convert the input protein information to readily detectable output DNA. Affinity binding of the specific protein to both the output DNA duplex and the competing DNA assembled them on AuNP scaffold and increased their local concentrations, resulting in binding-induced strand displacement. The displaced output DNA was easily detectable with fluorescent dyes as labels. Other molecular translator format, e.g. catalytic DNA circuits, could be achieved by incorporating functional DNA domains instead of fluorescent dyes in the output DNA and by using the principle of toehold-mediated strand-displacement. Furthermore, many proteins can bind to two affinity probes and are amenable to sandwich assays (e.g. ELISA). Thus, the concept and strategy reported here can also be applied to construct binding-induced molecular translators for these and other molecular targets for which two or more affinity probes can bind. Potential applications range from assays for specific molecular targets, to molecular imaging and point-of-care diagnostics, and binding-induced nano-devices.

## 5.5 References

1. a) B. Li, A. D. Ellington, X. Chen, *Nucleic Acids Res.* **2011**, *39*, e110; b) D. S. Seferos, D. A. Giljohann, H. D. Hill, A. E. Prigodich, C. A. Mirkin, *J. Am. Chem. Soc.* **2007**, *129*, 15477-15479; c) D. Zhang, D. S. Seferos, D. A. Giljohann, P. C. Patel, C. A. Mirkin, *Nano Lett.* **2009**, *9*, 3258-3261.
2. a) S. Liao, N. C. Seeman, *Science* **2004**, *306*, 2072-2074; b) J. J. Tabor, M. Levy, A. D. Ellington, *Nucleic Acids Res.* **2006**, *34*, 2166-2172; c) A. V. Garibotti, S. Liao, N. C. Seeman, *Nano Lett.* **2007**, *7*, 480-483; d) M. Endo, S. Uegaki, T. Majima, *Chem. Commun.* **2005**, *25*, 3153-3155; e) S. Beyer, F. C. Simmel, *Nucleic Acids Res.* **2006**, *34*, 1581-1587.
3. J. M. Picuri, B. M. Frezza, M. R. Ghadiri, *J. Am. Chem. Soc.* **2009**, *131*, 9368-9377.
4. D. Y. Zhang, E. Winfree, *J. Am. Chem. Soc.* **2009**, *131*, 17303-17314.
5. A. J. Genot, D. Y. Zhang, J. Bath, A. J. Turberfield, *J. Am. Chem. Soc.* **2011**, *133*, 2177-2182.
6. Y. Xing, Z. Yang, D. Liu, *Angew. Chem. Int. Ed.* **2011**, *50*, 11934-11936.
7. a) H. Yang, A. Z. Rys, C. K. McLaughlin, H. F. Sleiman, *Angew. Chem. Int. Ed.* **2009**, *48*, 9919-9923; b) H. Zhang, X-F. Li, X. C. Le, *Anal. Chem.* **2012**, *84*, 877-884; c) Y. Sun, H. Liu, L. Xu, L. Wang, Q-H. Fan, D. Liu, *Langmuir* **2010**, *26*, 12496-12499; d) C. Zhou, Z. Yang, D. Liu, *J. Am. Chem. Soc.* **2012**, *134*, 1416-1418.
8. L. P. Reynaldo, A. V. Vologodskii, B. P. Neri, *J. Mol. Biol.* **2000**, *297*, 511-520.
9. a) A. K. Lytton-Jean, C. A. Mirkin, *J. Am. Chem. Soc.* **2005**, *127*, 12754-12755; b) Y. F. Huang, H. T. Chuang, W. Tan, *Anal. Chem.* **2008**, *80*, 567-572; c) T.

Zhao, Z. Yang, D. Liu, *Nanoscale*, **2011**, 3, 4015-4021; d) W. Wang, H. Liu, D. Liu, Y. Xu, Y. Yang, D. Zhou, *Langmuir* **2007**, 23, 11956-11959.

## **Chapter Six: Conclusions and Future Work**

I have explored dynamic DNA nanotechnology towards 1) understanding and overcoming practical issues of biosensors based on DNA functionalized gold nanoparticles (DNA-AuNPs), and 2) constructing protein detection tools for potential point-of-care diagnostic applications. Specifically, Chapters 2 and 3 focus mainly on manipulating DNA assemblies on AuNPs to enhance sensor sensitivity, specificity, and robustness for protein detection. Chapters 4 and 5 focus mainly on constructing novel binding-induced DNA assembly systems for homogeneous protein assays. In the following paragraphs, I will summarize the conclusions from each chapter in detail.

In chapter 2, I focused on understanding the thermal stability of DNA-AuNPs due to its importance on building robust DNA-AuNP based biosensors. I observed that 1) thermal stability of DNA-AuNPs was affected both by organosulfur anchor groups modified on DNA oligonucleotides and by surface density of DNA oligonucleotides conjugated on AuNP; 2) DNA-AuNPs conjugated through different organosulfur anchor groups displayed opposite trends between the thermal stability and the chemical stability. These findings can potentially be used to guide designs of DNA-AuNPs for different sensing applications. For example, we designed a series of DNA-AuNP probes using double-stranded DNA both modified with organosulfur anchors, and demonstrated the potentials on enhancing the chemical stability of DNA-AuNPs and thermal stability of short internal complementary DNA on DNA-AuNPs.

In chapter 3, I focused on understanding nonspecific protein adsorptions on aptamer functionalized AuNPs (Apt-AuNPs). By applying Apt-AuNPs as detection probes for analyzing membrane blotted serum proteins, I observed strong nonspecific adsorption of serum proteins on Apt-AuNPs. To overcome this practical problem, I developed a competitive protection strategy using dynamic DNA assembly on Apt-AuNPs and achieved highly selective detection of human  $\alpha$ -thrombin from human serum samples in a colorimetric format. This strategy can be generalized to different oligonucleotide-functionalized nanoparticle systems to control selectivity. Based on dynamic DNA assembly on Apt-AuNPs, I have also developed strategies of the directed growth of AuNP layers through controlled assembly and the targeted growth of AuNPs with gold enhancement, which can be used to enhance signals for visual detection of many different targets of clinical and prognostic significance.

In chapter 4, I focused on expanding the scope of dynamic DNA nanotechnology to proteins. To achieve this research goal, I have successfully developed a binding-induced DNA strand-displacement strategy that was able to convert protein bindings to the release of pre-designed output DNA molecules. Using this unique strategy, I have successfully developed two binding-induced DNA assembly systems, including a binding-induced strand-displacement beacon and a binding-induced catalytic DNA circuit. Both systems can be applied to the detection of specific proteins for potential point-of-care diagnostics.

In chapter 5, I described nano-sensors for homogeneous proteins assays (termed binding-induced molecular translator) by applying binding-induced DNA

strand-displacement strategy on DNA-AuNPs. The use of binding-induced molecular translator enabled sensitive and specific detection of streptavidin and the homodimer of platelet derived growth factor (PDGF-BB) without any separation steps.

The strategies and principles described in this thesis are not limited to construction of bioassays and biosensors. They can potentially be used to develop new tools for molecular imaging, drug delivery, material assemblies, and controlling cell functions. However, to transform our concept and strategies to real-life applications, we need much more efforts to overcome many remaining challenges. First, many important protein biomarkers are present in pM or even lower concentrations, requiring reliable signal amplification strategies to push the detection limit. Second, disease related protein biomarkers are always present in extremely complicated sample matrix, e.g. blood samples. Thus, affinity ligands with excellent selectivity and stability are required. Third, point-of-care diagnostics usually require analysis to be completed within one hour. Thus, techniques for signal generation and/or amplification need to meet this requirement.

Confronting these challenges presents new opportunities for further research on protein detections using dynamic DNA assemblies, in particular better selection of affinity ligands, innovative applications of nanomaterials with rational design of DNA probes, and novel isothermal DNA amplification strategies.

A recently developed technique for selection of a slow off-rate modified aptamer (SOMAmer) from modified oligonucleotide libraries has the potential to generate aptamers for almost any protein target.<sup>1</sup> Containing modified nucleoside deoxyuridine triphosphate (dUTP) mimicking amino acid side chains, aptamers (SOMAmers) selected for 813 proteins have shown high specificity and binding affinity, with dissociation constant values ranging from  $10^{-11.5}$  to  $10^{-7.5}$  M. Application of these new aptamers to dynamic DNA assemblies could overcome the limitation of many current DNA assembly systems that focus on DNA detection, by broadening the scope to the detection of proteins. The dramatic increase in the number of aptamers available for proteins should open up opportunities for developing assays for multiple proteins, which could greatly speed up the diagnostic process.

Rationale designs of DNA probes incorporating unique properties of novel nanomaterials could overcome some of the problems encountered by protein assays using dynamic DNA assemblies. For example, AuNPs have been demonstrated to protect nucleic acids from enzymatic degradation in biofluids.<sup>2</sup> QDs can be engineered to emit in the near-IR region, avoiding autofluorescence from a clinical sample matrix.<sup>3</sup> Diverse nanomaterials with extraordinary photonic, electronic, and catalytic properties can be applied to improve assay performance.<sup>4</sup>

Isothermal DNA amplification strategies can easily be adapted to dynamic DNA assembly systems to push the detection limit for protein detection. Many successful isothermal DNA amplification strategies have been designed and applied to the detection of nucleic acids.<sup>5</sup> These strategies could contribute to

enhancing protein detections by translating protein bindings to release/form pre-designed nucleic acids that trigger subsequent isothermal DNA amplifications. Furthermore, DNA probes or aptamers can be immobilized onto solid supports, e.g. magnetic beads, lateral flow paper sticks, microfluidic devices, to isolate and/or preconcentrate specific proteins from complicated sample matrix. These approaches could potentially eliminate the matrix effect and enhance the assay sensitivity and specificity.

I am currently conducting several ongoing projects, including 1) developing binding-induced molecular amplifier that is able to convert one protein binding event to the release of hundreds of pre-designed output so that the detection signal of target proteins can be amplified; 2) studying the kinetics of binding-induced DNA strand displacement to explore new approaches for further improvement; 3) developing monolithic materials that can be controlled by dynamic DNA assemblies for detecting specific proteins and protein-protein interactions from complicated sample matrix.

## References

1. Gold, L.; Ayers, D.; Bertino, J.; et al. *Plos One* **2010**, *5*, e15004.
2. Seferos, D. S.; Prigodich, A. E.; Giljohann, D. A.; Patel, P. C.; Mirkin, C. A. *Nano Lett.* **2009**, *9*, 308.
3. Smith, A. M.; Mancini, M. C.; Nie, S. *Nat. Nanotechnol.* **2009**, *4*, 710.
4. Giljohann, D. A.; Mirkin, C. A. *Nature* **2009**, *462*, 461.
5. Zhang, H.; Li, F.; Dever, B.; Li, X.-F.; Le, X. C. *Chem. Rev.* Published online, DOI: 10/1021/300340p.

## Appendix A: List of Publications from the PhD Program

### Published or submitted

1. **Li, F.**; Zhang, H.; Dever, B.; Li, X.-F.; Le, X. C. Thermal stability of DNA functionalized gold nanoparticles. *Bioconjugate Chemistry*. Submitted (**Chapter 2**)
2. **Li, F.**; Zhang, H.; Wang, Z.; Li, X.; Li, X.-F.; Le, X. C. Dynamic DNA assemblies mediated by binding-induced DNA strand displacement. *Journal of the American Chemical Society*, **2013**, *135*, 2443-2446. (**Chapter 4**)
3. Zhang, H.; **Li, F.**; Dever, B.; Wang, C.; Li, X.-F.; Le, X.C. Assembling DNA through Affinity Recognitions for Protein Detection. *Angewante Chemie International Edition*, Submitted. (Invited Review) (**Chapter 1**)
4. Zhang, H. \*; **Li, F.** \*; Dever, B.; Li, X.-F.; Le, X. C. Homogeneous Binding Assays for Nucleic Acids and Proteins. *Chemical Reviews*, Published online Dec. 11, 2012. DOI: 10/1021/300340p. (\* These authors contributed equally to this paper) (**Chapter 1**)
5. **Li, F.**; Zhang, H.; Lai C.; Li, X.-F.; Le, X. C. A Molecular Translator that Acts by Binding-Induced DNA Strand Displacement for a Homogeneous Protein Assay. *Angewante Chemie International Edition*, **2012**, *51*, 9317-9320. (**Chapter 5**)
6. **Li, F.**; Li, J.; Wang, C.; Zhang, J.; Li, X.-F.; Le, X. C. Competitive protection of aptamer-functionalized gold nanoparticles by controlling DNA assembly. *Analytical Chemistry*, **2011**, *83*, 6464-6467. (**Chapter 3**)
7. **Li, F.**; Dever, B.; Zhang, H.; Li, X.-F.; Le, X. C. Mesoporous materials in peptidome analysis. *Angewandte Chemie International Edition*, **2012**, *51*, 3518-3519. (**not included in this thesis**)
8. Hamula, C.L.A.; Zhang, H.; **Li, F.**; Wang, Z.; Le, X. C.; Li, X.-F. Selection and analytical applications of aptamers binding microbial pathogens. *Trends in Analytical Chemistry*, **2011**, *30*, 1587-1597. (**not included in this thesis**)
9. Liu, Y.; Wang, C.; **Li, F.**; Shen, S.; Le, X. C.; Li, X.-F. DNase I-Mediated Single-Cycle Selection of Aptamers for Blotted Proteins on a Membrane. *Analytical Chemistry*, **2012**, *84*, 7603-7606. (**not included in this thesis**)
10. **Li, F.**; Zhao, Q.; Wang, C.; Lu, X.; Li, X.-F.; Le, X. C. Detection of *E. coli* O157: H7 using gold nanoparticle labeling and inductively coupled plasma-mass spectrometry. *Analytical Chemistry*, **2010**, *82*, 3399-3403. (**Appendix B**)

11. Wagner, M.K.; **Li, F.**; Li, J.; Li, X.-F.; Le, X. C. Quantum dot based assays for cancer biomarkers. *Analytical and Bioanalytical Chemistry*, **2010**, 397, 3213-3224. (**not included in this thesis**)
12. Goulko, A.A.; **Li, F.**; Le, X. C. Bioanalytical applications of aptamer and molecular beacon probes in fluorescence affinity assays. *Trends in Analytical Chemistry*, **2009**, 28, 878-892. (**not included in the thesis**)

### Manuscripts in preparation

13. **Li, F.**; Li, J.; Wang C.; Naranmandura, H.; Li, X.-F.; Le, X. C. Target growth of aptamer-functionalized gold nanoparticles for direct visualization of membrane blotted proteins. (**Chapter 3**)
14. **Li, F.**; Zhang, H.; Li, X.-F.; Le, X. C. Kinetics of binding-induced DNA strand-displacement reactions. (**not included in this thesis**)
15. **Li, F.**; Lau, A.; Zhang, H.; Li, X.-F.; Le, X. C. A binding-induced molecular amplifier for homogeneous detection of nucleic acids and proteins. (**not included in this thesis**)

### Conference Presentations

#### Oral presentations:

1. **Li, F.**; Le, X.C., Binding-induced molecular translator for homogeneous protein assays. The 28<sup>th</sup> International Symposium on MicroScale Bioseparations and Analyses (October 21st, 2012, Shanghai, China). Award presentation.
2. **Li, F.**; Le, X.C., Binding-induced nano-switch for homogenous protein detection. The 243<sup>rd</sup> American Chemical Society National Meeting and Exhibition (March 25th, 2012, San Diego, California, the United States of America)
3. **Li, F.**; Le, X.C., Thermal stability of thiol-modified DNA on gold nanoparticles. The 57<sup>th</sup> International Conference on Analytical Sciences and Spectroscopy and 3<sup>rd</sup> Canada-China Analytical Chemistry Conference (August 28th, 2011, Toronto, Canada)
4. **Li, F.**; Le, X.C., Dynamic protection of aptamer functionalized gold nanoparticles. The 56th International Conference on Analytical Sciences and Spectroscopy (August 16th, 2010, Edmonton, Canada). Invited graduate student presentation.

5. **Li, F.**; Le, X.C., Detection of *E. coli* O157: H7 using gold nanoparticle amplification and inductively coupled plasma-mass spectrometry. The 93rd Canadian Chemistry Conference and Exhibition (May 29th, 2010, Toronto, Canada)

**Poster presentations:**

1. Lau, A.; **Li, F.**; Le, X.C., Fluorescence-based method for homogeneous detection of nucleic acids and proteins. John W. Macgregor Memorial Lecture Student and Resident Research Day (November 6th, 2012, Edmonton, Canada)
2. **Li, F.**; Le, X.C., Binding-induced nano-switch for homogenous protein detection. John W. Macgregor Memorial Lecture Student and Resident Research Day (October 11th, 2011, Edmonton, Canada)
3. **Li, F.**; Le, X.C., Application of aptamer functionalized gold nanoparticles for protein analysis in the western blot format. John W. Macgregor Memorial Lecture and Student and Resident Research Day (October 7th, 2010, Edmonton, Canada)
4. **Li, F.**; Le, X.C., Detection of *E. coli* O157: H7 using gold nanoparticle amplification and inductively coupled plasma-mass spectrometry. The Second China-Canada Conference on Analytical Chemistry for Life Sciences (October 14th, 2009, Beijing, China)
5. **Li, F.**; Le, X.C., Detection of *E. coli* O157: H7 using gold nanoparticle amplification and inductively coupled plasma-mass spectrometry. John W. Macgregor Memorial Lecture Student and Resident Research Day (October 1st, 2009, Edmonton, Canada)
6. **Li, F.**; Zhang, H.; Le, X. C., Multiple protein analysis by tunable aptamer capillary electrophoresis, John W. Macgregor Memorial Lecture and Student and Resident Research Day (October 2nd, 2008, Edmonton, Canada)

## Appendix B: Detection of *Escherichia coli* O157:H7 Using Gold Nanoparticle Labeling and Inductively Coupled Plasma Mass Spectrometry<sup>5</sup>

### Introduction

The analysis of pathogenic bacteria is vital for protection of food and water safety, health surveillance, and clinical diagnosis. Among more than 100 known serotypes of *E. coli*, O157: H7 is a notorious pathogen confirmed in many outbreaks of food borne illnesses.<sup>1,2</sup> It causes bloody diarrhea, haemorrhagic colitis and occasionally haemolytic uremic syndrome (HUS, a type of kidney failure). An infection dose as low as ~100 cells can lead to diseases or even deaths, especially in children, elderly, and immune compromised people.<sup>1</sup> Therefore, clinical diagnosis as well as food, water industry continue to demand for fast and sensitive assays for *E. coli* O157: H7.<sup>3-5</sup> Conventional methods for detection of pathogenic bacteria, includes culture techniques,<sup>6</sup> polymerase chain reaction (PCR),<sup>7-9</sup> and enzyme-linked immunosorbent assays (ELISAs).<sup>10,11</sup> To improve the sensitivity and speed of analysis, much recent effort has focused on the use of fluorescence nanoparticles<sup>12</sup> or nanovesicles,<sup>13</sup> quantum dots,<sup>14-16</sup> bioluminescence,<sup>17-18</sup> mass spectrometry,<sup>19</sup> infrared (IR) spectrometry,<sup>20-21</sup> surface enhanced Raman spectrometry (SERS),<sup>22-23</sup> Rayleigh scattering spectrometry,<sup>24</sup> piezoelectric biosensors,<sup>25-26</sup> and amperometric biosensors.<sup>27</sup> The objective of the present study was to develop a new analytical strategy for bacteria detection that could achieve high speed and high sensitivity by taking advantages of antibody

---

<sup>5</sup> This chapter has been published in Li, F.; Zhao, Q.; Wang, C.; Lu, X.; Li, X.-F.; Le, X.C. *Anal. Chem.* **2010**, *82*, 3399-3403.

affinity, gold nanoparticles (Au NPs) amplification, and inductively coupled plasma-mass spectrometry (ICP-MS) detection.

ICP-MS is one of the most sensitive techniques for trace element analysis, providing large dynamic range, low detection limits, and multi-element and rapid analysis capability.<sup>28,29</sup> Recently, the use of elemental tags and inorganic nanoparticles has also made ICP-MS amenable for analysis of bio-molecules.<sup>28-34</sup> Although inorganic nanoparticles, such as Au NPs, have been applied as detection and imaging probes,<sup>35</sup> they have not been demonstrated in ICP-MS assays for whole bacterial cells. We show here for the first time an affinity assay for bacterial cells using nanoparticle amplification and ICP-MS detection.

To demonstrate the proof of principle, we chose *E. coli* O157: H7 as the target analyte. A monoclonal antibody for *E. coli* O157:H7 is conjugated to gold nanoparticles (Au NPs, 10 nm diameter), and these Au NPs serve as affinity probes to recognize the *E. coli* O157:H7 target. Subsequent detection of Au NPs by ICP-MS leads to quantitative analysis of the bacterial cells. Because ICP-MS measures Au elemental ions produced by Au atoms, and a 10-nm-diameter Au NP contains ~30 000 Au atoms,<sup>31,34</sup> the use of 10-nm Au NPs could potentially enhance the ICP-MS signal by up to 30 000 folds, thereby dramatically improving sensitivity of the assay.

## **Experimental Section**

### **Chemicals and Materials.**

Mouse monoclonal antibody (mAb) against *E. coli* O157: H7 was purchased from Biodesign International (Meridian Life Science). Biotin conjugated rabbit polyclonal antibody to *E. coli* O and *E. coli* K was obtained from Abcam (Product No. ab33839). *E. coli* O157: H7 cultures (strain ADRI V241) were provided by the Agri-Food Laboratories Branch, Alberta Agriculture and Food (Edmonton, Alberta, Canada). *E. coli* DH5 $\alpha$ , ATCC35218, ATCC25922 were obtained from the American Type Culture Collection. Solution of gold standard was purchased from Agilent (Multi-Element Calibration Standard-3, 10  $\mu\text{g}/\text{mL}$ ). Solutions of gold nanoparticles (Au NPs) (10 nm in diameter,  $5.4 \times 10^{12}$  Au NPs per mL) and streptavidin-labelled Au NPs (10 nm in diameter,  $1.4 \times 10^{13}$  Au NPs per mL) were purchased from Sigma. Bovine serum albumin (BSA) was also purchased from Sigma. Phosphate buffered saline (PBS) 10X solution and nitric acid (Optima) were obtained from Fisher Scientific.

#### **Bacteria culture and plate counting.**

The culture conditions were previously described in detail.<sup>7</sup> Briefly, *E. coli* O157:H7 was grown in tryptic soy broth (TSB) at 37 °C with shaking (125 rpm). To count the number of bacteria cells, cultures were serially diluted with sterile water, and 100  $\mu\text{L}$  of the selected dilution was mixed with warm tryptic soy agar (TSA) and poured to plates in triplicate. Plates were incubated at 37 °C for 24 h. For calculation of the numbers of Colony-forming units per mL (CFU/mL), dilutions showing between 30 and 300 colonies on TSA were used.

### **Preparation and characterization of antibody modified Au NPs.**

*Direct modification:* Anti- *E. coli* O157 mAb was modified onto Au NPs according to the literature procedures.<sup>36</sup> A measured amount of mAb was added to 1 mL of Au NP solution (undiluted) at pH 9.0. After incubation at room temperature for 30 minutes, the mixture was passivated and stabilized with 500  $\mu$ L of a 5% BSA solution for 1 hr. The final solution was centrifuged at 17,000 g for 1 hr at 4 °C, and the supernatant was removed. After washing with PBS buffer 2 times, the pellet was re-dispersed in 1 mL of PBS buffer with 0.5% BSA at pH 7.4. The modified Au NPs solution could be stored at 4 °C for more than one month. The loading of mAb onto Au NPs was determined by a modified colorimetric method.<sup>36</sup> In this experiment, various amounts of mAbs were added to 1 mL of Au NP solutions ( $5.4 \times 10^{12}$  Au NPs per mL) at pH 9.0. After 30 min incubation at room temperature, 100  $\mu$ L of 3 M NaCl was added to each solution, and the final color of each solution was observed and recorded using a digital camera.

*Modification through streptavidin-biotin interaction:* 7.0  $\mu$ g of polyclonal antibody (pAb) and 200  $\mu$ L of streptavidin-labelled Au NP solution ( $1.4 \times 10^{13}$  Au NPs per mL) were added together and diluted to 1 mL with 1 $\times$ PBS buffer containing 1% BSA. The mixture was incubated at room temperature for 30 min and then stored at 4 °C.

### **Incubation of cells with antibody modified Au NPs.**

Anti- *E. coli* O157: H7 mAb-modified Au NPs (10  $\mu$ L) were added to 100  $\mu$ l of sample solution containing  $0-5 \times 10^7$  CFU/mL of *E. coli* O157: H7, suspended in  $1 \times$  PBS with 0.5% BSA. The mixtures were incubated at room temperature for 20 min, followed by washing 3 times with  $1 \times$  PBS buffer (centrifugation at 17,000 g for 1 min). Finally, the cell pellets were re-dispersed and digested in a 200  $\mu$ L solution of 1% HNO<sub>3</sub> with 1% BSA for digestion. The digest was introduced into ICP-MS to detect Au at m/z 197. For each sample and calibration solution, triplicate analyses were performed using ICP-MS.

To demonstrate specificity, a control experiment was performed in the same manner as described above, except that *E. coli* O157: H7 cells were replaced by non-specific *E. coli* cells (DH5 $\alpha$ , ATCC35218 or ATCC25922). To determine the detection limit, replicate analyses of blanks were performed. Six replicates of blanks were treated the same way as for *E. coli* O157: H7 and the standard deviation was calculated from 18 analyses (triplicate ICP-MS analyses of each blank).

### **ICP-MS analysis.**

An Agilent 7500cs octopole reaction system ICP-MS, operated in the helium mode, was used for the elemental analysis of Au NPs. The operating parameters of ICP-MS are summarized in Supporting Information Table S1. A 20- $\mu$ L sample was injected using a Rheodyne six-port injector (Model 7725i, Rheodyne, CA, USA) to a 1% HNO<sub>3</sub> carrier stream. Detailed information about tuning and operating conditions was described previously.<sup>34</sup>

**Caution:** *E. coli* O157:H7 is pathogenic and should be handled in a Level 2 biohazard hood.

## **Results and Discussion**

The principle of the assay is schematically shown in Figure 1. To carry out an analysis, the antibody-conjugated Au NPs are added to a sample solution. The target bacterial cells bind with the antibody to form affinity complexes, linking the cell, antibody, and Au NPs. The mixture is centrifuged to separate the Au NPs bound to the cells from the unbound Au NPs. The fraction of the cell-bound Au NPs is then acid digested and quantified by the determination of Au using ICP-MS. The key components in developing this assay include the conjugation of antibodies to Au NPs, the specific binding of these conjugates to the bacterial cells, and sensitive detection of Au NPs using ICP-MS. Each of these components contributes to the sensitivity and specificity of the assay. These components are optimized and discussed below.

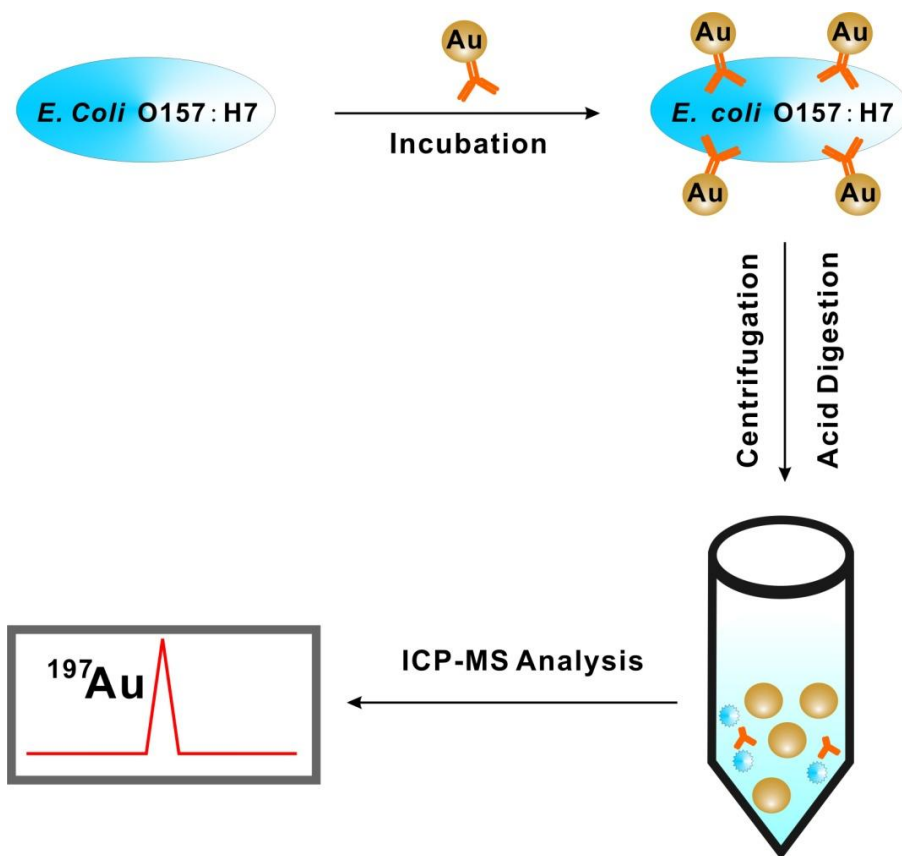


**Figure 1.** Schematic diagram showing the principle of the assay. *E. coli* O157:H7 cell was incubated with antibody-conjugated gold nanoparticles (Au NPs, shown in gold). The unbound Au NPs were separated from cell complex by centrifugation. After washing, the cell pellets containing Au NPs were digested with 1% nitric acid, and the solution was analyzed by ICP-MS. The intensity of the ICP-MS measurement of Au at  $m/z$  197 corresponds to the concentration of *E. coli* O157:H7 cells in the original sample.

## Characterization of antibody-modified Au NPs

To attach antibody to Au NPs, we adapted a well-documented technique of protein adsorption onto Au NPs.<sup>35,37</sup> The adsorption process is dependent on pH and the amount of protein loading. Consistent with the reported observations,<sup>37</sup> we found that a pH value of 9.0 was suitable for achieving Au NP modification with monoclonal antibody against *E. coli* O157:H7. To monitor the amount of antibody loading on the Au NPs, we used a simple colorimetric assay. In the absence of antibody modification, Au NPs in water appears red (Figure 2, far left tube). The addition of 1 M of NaCl to this Au NPs solution causes an immediate color change from red to blue (Figure 2 far right tube). This color change is due to flocculation of nanoparticles. With the addition of antibody to Au NPs solution, the electrolyte-induced flocculation was reduced or eliminated. This is due to the presence of antibodies on the surface of Au NPs. With increasing amount of antibody, the color of the Au NPs solution was reversed back to red, as shown from right to left in Figure 2. An amount of 7  $\mu\text{g}$  per mL was selected since we found that the Au NPs were well stabilized when the amount of antibody was greater than 6  $\mu\text{g}$  per mL. This amount (7  $\mu\text{g}/\text{mL}$ ) corresponds to  $\sim 5$  protein molecules on each Au NP.

The Au NPs with antibody modification were further characterized by using ICP-MS. Previous work has shown that Au NPs could be quantified by ICP-MS and that the atomization efficiency of ICP-MS for nanoparticles were the same as for Au ions in solution.<sup>30,34</sup> Thus, by calibrating the number of Au NPs against concentration of Au in standard solutions (Figure 3), we are able to measure the

amount of Au atoms in each Au NP. Our results show that each Au NP (10 nm size) contained 21,400 Au atoms, which is consistent with other reports.<sup>31,34</sup>



**Figure 2.** Result of antibody loading test. The far left tube contains Au NPs in water with no salt or antibody added. To the other tubes containing the same amount of Au NPs was added varying amounts (0–10 µg) of antibody and 1 M NaCl.

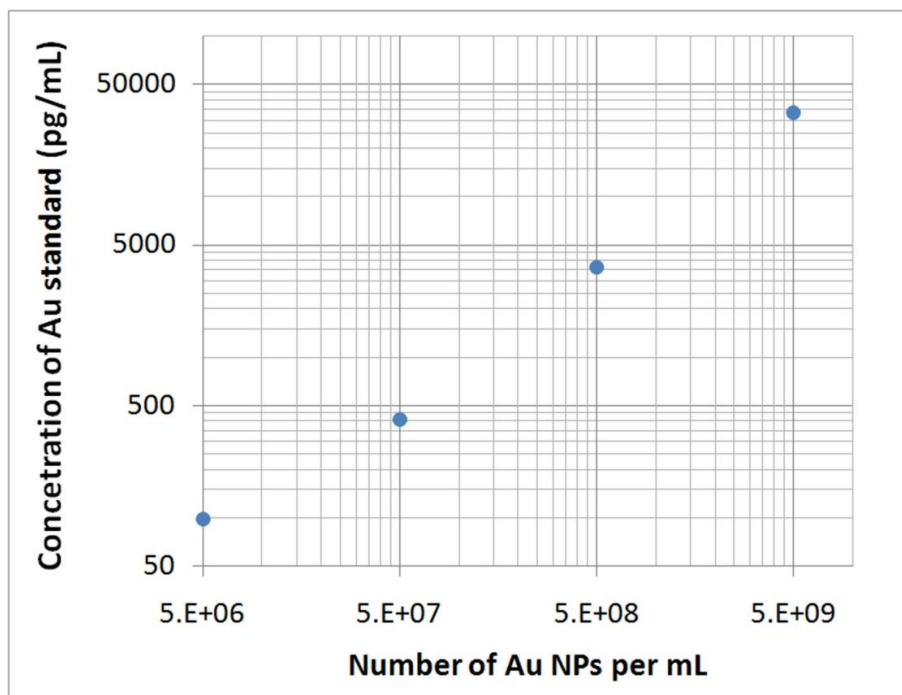


**Figure 3.** ICP-MS analyses of Au NPs, calibrated against Au standard solutions. Au NP solutions containing varying amounts of gold nanoparticles ( $5 \times 10^6$  /mL to  $5 \times 10^9$  /mL) and Au standard solutions were analysed by ICP-MS. The concentration of Au NPs (number of Au NPs per mL) and Au standard solutions (pg/mL) that resulted in identical signal intensities were correlated. Error bars (one standard deviation from triplicate analyses) were smaller than the size of the symbol.

### **Detection of *E. coli* O157: H7 by ICP-MS**

Using monoclonal antibody attached to Au NPs as affinity probes to recognize *E. coli* O157: H7, we have developed a sensitive assay for this pathogen. Figure 4 shows typical results from one set of experiments with different concentrations of *E. coli* O157:H7 cells, ranging from 50 to  $5 \times 10^6$  CFU/mL. The signal intensity increases with increasing cell concentrations. A detection limit of 500 CFU/mL was achieved. This conservative estimate was based on 3 times the standard deviation of the background plus the mean blank values from triplicate analyses of each of 6 blanks. The linear dynamic range was between 500 CFU/mL and  $5 \times 10^5$  CFU/mL with a linear correlation  $r=0.964$ .

The assay procedures involve a short incubation, a simple centrifugation to separate the cells, acid digestion, and ICP-MS analysis. Because both *E. coli* O157: H7 cell labelling and ICP-MS detection require only minimum sample preparation, the assay is simple and fast, taking less than 40 min for each sample: 20 min for incubation, <15 min for washing and acid digestion, and <5 min for ICP-MS detection. Triplicate ICP-MS analyses showed a relative standard deviation (RSD) of <5%, and triplicate sample preparations exhibited RSD of <10%.

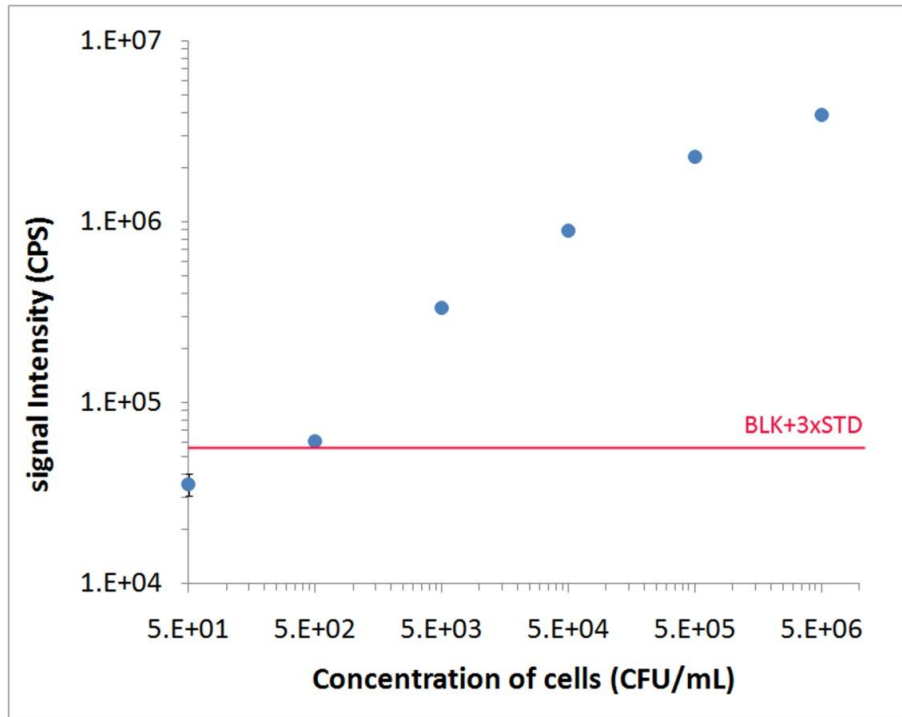


**Figure 4.** The measured signal intensity as a function of the concentration of *E. coli* O157: H7 cells in water samples. Error bars represent one standard deviation from triplicate analyses.

The specificity of this assay is mainly dependent on the antibodies used. *E. coli* O157: H7 contains two specific antigens: O polysaccharide (O157) and flagella protein (H7). The antibody we used specifically recognizes the lipopolysaccharides (LPS) oligosaccharide region of the cell and has no reactivity with most other *E. coli* serotypes, such as O111, O125, O20, O155 and K12. However, any non-specific binding or adsorption of Au NPs would produce background signals. To test the specificity of the assay, we used several non-specific *E. coli* cells, DH5 $\alpha$ , ATCC35218, and ATCC25922. As shown in Figure 5, at a concentration of  $5 \times 10^5$  CFU/mL, all three non-specific cells showed only background signals, all at much lower intensities than that for the specific O157:H7 cells. The background from DH5 $\alpha$  and ATCC25922 cells were negligible. We also tested different concentrations of all three non-specific cells, from  $5 \times 10^3$  to  $5 \times 10^6$  CFU/mL, and they all had signal intensities similar to the blank.

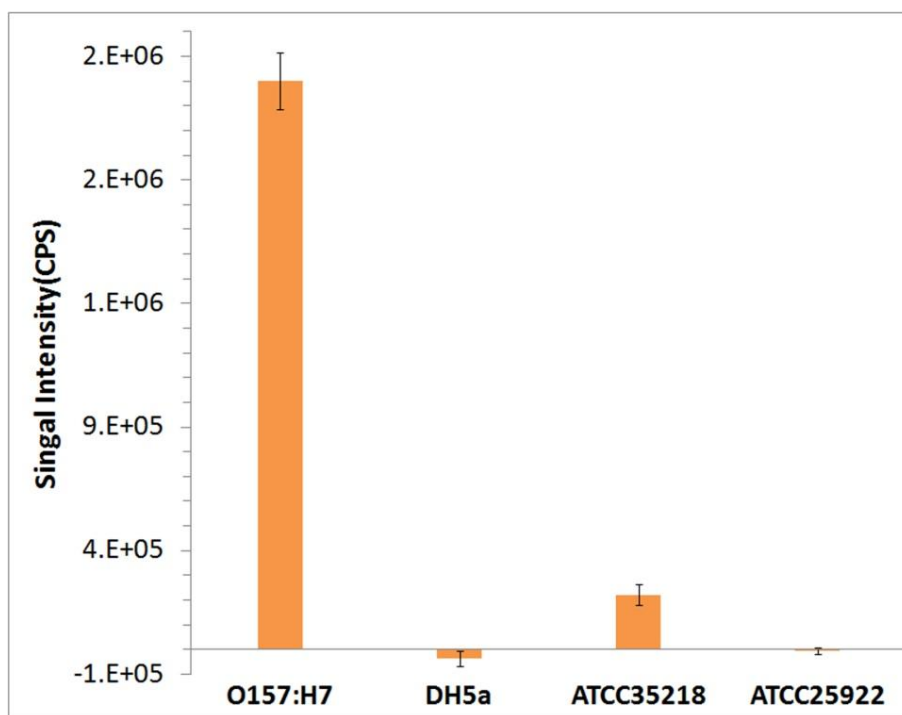


**Figure 5.** Results of specificity test. Samples contained either *E. coli* O157:H7 cells or one of the non-specific cells (DH5 $\alpha$ , ATCC35218, or ATCC 25922). Concentrations of bacterial cells were  $5 \times 10^5$  CFU/mL. Error bars represent one standard deviation from triplicate analyses.

We noted that the signal intensities increased with the increase of *E. coli* cell concentrations in the sample as expected, but these increases were not completely linear over the large concentration range (Figure 4). We suspected that the non-linearity observed at the high bacterial concentrations could be due to cell aggregation, reducing the cell surface area for binding to the antibody. Because we had on average 5 antibody molecules attached to each Au NP. These Au NPs could bring bacterial cells together. Aggregation of the cells would decrease their surface area available for binding to the antibody-conjugated Au NPs, which would result in signals lower than expected for high concentration of cells. In order to test this hypothesis, we measured the average number of Au NPs bound

to each CFU (colony forming unit) after we incubated a fixed amount of Au NPs with increasing concentrations of bacterial cells (Figure 6). We found that as the cell concentration increased from  $5 \times 10^2$  CFU/mL to  $5 \times 10^6$  CFU/mL, the amount of Au NPs bound to each CFU decreased from  $1.1 \times 10^6$  to  $7.8 \times 10^3$ . These results support our hypothesis, and suggest that the assay is more useful for detecting low concentrations of the target cells. Decreasing the loading of antibodies on Au NPs and increasing the concentration of Au NPs may improve linearity for the high bacterial concentration range; however aggregation of Au NPs could potentially be an issue.

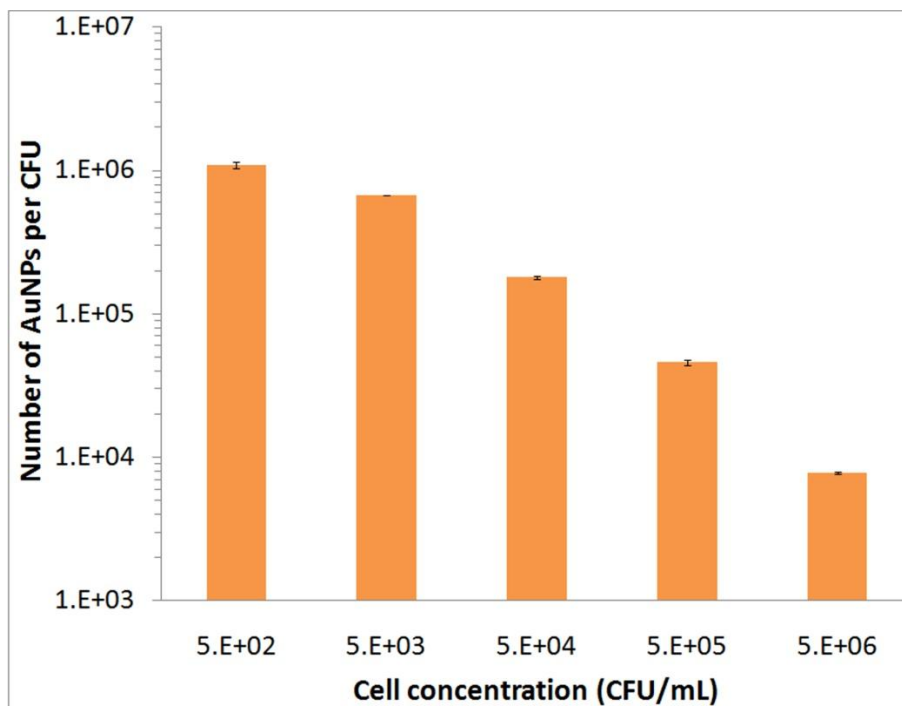


**Figure 6.** Average number of Au NPs bound to each CFU as a function of increasing concentrations of *E. coli* O157: H7 cells. Error bars represent one standard deviation from triplicate analyses.

We also explored the use of commercially available biotinylated polyclonal antibody and streptavidin-coated Au NPs, in an attempt to broaden the application of the assay. Because of the strong binding between biotin and streptavidin, streptavidin-coated Au NPs could be used with a range of biotinylated antibodies for other targets. Our preliminary results from the use of biotinylated polyclonal antibody to all *E. coli* O and K strains showed lower specificity and binding ability to *E. coli* O157:H7 compared to the use of directly modified Au NPs with monoclonal antibody. Nonetheless, a dynamic range from  $5 \times 10^4$  to  $5 \times 10^7$  CFU/mL was achieved with a detection limit of  $5 \times 10^4$  CFU/mL (Figure 7).

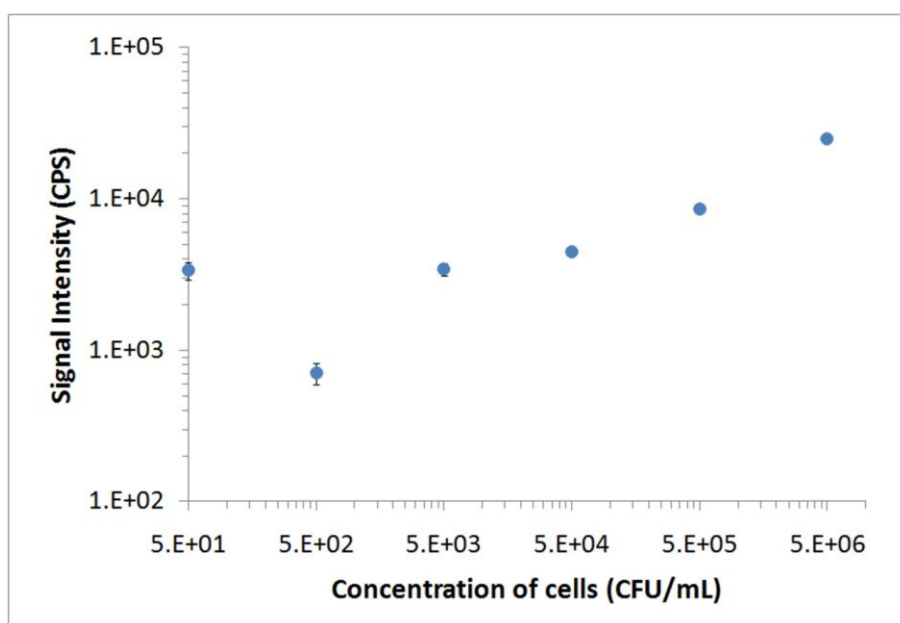


**Figure 7.** Assay for *E. coli* O157:H7 by using biotinylated polyclonal antibody (anti all *E. coli* O and K strains) and streptavidin-coated Au NPs. Error bars represent one standard deviation from triplicate analyses.

In conclusion, we have demonstrated a sensitive, specific, and rapid assay for *E. coli* O157:H7 based on the combination of monoclonal antibody recognition, gold nanoparticle amplification, and inductively coupled plasma-mass spectrometry detection. The assay was able to detect bacterial cells in a large concentration range and with a detection limit comparable to most immunoassays or sensor-based assays. Commonly used sample pre-concentration techniques (e.g., the use of antibody-coated magnetic beads or immuno membrane filtration) could further improve the detection limit of the assay. In addition to Au NPs, other nanoparticles (e.g., silver nanoparticles and rare earth nanoparticles) could also be used as specific labels. Because ICP-MS is capable of specific detection of multiple elements, high-throughput analyses of multiple bacterial cells could be achieved by labeling antibodies for different cells with different nanoparticles. The feasibility demonstrated here for the analysis of *E. coli* O157:H7 suggests the potential of similar immunoassays for wide variety of bacterial pathogens.

## References

1. Nataro, J. P.; Kaper, J. B. *Clin. Microbiol. Rev.* **1998**, *11*, 142-201.
2. Tarr, P. I.; Neill, M. A. *Gastroenterol Clin. North Am.* **2001**, *30*, 735-751.
3. Muniesa, M.; Jofre, J.; Garcia-Aljaro, C.; Blanch, A. R. *Environ. Sci. Technol.* **2006**, *40*, 7141-7149.
4. de Boer, E.; Beumer, R. R. *Int. J. Food. Microbiol.* **1999**, *50*, 119-130.
5. Deisingh, A. K.; Thompson, M. *J. Appl. Microbiol.* **2004**, *96*, 419-429.
6. March, S. B.; Ratnam, S. *J. Clin. Microbiol.* **1986**, *23*, 869-872.
7. Liu, Y.; Gilchrist, A.; Zhang, J.; Li, X. F. *Appl. Environ. Microbiol.* **2008**, *74*, 1502-1507.

8. Rodriguez-Lazaro, D.; D'Agostino, M.; Herrewegh, A.; Pla, M.; Cook, N.; Ikononopoulos, J. *Int. J. Food Microbiol.* **2005**, *101*, 93-104.
9. Jofre, A.; Martin, B.; Garriga, M.; Hugas, M.; Pla, M.; Rodriguez-Lazaro, D.; Aymerich, T. *Food. Microbiol.* **2005**, *22*, 109-115.
10. Park, S.; Kim, H.; Paek, S. H.; Hong, J. W.; Kim, Y. K. *Ultramicroscopy* **2008**, *108*, 1348-1351.
11. Lazcka, O.; Del Campo, F. J.; Munoz, F. X. *Biosens. Bioelectron.* **2007**, *22*, 1205-1217.
12. Zhao, X.; Hilliard, L. R.; Mechery, S. J.; Wang, Y.; Bagwe, R. P.; Jin, S.; Tan, W. *Proc. Natl. Acad. Sci. U. S. A.* **2004**, *101*, 15027-15032.
13. Chen, C. S.; Durst, R. A. *Talanta* **2006**, *69*, 232-238.
14. Su, X. L.; Li, Y. *Anal. Chem.* **2004**, *76*, 4806-4810.
15. Hahn, M. A.; Tabb, J. S.; Krauss, T. D. *Anal. Chem.* **2005**, *77*, 4861-4869.
16. Hahn, M. A.; Keng, P. C.; Krauss, T. D. *Anal. Chem.* **2008**, *80*, 864-872.
17. Liu, Y.; Brandon, R.; Cate, M.; Peng, X.; Stony, R.; Johnson, M. *Anal. Chem.* **2007**, *79*, 8796-8802.
18. Wolter, A.; Niessner, R.; Seidel, M. *Anal. Chem.* **2008**, *80*, 5854-5863.
19. Chen, W. J.; Tsai, P. J.; Chen, Y. C. *Anal. Chem.* **2008**, *80*, 9612-9621.
20. Ravindranath, S. P.; Mauer, L. J.; Deb-Roy, C.; Irudayaraj, J. *Anal. Chem.* **2009**, *81*, 2840-2846.
21. Yu, C.; Ganjoo, A.; Jain, H.; Pantano, C. G.; Irudayaraj, J. *Anal. Chem.* **2006**, *78*, 2500-2506.
22. Naja, G.; Bouvrette, P.; Hrapovic, S.; Luong, J. H. *Analyst* **2007**, *132*, 679-686.
23. Sengupta, A.; Mujacic, M.; Davis, E. J. *Anal. Bioanal. Chem.* **2006**, *386*, 1379-1386.
24. Singh, A. K.; Senapati, D.; Wang, S.; Griffin, J.; Neely, A.; Candice, P.; Naylor, K. M.; Varisli, B.; Kalluri, J. R.; Ray, P. C. *ACS Nano* **2009**, *3*, 1906-1912.
25. Serra, B.; Gamella, M.; Reviejo, A. J.; Pingarron, J. M. *Anal. Bioanal. Chem.* **2008**, *391*, 1853-1860.
26. Su, X. L.; Li, Y. *Biosens. Bioelectron.* **2004**, *19*, 563-574.

27. Cheng, Y.; Liu, Y.; Huang, J.; Xian, Y.; Zhang, W.; Zhang, Z.; Jin, L. *Talanta* **2008**, *75*, 167-171.
28. Lu, Y.; Wang, W.; Xing, Z.; Wang, S.; Cao, P.; Zhang, S.; Zhang, X. *Talanta* **2009**, *78*, 869-873.
29. Baranov, V. I.; Quinn, Z.; Bandura, D. R.; Tanner, S. D. *Anal. Chem.* **2002**, *74*, 1629-1636.
30. Zhang, C.; Zhang, Z.; Yu, B.; Shi, J.; Zhang, X. *Anal. Chem.* **2002**, *74*, 96-99.
31. Ornatsky, O.; Baranov, V. I.; Bandura, D. R.; Tanner, S. D.; Dick, J. J. *J. Immunol. Methods* **2006**, *308*, 68-76.
32. Razumienko, E.; Ornatsky, O.; Kinach, R.; Milyavsky, M.; Lechman, E.; Baranov, V.; Winnik, M. A.; Tanner, S. D. *J. Immunol. Methods* **2008**, *336*, 56-63.
33. Bandura, D. R.; Baranov, V. I.; Ornatsky, O. I.; Antonov, A.; Kinach, R.; Lou, X.; Pavlov, S.; Vorobiev, S.; Dick, J. E.; Tanner, S. D. *Anal. Chem.* **2009**, *81*, 6813-6822.
34. Zhao, Q.; Lu, X.; Yuan, C. G.; Li, X. F.; Le, X. C. *Anal. Chem.* **2009**, *81*, 7484-7489.
35. Hayat, M. A. *Colloidal Gold: Principles, Methods, and Applications*, Academic Press, San Diego, CA, **1989**
36. Hill, H. D.; Mirkin, C. A. *Nat. Protoc.* **2006**, *1*, 324-336.
37. Bullock, G. R.; Petrusz, P. *Techniques in Immunocytochemistry*. Academic Press, New York, **1983**, vol. 2, pp. 217-284.